The Effect of Seasonal Variation in Birth and Transmission Rates on Host-Parasite Relationships

Charlotte Ward

SUBMITTED FOR THE DEGREE OF
DOCTOR OF PHILOSOPHY

School of Mathematics and Statistics
University of Sheffield

November 2020

Supervisor: Dr. Alex Best

For Grandma Ward, and Grandma Kirby.

Abstract

Climate change is impacting ecosystems, and its effect on host-parasite systems is being noticed globally. With changing seasons comes changing species behaviour, and how these alternative behaviours might impact host-parasite systems is an important study area. Here we use and adapt classic susceptible-infected-recovered (SIR) compartmental disease models of hosts and parasites to consider how seasonality in both birth and transmission affect dynamics. We use the models to explore how seasonality drives behaviour of a population and its disease dynamics. We summarise how each seasonal component impacts population dynamics individually before incorporating both seasonal terms into the theoretical models. Simultaneous incorporation of seasonality in birth rate and seasonality in transmission leads to a wide range of population dynamics in each case where notably the timing of birth and transmission in relation to each other plays a pivotal role in determining the recurrence of disease cycles. The results obtained help us to understand, for example, how a host-parasite system might react after changing their behaviour due to a changing climate. We explore population management, or *harvest*, strategies with the aim of controlling the size of disease outbreaks without reducing population levels to critically low values. The timing of harvesting, in relation to the seasonal birth and transmission, is an important factor in determining the most appropriate disease control strategy. Overall, we show that the presence of seasonality in both birth and transmission plays a large role in determining population and disease dynamics, and that harvesting strategies can help to reduce disease whilst maintaining population size.

Acknowledgements

Firstly I would like to thank my supervisor, Dr. Alex Best, for his unrivalled support throughout the three years of my PhD research. Without his support and guidance this thesis would not have come to fruition so successfully.

Endless thanks to my Mum and Dad for supporting me and being excited about everything I do, from academics to bird watching to running. Thanks especially for supplies of sweets and chocolate, which kept me going in the toughest times.

To Fay, for being the best officemate and friend I could wish for. From the beginning of our undergraduate degrees in 2011, to the completion of our PhD projects in 2021, we've come a long way together!

Further thanks go to my running and orienteering coach, and general life mentor, Rob. You have kept me calm, supported and motivated me to complete the PhD, and helped me to achieve things I never thought possible in my sporting endeavours.

My final thanks go to Tom. There are not enough words to describe how well you have supported and encouraged me throughout the whole PhD process. I am so grateful for the time we have spent together over the last three years, and look forward to the many more to follow.

Contents

List of Figures

Chapter 1

Introduction

The Intergovernmental Panel on Climate Change (Houghton et al., 2001) define Climate Change as:

> *A statistically signifiant variation of the mean state of the climate or of its variability, typically persisting for decades or longer.*

Since climate change encompasses several different areas, including global warming, changes in ocean pH, and air and water quality, an understanding of how each of these components is impacting our ecosystems is vital. The effects are being noticed in both human and wildlife populations, where species interactions are changing in response. With climate change progressing faster than we have previously observed and documented (IPCC Core Writing Team, 2014), there is an urgent need to tackle the climate crisis if we wish to ameliorate damaging environmental consequences (Gilman et al., 2010).

Climate change can be considered anthropogenic (Parratt et al., 2016); it is a consequence of human initiated actions. The shifting of our seasons, observed through changes in weather events, can lead to changing transmission dynamics of infectious diseases. Since wildlife behaviour and physiology can be driven by changes in temperature, global warming will be likely to impact the habitual behaviour of species (Lafferty, 2009). Wildlife hosts and their parasites co-exist in their environments where interactions between the two, under specific environmental conditions, lead to the spread of disease. Climate change can affect the geographic distribution, life-cycle traits and physiology of both hosts and parasites, which can lead to changes in host-parasite relationships (Gallana et al., 2013). Also, climate change can alter the seasonal contacts between population members and hence cause the force of infection to change, which in turn can result to changes in disease dynamics (Silk et al., 2017). There have been theoretical studies, with models showing that seasonal changes, either in host or parasite, can create surges in disease incidence within a population (Fisman, 2007). Considering that climate change can influence both hosts and parasite behaviour, this result is vitally important. Further, empir-

ical studies have shown that warming can increase the virulence of parasites. Paull and Johnson (2011) indicated the negative implications of rising temperatures on a snail host-parasite system, where warming shifted the infection season to match the vulnerable life-stages of the snail host. Avian population behaviour, as changes in response to climate, has also been investigated. There is evidence of both shifting breeding time, and in the timing and duration of migration. In fact, studies have shown that migration may not be completed at all by some species (Ketterson et al., 2015). Such findings provide evidence that ecological systems can be subject to behavioural alterations due to climate change. We also know that different parasites will respond to climate change (global warming) in different ways. For example, an infectious disease such as malaria thrives in warm and damp conditions, and is thus more likely to benefit under current climate change predictions (Lafferty, 2009).

Infectious diseases can impact population dynamics through reducing survival rates and/or fecundity (Dobson and Hudson, 1992; Hudson et al., 1998). If the impact of disease on these rates is sufficiently strong, populations can dramatically change, and this is particularly true in seasonal (heterogeneous) environments (Smith et al., 2008). It has been shown, however, that parasites may actually regulate population abundance (Tompkins and Begon, 1999; Tompkins et al., 2001). Albon et al. (2002) give empirical evidence that, for a reindeer population infected by a parasitic nematode of the intestine, the parasite can regulate population abundance of hosts.

As the behaviour of wildlife populations and parasites change due to our changing climate, an understanding of how these interactions are altering is an important area of study. Mathematical modelling can help us explore how climate change affects host-parasite relationships. We can use mechanistic modelling techniques to understand these complex systems, examining individual components and their connections to each other. The models devised are known as compartmental models, and are used extensively in infectious disease modelling.

§ 1.1 SIR Models

Mathematical modelling of infectious diseases using the susceptible-infected-recovered (SIR) compartmental model framework was first introduced by Kermack and McKendrick (1927), and since its introduction (with formalised work by Dietz (1967)), it has been widely used in the field of mathematical biology modelling. To model a host-parasite relationship using the SIR framework, we formulate a system of ordinary differential equations (ODEs). We have three variables of interest; the population size of susceptible individuals, of infected individuals and of those recovered from disease, and we want to know how these populations change through time, a dynamic variable. Since we assume that time is the only dynamic variable, we are therefore neglecting spatial variations, allowing the formulation of a simple ODE system. We model disease at the population-level, hence the deterministic

framework here uses a *mean-field* approach. This means that we use the assumption that the individual effect of population members on each other can be given by a single approximation (Sharkey, 2008). Our ODE system thus has an equation for each of: S; susceptible individuals, I; those infected, and R; individuals who are recovered (either permanently or temporarily) from the disease. The total population size is given by $N = S + I + R$. Population members move from being susceptible, to infected, to recovered (and back to susceptible if appropriate) according to certain rates. Other demographic processes are considered when formulating a model. We consider the process of new population members being added (births), and individuals leaving the population (deaths). A flow diagram helps to visualise the demographics, and thus prepare a system of ODEs from which we can explore population dynamics of a host-parasite system:

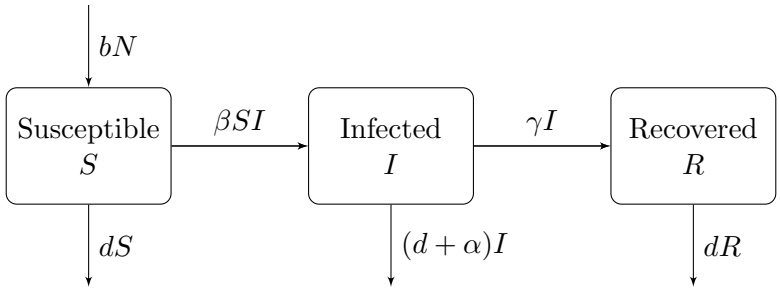

Figure 1.1: Schematic diagram of an SIR compartmental model.

We assert that all newborn population members are susceptible, and these new individuals enter the population at per capita rate b. That is, the offspring of an infected individual is not born with the disease and instead is another susceptible individual. This means that we do not consider our disease to be able to transmit via *vertical* means (i.e. we have no mother-offspring transmission). The absence of vertical transmission is true for many diseases, such as Chronic Wasting Disease in cervids (Miller et al., 2006). More recent studies have found that there is no evidence of vertical transmission for SARS-CoV-2 (Grimminck et al., 2020). The per capita death rate of members is given by the parameter d, and infected members are subject to an increased death rate due to disease; we call this a *virulence* and denote it by α. If recovery is possible, this happens at the per capita rate γ. In this system, transmission occurs upon direct contacts between susceptible and infected population members, with transmission coefficient β. This type of transmission is known as *density-dependent* (Anderson and May, 1981), since it assumes contact rates increase as population sizes increase. Other types of transmission are possible, depending on the system being studied. The most commonly used transmission, aside from the density-dependent transmission described above, is known as *frequency-dependent* transmission. For frequency-dependent direct contact trans-

mission, the likelihood of contracting infection is *independent* of the total population size. We may consider this transmission most appropriate for sexually transmitted infections in human populations, or for vector-borne diseases, for example. There has been debate on how best to model transmission of infectious diseases in wildlife populations (Mccallum et al., 2001), though in this thesis we will only consider density-dependent transmission.

Using the flow diagram, we can write our system of ODEs representing the host-parasite system:

$$\frac{dS}{dt} = bN - \beta SI - dS \tag{1.1}$$

$$\frac{dI}{dt} = \beta SI - (d + \alpha + \gamma)I \tag{1.2}$$

$$\frac{dR}{dt} = \gamma I - dR \tag{1.3}$$

The total population, $N = S + I + R$, is a dynamic variable with

$$\frac{dN}{dt} = (b - d)N - \alpha I.$$

The allowance for N to be dynamic, i.e. population size is not fixed, is important for modelling host-parasite systems where births and deaths are not equal, and when virulence has a significant impact on the population (Hethcote, 1994). The average infectious period is given by $\frac{1}{\Gamma}$, where $\Gamma = d + \alpha + \gamma$; this is the average time that an individual will spend infected, and is an important quantity in the formulation of the *Basic Reproductive Ratio* (see section 1.2).

To solve this system of ordinary differential equations, we set each equation equal to 0 and solve to find steady-state solutions S^*, I^*, R^*. For our system of equations (1.1)-(1.3) we obtain the following solutions:

- an extinction equilibrium, $(S^*, I^*, R^*) = (0, 0, 0)$;
- a disease-free equilibrium, $(S^*, I^*, R^*) = (S, 0, 0)$ (occurring only when $b = d$);
- and an endemic equilibrium,

$$(S^*, I^*, R^*) = \left(\frac{\Gamma}{\beta}, \frac{-d\Gamma(b-d)}{bd\beta + \gamma\beta - d\beta\Gamma}, \frac{-\gamma\Gamma(b-d)}{\beta(bd + \gamma - d\Gamma)}\right).$$

We notice in particular here that the disease-free equilibrium occurs only when the birth and death rates are equal; i.e. $b = d$. Stability of the equilibrium points can be found by considering the Jacobian matrix, and the corresponding eigenvalues, for the equations (1.1)-(1.3). In this system, infection will persist if the extinction and disease-free equilibriums are unstable, and the endemic equilibrium is stable. Computing the Jacobian and corresponding eigenvalues in the extinction state, we

have: $\lambda_1 = b - d$, $\lambda_2 = -d$, and $\lambda_3 = -d - \alpha - \gamma$. Since parameters in the model will be positive, both $\lambda_2 < 0$ and $\lambda_3 < 0$. Therefore for an unstable equilibrium we require $\lambda_1 > 0$, i.e. $d < b$. For the disease-free state, we have eigenvalues: $\lambda_1 = 0$, $\lambda_2 = -d$ and $\lambda_3 = \beta S^* - d - \alpha - \gamma$. Therefore, an unstable equilibrium occurs when $S^* > \frac{d+\alpha+\gamma}{\beta}$. This requirement is related to both the *basic reproductive ratio* and the *threshold for disease outbreak* covered in the next sections.

§ 1.2 The Basic Reproductive Ratio

The *Basic Reproductive Ratio*, R_0, is an important number that can be found from an SIR epidemiological model. It is defined as:

> *The average number of secondary infections arising from the introduction of a single infectious individual in an entirely susceptible population.* (Anderson and May, 1991)

Using the value of R_0 computed, we can determine whether an infectious disease can spread in a naive population (a population who have not previously been exposed to the emerging disease). When $R_0 > 1$, infection will be able to spread through the susceptible population, but if $R_0 < 1$, this will not be possible. Larger values of R_0 indicate that an epidemic outbreak will be harder to control.

Using the definition by Anderson and May (1981), R_0 is computed in the following way:

$$R_0 = (\text{expected number of secondary infections}) \times (\text{infectious period})$$

That is, for the system described in section 1.1,

$$R_0 = \frac{\beta N}{d + \alpha + \gamma} \tag{1.4}$$

since βN gives the number of secondary infections and $\frac{1}{d+\alpha+\gamma}$ indicates amount of time an individual spends in the infected class.

§ 1.3 Thresholds for Disease Outbreak

The threshold level determining whether a disease will occur in a population is a key tool in infectious disease research since diseases cannot spread through a population if a proportion of members exceeds a certain threshold level (Potapov et al., 2012). Thresholds can only be calculated using data available; it can be difficult to obtain sufficient empirical data for their formulation (Deredec and Courchamp, 2003). Therefore, empirically derived thresholds may be miscalculated due to complex host-parasite structure, missing data or inaccuracies (Lloyd-Smith et al., 2005). Hence, theoretically derived thresholds are important.

The growth of infection in a population depends on the rate of change of infected population members through time. Using the framework of Kermack and McKendrick (1927), infections will rise when

$$\frac{dI}{dt} > 0. \tag{1.5}$$

For the basic model, as defined in section 1.1, we can see that this condition is equivalent to the following:

$$\begin{aligned} \frac{dI}{dt} = \beta SI - (d+\alpha+\gamma)I &> 0 \\ \beta SI &> (d+\alpha+\gamma)I \\ S &> \frac{d+\alpha+\gamma}{\beta} \\ \frac{S}{N} &> \frac{1}{R_0}. \end{aligned}$$

Thus, infection will break-out when the number of susceptible population members is sufficiently high; the proportion of these individuals in the whole population must be greater than the inverse of the basic reproductive ratio. We call this the *threshold* for disease outbreak (Keeling and Rohani, 2008).

This threshold is related to R_e, the *Effective Reproduction Number*. The basic reproduction number R_0 was computed assuming an entirely disease-free population, however in established host-parasite systems, it is likely that disease will already exist in the population. The effective reproduction number gives an expression for the average number of new infections occurring at time t, from an infected population member, in an environment where infection already exists in the population. To compute R_e, the basic reproductive ratio is multiplied by the current proportion of susceptible population members. That is:

$$R_e = \frac{S}{N} R_0. \tag{1.6}$$

Rearranging the equation for the threshold, we find the relationship to R_e. That is, we find that disease incidence will increase when

$$\begin{aligned} \frac{S}{N} R_0 &> 1 \\ \text{i.e.} \qquad R_e &> 1. \end{aligned}$$

Therefore, we have determined that infection will continue to persist in the population if $R_e > 1$. We can see that this is in line with the condition for emerging disease growth in a naive population, since we have $R_0 > 1$ leading to infection spreading.

In the seasonal models presented in this thesis, the threshold is an important concept and tool for analysing the behaviour of our systems and will be used to help explain the behaviours we observe.

§ 1.4 Other Compartmental Disease Models

In Anderson and May (1979) and Anderson and May (1981), variations of the classic SIR compartmental disease model are defined, analysed and discussed. These models form the frameworks exhibited in theoretical modelling to date. In this section we introduce the two types of models we will use in later sections of this thesis, and additionally introduce a model that has been popularly used in infectious disease modelling.

1.4.1 $SIR - D$ Model

We now introduce the model that will form the framework of the model used in Chapter 3. The model is described by the term $SIR - D$, or susceptible-infected-recovered-decaying, and is based on Model G from Anderson and May (1981). The decaying class represents an environmental reservoir of disease, which Anderson and May (1981) coined in their model as a *free-living* parasite stage. We define an additional transmission pathway, whereby susceptible hosts can contract disease through direct contacts with an environmental reservoir of infectious material. The material within this class originates from the death of infected population members, and from living infectious material expelled by infected individuals. We maintain the assumption that disease can transmit directly from infected to susceptible members via the transmission term βSI, which is in contrast to Anderson and May (1981) who assume only free-living infection transmission of disease. A schematic diagram helps to view the transitions between compartments in this model:

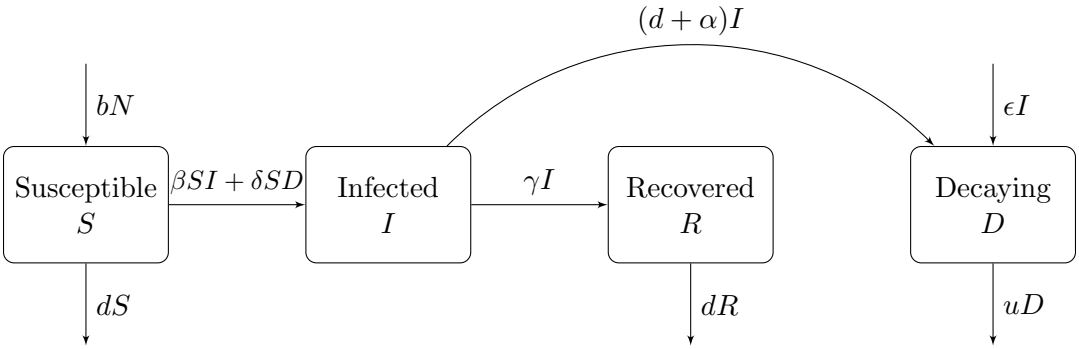

Figure 1.2: Schematic diagram of an SIR-D compartmental model.

The system of ordinary differential equations representing the population and

disease dynamics for this model is then:

$$\frac{dS}{dt} = bN - \beta SI - dS - \delta SD \tag{1.7}$$

$$\frac{dI}{dt} = \beta SI + \delta SD - (d + \alpha + \gamma)I \tag{1.8}$$

$$\frac{dR}{dt} = \gamma I - dR \tag{1.9}$$

$$\frac{dD}{dt} = (d + \alpha)I + \epsilon I - uD \tag{1.10}$$

where parameters are as described in section 1.1, with some additions. The transmission coefficient of decaying matter to susceptible individuals is given by δ; ϵ is a shedding rate of infectious material from living infected members that reaches the decay pool; and u is the per capita rate at which decaying material ceases to be infectious.

It is worth noting here that it is possible to obtain a stable limit cycle as a solution to this model; i.e. population abundances can oscillate without an external force added. Anderson and May (1981) note that this is most likely to occur in their model (the model above, without the direct transmission βSI) for systems where infectious material exists for a long time (u small), and where the infectious disease is highly pathogenic (high α). In the model described by equations (1.7)-(1.10) presented here, we found existence of stable limit cycles through numerical simulations, and this is explored further in chapter 3.

1.4.2 SIR with Constraints

For many populations, it is possible that the density of hosts will impact their relationship with parasites. For example, an increased density of hosts could lead to competition for resources such as space, and food, which could ultimately lead to an increased death-rate in the population, or a reduction in host fecundity, for example. In this situation, we may need to incorporate additional density-dependent constraints into our SIR model to account for such effects. If the density-dependence acts on the population death rate, it does so in a manner that is linearly proportional to the total population size, N, as described by Model F in Anderson and May (1981). For a density-dependent factor given by the parameter q, the natural death rate d changes to the form $d + qN$. The system of differential equations for the SIR model as in 1.1 then becomes:

$$\frac{dS}{dt} = bN - \beta SI - (d + qN)S \tag{1.11}$$

$$\frac{dI}{dt} = \beta SI - (d + qN + \alpha + \gamma)I \tag{1.12}$$

$$\frac{dR}{dt} = \gamma I - (d + qN)R \tag{1.13}$$

For the models formulated in chapters 2, 3 and 4, we will consider density-dependence in the host death rate.

1.4.3 $SEIR$ Model

One of the most widely applied compartmental disease models is that of an $SEIR$ form, where this stands for susceptible-exposed-infectious-recovered. Though not used in this thesis, the extensive studies of the $SEIR$ model framework have produced some key results for the field of infectious disease modelling (to be noted later), and so we feel it appropriate to include a brief description of such a model here. This type of compartmental disease model is used when there is a latent period of infection from the disease, i.e. an individual becomes infected (exposed), but is not yet infectious. There is a time-lag between contracting disease, and being able to pass the disease on. An example system of ordinary differential equations for this type of model is:

$$\frac{dS}{dt} = bN - \beta SI - dS \tag{1.14}$$

$$\frac{dE}{dt} = \beta SI - (d+v)E \tag{1.15}$$

$$\frac{dI}{dt} = vE - (d+\alpha+\gamma)I \tag{1.16}$$

$$\frac{dR}{dt} = \gamma I - dR \tag{1.17}$$

where parameters are as described in section 1.1, and v is the constant rate at which exposed members become infectious.

§ 1.5 Seasonality in SIR Models of Wildlife Systems

Seasonality can be considered as the driving force of disease incidence and epidemics in host-parasite systems (Schwartz, 1985), since both host and pathogen behaviour can alter throughout the course of a season. For example it is common for wildlife hosts to have a defined breeding season (Rowan, 1938), for species to exhibit seasonal social patterns, and for pathogens to be more prevalent at certain time-points during the year (Lafferty, 2009). Empirical evidence showing that changes in social contacts within a population, hence driving seasonality in disease transmission, is mounting (Silk et al., 2017) and there is increasing evidence that wildlife populations with seasonal social behaviour can cause seasonal disease transmission (Duke-Sylvester et al., 2011). To fully understand host-parasite relationships, therefore, it is of great importance to acknowledge and understand the impact of seasonality (Altizer et al., 2006), and accept that seasonal forcing is ever-changing with the increasing rate of climate-change (Walther et al., 2002).

Seasonality is incorporated into SIR models as an external periodic force. Classically, modelling efforts for wildlife populations have incorporated only one external forcing; usually either in the species birth rate, or the transmission. In this thesis our models will consider more than one seasonal component and their impact on host-parasite dynamics. With incorporation of seasonal forcing, theoretical studies thus far have shown that any pattern of recurrent epidemics, from annual dynamics to chaos, are possible (Stone et al., 2007). The precise configuration of external forcing, i.e. which parts of a system experience seasonality, is important in determining output dynamics. With multiple seasonal forcing functions, interactions between the different functions can lead to changes in the system (Greenman and Pasour, 2011).

The standard SIR model (section 1.1), with seasonality in transmission (or contact rate), can have multiple stable solutions of varying cycle lengths (Dietz, 1976; Smith, 1983). Inclusion of a seasonal birth rate into an SIR disease model can also decrease the stability of the system; this is partly due to the time-delay induced by such seasonality (May, 1974; White et al., 1996). The reduction in stability in both cases can in turn lead to highly complex dynamics (May, 1976). In general, deterministic SIR models possess a stable fixed point, but the addition of seasonal forcing can lead to series of period-doubling bifurcations (Keeling et al., 2001). In an $SEIR$ model (section 1.4.3), for example, seasonality in birth rate, where birth rate is given by a pulse, has been shown to be destabilising. Depending on initial conditions, the induced dynamics can become highly complex (White et al., 1996). With periodic contact rate (transmission) in the standard $SEIR$ model, the initial population conditions are important for determining the occurrence of disease outbreaks. Multiple stable solutions exist, where small changes can change the period of epidemics. The seasonality is the driving force of disease incidence (Schwartz, 1985). The magnitude and timing of seasonal forcing has been shown to play a role in driving disease dynamics in a system (Schwartz, 1985; Keeling et al., 2001; Begon et al., 2009). It can also be noted that, with multiple forcing functions acting on a host-parasite model, dynamics are sensitive to the relative timings and amplitude of both of the seasonal components (Greenman and Pasour, 2011).

In addition to natural seasonal forcing, such as birth and contact rates, it is possible that human-mediated forcing could impact a host-parasite system. For example seasonality can come in the form of human intervention practices (Greenman and Norman, 2007), a means of controlling the size of a population with the aim of limiting disease spread or attaining management targets. Unlike natural forcing mechanisms from birth or transmission rates, anthropogenic forcing can be manipulated to achieve desired results, and thus has the potential to control the dynamics of a system.

Including a seasonally varying process, or multiple seasonal components, in an SIR model increases the complexity of analysis. Simulation-based approaches to analysis provide an opportunity to explore a wide-range of parameter values. Nu-

merical simulations can show how the addition of seasonality impacts the population dynamics, persistence of disease and the stability of the host-parasite system being studied. Therefore, such approaches are very useful in monitoring the changing relationships between wildlife populations and infectious diseases, and can help inform management strategies for infectious disease control. Previous studies have used numerical simulation methods to explore seasonality in host-parasite disease systems (Dorélien et al., 2013; Peel et al., 2014; Maji et al., 2018). Bifurcation analyses with numerical continuation software (He and Earn, 2007; Best, 2013; Taylor, 2014) have also been explored, and these are often used in tandem with numerical simulations. In addition, studies such as those in Hosseini et al. (2004) and Swinton et al. (1998) were able to compare their theory with empirical data to show consistency between theoretical modelling and real-world data. It is possible to conduct algebraic analysis, but only in more simple systems where linearisation of the system is possible (Greenman and Pasour, 2011).

§ 1.6 Disease Control and Management Strategies

With the increasing emergence of highly infectious diseases, modelling different management strategies to determine appropriate controls is becoming ever-more important. Population management of wildlife can be incorporated into SIR models in several different ways. The strategy which needs to be implemented in a system to control or eradicate disease depends on different factors, for example we might need to consider:

- if the disease is fatal;
- if vaccinations are available;
- if harvest can be targeted at only those infected, and
- what results we want to obtain from the management.

When determining an appropriate management strategy, the desired outcome is an important factor in the decision making process. It may be that the harvest strategy needs to maximise yield, for example if the wildlife population is harvested for meat, fur or skin. Traditionally referred to in fisheries management processes, and without consideration of disease, the concepts of Maximum Sustainable Yield (MSY) and Maximum Annual Yield (MAY) are theoretical concepts giving values for the highest numbers of fish that can be taken from a population, without such population being driven to local extinction (Maunder, 2008; Tsikliras and Froese, 2019). The concepts of MSY and MAY can be used for management considerations of other wildlife populations since its goals, described above as maximising yield whilst maintaining population numbers, can be generalised to suit other populations such as wild herds of reindeer.

Due to the cost of implementing management strategies, it is important that quantitative results from modelling infectious diseases with management are accurate, and hence it is crucial to have an appropriate model for the system being studied. Some of the types of management strategies that can be used are highlighted in the following sections.

1.6.1 Mass Vaccination

Mass vaccination strategies are most commonly used to help control human infectious diseases, such as smallpox, measles and meningitis, and involve administering vaccines to large populations in a short time interval. The goal of such vaccination programmes is often to develop herd-immunity, a strategy that means an appropriate proportion of the population is immunised giving protection to those not immune and helping to prevent disease outbreaks. The basic reproductive ratio of a disease helps to determine the proportion of the population that is required to be immunised to prevent epidemics. This herd-immunity threshold, denoted by HT is:

$$HT = 1 - \frac{1}{R_0} \tag{1.18}$$

For example, for a disease with a high R_0 such as measles where estimates have shown the basic reproductive rate to be as high as $R_0 = 18$ (Guerra et al., 2017), we require $HT = 1 - 1/18 = 0.94$ or 94% of the population to be immunised to prevent further disease spread. However, for a disease with a smaller R_0 such as Ebola with estimates around $R_0 = 2$ (Camacho et al., 2014; Khan et al., 2015), only 50% of the population ($HT = 1 - 1/2 = 0.5$) are required to be immune to stop epidemics. Mass vaccinations can also be routinely performed, i.e. they can be carried out annually at the same time as a measure to control seasonal outbreaks of disease such as influenza.

1.6.2 Contact Tracing and Isolation

Contact tracing is an effective means of controlling infectious diseases. An individual known to be infected traces all of their recent contacts, and these individuals can then be tested and treated for the disease if required. Using isolation as a method to prevent further spread by those contacts is also an effective solution which goes hand-in-hand with contact tracing. We may typically think of these methods for the control of sexually transmitted infections, but more recently we have seen this method used for the SARS epidemic (Donnelly et al., 2003a) and the 2020 coronavirus outbreak (Kucharski et al., 2020). Again, this method is most appropriate for human diseases, and is particularly successful when cases of infection are low (Eames and Keeling, 2003). Contact tracing is not likely to be an effective means of infectious disease control in free-ranging wildlife populations, such as the ones considered when formulating the models in this thesis. This is because contact tracing

relies on known contact structure within the population being studied, whereas our models assume random interactions between population members.

To demonstrate how contact tracing can be incorporated into an SIR model, we show a framework based on the method used by Eames and Keeling (2003). A new class is implemented to consider traced (or isolated) individuals, T. The $SITR$ model could be described by the following set of ordinary differential equations:

$$\frac{dS}{dt} = -\beta SI \tag{1.19}$$

$$\frac{dI}{dt} = \beta SI - \gamma I - cIT \tag{1.20}$$

$$\frac{dT}{dt} = cIT - aT \tag{1.21}$$

$$\frac{dR}{dt} = \gamma I + aT \tag{1.22}$$

Individuals in the treatment class are there for only a short time, to represent the speed at which tracing can be implemented. Treated individuals cannot spread infection further, for example due to their isolation, or their decision to avoid further contacts. In this model, β is the contact rate of susceptible and infected individuals, γ the per capita recovery rate in the absence of tracing, a is the length of time in the traced class, and c is the contact tracing rate. This is a simple example of how contact tracing may be incorporated in the model.

1.6.3 Constant Catch and Constant Effort

Constant catches and constant efforts are typically associated with fisheries management, and have previously been studied in conjunction with the concept of Maximum Sustainable Yield (MSY) (Azar et al., 1994; Duarte, 1994; Azar et al., 1996).

The constant catch process involves the removal of individuals in a population using the same abundance each time harvest is performed, e.g. per day, 20 fish are removed from a lake. This strategy is most suited to a population where such constant removal will not lead to the depletion of the population to a level which would not allow the constant catch to be sustained. Constant effort is performed in relation to the existing population abundance, where a proportion of individuals are removed continuously at a certain rate.

Suppose we model the population dynamics of our species by the following equation:

$$dF = (b - d)F - H(F) \tag{1.23}$$

where b represents a birth rate, d a death rate, and $H(F)$ gives the function for the harvest strategy. Then, a constant catch harvest would be given by a constant function, e.g. $H(F) = c$, whilst a constant effort harvest would involve the population, e.g. $H(F) = cF$, where $c \in \mathbb{R}$. The more effective method of these two strategies is system dependent (Azar et al., 1996).

This method can be applied to a host-parasite system using an SIR model, where we can choose to harvest any combination of the population members, depending on the system being studied. Supposing it is not possible to distinguish susceptible, from infected, or recovered individuals, we would need to apply the harvest function to all three compartments of the disease model. Then, our system of equations would look something like the following:

$$\frac{dS}{dt} = bN - \beta SI - dS - cS \tag{1.24}$$

$$\frac{dI}{dt} = \beta SI - (d + \alpha + \gamma)I - cI \tag{1.25}$$

$$\frac{dR}{dt} = \gamma I - dR - cR \tag{1.26}$$

where $c \in \mathbb{R}$ represents the proportion of each population class harvested as a constant effort.

1.6.4 Seasonal Harvest

Wildlife populations are frequently managed in short harvest seasons, performed at a specific time with the aim of achieving a maximised yield whilst maintaining a sustainable population (Choisy and Rohani, 2006). Seasonal harvesting can follow constant-catch, or constant-effort frameworks, where the harvest takes an "on/off"approach, being performed only for a short time-frame rather than continuously through a season.

For example, if a harvest function is represented by the term H, a seasonal harvest could be given by the piecewise continuous function:

$$H = \begin{cases} c & \text{if } \ n + s < t \leq n + r, \\ 0 & \text{otherwise.} \end{cases} \tag{1.27}$$

Here, $c \in \mathbb{R}$ is the harvest rate, $n \in \mathbb{Z}$ is the year of harvest, and $s, r \in \mathbb{R}$ with $0 < s < r < 1$ and $r - s$ the length of the harvest season. To apply this is an SIR framework, with H as defined by the piecewise function above, we can write the system of equations as:

$$\frac{dS}{dt} = bN - \beta SI - dS - HS \tag{1.28}$$

$$\frac{dI}{dt} = \beta SI - (d + \alpha + \gamma)I - HI \tag{1.29}$$

$$\frac{dR}{dt} = \gamma I - dR - HR. \tag{1.30}$$

With this framework c is the harvest rate of the population during the defined season, representing the constant effort style management.

§ 1.7 Methodology

1.7.1 ODE15S

For the numerical simulations in this thesis, Matlab (*MATLAB version R2018a*) software is used and the *ode15s* solver implemented in order to solve our systems of ordinary differential equations. This *stiff* ODE solver is used as it increases the efficiency of our numerical simulations over a non-stiff solver such as the widely used *ode45* solver. The ode15s solver uses a multistep process and uses a quasi-constant step size (it is a variable order and variable step solver) (Shampine and Reichelt, 1997) to solve our system of ordinary differential equations numerically. It is better able to cope with the rapidly changing solutions from our system of differential equations that describe disease dynamics. An example (dummy) code using the *ode15s* solver for an SIR system is shown in figure 1.3.

We choose to analyse our system via numerical simulation methods since our model is highly complex. This allows us to explore a wide range of parameter combinations, detailing the possible outcome of population and disease dynamics for different host-parasite scenarios.

1.7.2 Bifurcation Diagrams

A *bifurcation diagram* shows qualitative and quantitative changes in model dynamics as one model parameter is varied. Figure 1.4 shows an example of the type of bifurcation diagram used throughout this thesis. Across the x-axis of our bifurcation diagram (bottom panel in figure 1.4) we vary a control parameter, in this case β_2, and the y-axis reads the corresponding level of infection in the population (proportion infected; on a log-scale) for the specific value of β_2. The number of points corresponding to any one x value at any one time indicates how often the disease dynamics re-occur, i.e. one point above an x value translates to annual dynamics, two points a biennial cycle, and so forth. The dynamics are sampled at the same time-point each year, and the corresponding plotted points/branches show those values. The top two figures in 1.4 show the proportion of infected population members in time-series data, for two different values of β_2. We show where these correspond to the bifurcation via the vertical lines overlaying the bifurcation diagram.

We compute our bifurcation diagrams using code written in Matlab (*MATLAB version R2018a*). Our code is adapted for our specific models using the available program files in Keeling and Rohani (2008), accessible from Chapter 5: Program 5.2 at the following webpage:

- https://homepages.warwick.ac.uk/ masfz/ModelingInfectiousDiseases/index.html

We begin by defining the fixed model parameters, and define a vector of values for the bifurcation parameter of interest. For example, if we want to vary β_2 between 0 and 1, we may specify $\beta_2 = [0 : 0.001 : 1]$, so that 1000 different values of β_2 are

```
% Calling the differential equations
function [t,S,I,R] = SIR11(beta,gamma,b,d,S0,I0,MaxTime)

% Set up default parameters and initial conditions
   beta=1;
   gamma=1;
   b=2;
   d=1;
   S0=90;
   I0=10;
   MaxTime=500;

S=S0; I=I0; R=1-S-I;

% The main iteration
[t, pop]=ode15s(@SIR1,[0 MaxTime],[S I R],options,[beta gamma b]);

S=pop(:,1); I=pop(:,2); R=pop(:,3);

% Plots the population dynamics
subplot(3,1,1)
plot(t,S,'g');
xlabel 'Time';
ylabel 'Susceptible'

subplot(3,1,2)
plot(t,I,'r');
xlabel 'Time';
ylabel 'Infectious'

subplot(3,1,3)
plot(t,R,'b');
xlabel 'Time';
ylabel 'Recovered'

% System of differential equations
function dPop=SIR1(t,pop,parameter)

beta=parameter(1); gamma=parameter(2); b=parameter(3); d=parameter(4);
S=pop(1); I=pop(2); R=pop(3);

dPop=zeros(3,1);

dPop(1)= b - beta*S*I - d*S;
dPop(2)= beta*S*I - gamma*I - d*I;
dPop(3)= gamma*I - d*R;
```

Figure 1.3: Example code using *ode15s* to solve an SIR model.

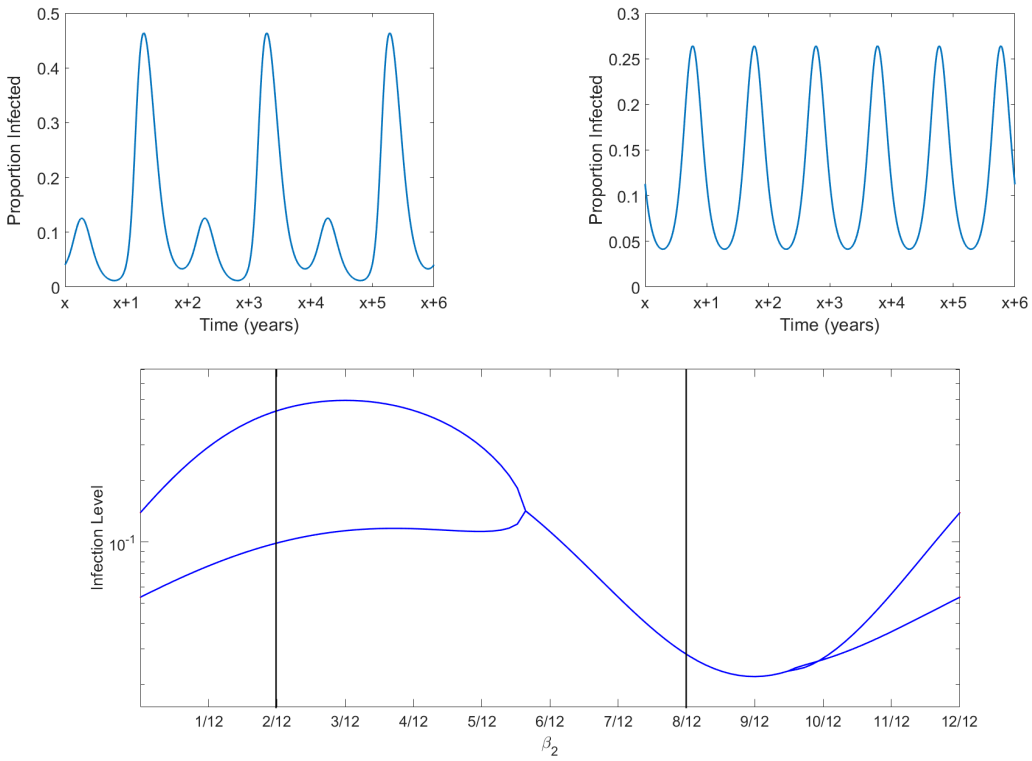

Figure 1.4: An example bifurcation diagram showing changing dynamics as the control parameter β_2 is varied, with time-series plots above to highlight the corresponding patterns shown by the bifurcation.

used in computing the bifurcation diagram. As standard, we use 1000 values of each bifurcation parameter of interest in this thesis. Additionally at this stage, we define a maximum run time $t \in \mathbb{Z}$ (years) for which the iterative process will run, and specify initial population conditions. The maximum time used is 500 years in all bifurcations following, unless otherwise stated, and initial population conditions are defined in the relevant sections. We use a *for* loop to run through each value of the control parameter, and implement the *ode15s* solver (see above) for each such value. Unless otherwise stated for all bifurcations, following the completion of one simulation cycle for a control parameter the bifurcation code uses *extrapolated* initial conditions to continue the bifurcation for the next parameter value. This means that the number of population members at the end of one simulation is used to start the next, and therefore initial conditions are continuously changing throughout the bifurcation process. Then, the code uses the *interp1* function to perform a linear interpolation between the time-sampled points t and the corresponding infection abundance (obtained from the ode15s output) for the final 10 years of simulations ($[t-9:t]$). Finally, we use the *semilogy* function to plot the bifurcation parameter values on the x-axis, and the associated log-scaled interpolated infection abundances on the y-axis. The code in figure 1.5 gives an example (dummy) code for this process.

We recognise that this definition/use of the term *Bifurcation Diagram* may not be familiar to the reader. We have used this definition as it is used by Keeling and Rohani (2008) to consider seasonally-forced systems where the forcing has a one-year period. Due to the use of annually forced seasonal parameters throughout this thesis, we are therefore largely interested in the qualitative patterns, and consequently take the approach described above where we sample one time-point per year, almost as in a discrete-time system.

1.7.3 Pie Diagrams

Throughout the thesis, pie diagrams are used to explore different combinations of parameter values and initial conditions when solving our systems of differential equations (see example figure 1.6). Using nested *for* loops in Matlab (*MATLAB version R2018a*), different combinations of parameter pairings were inputted into the ode15s solver, along with a vector of initial population conditions. For every combination of parameter values and initial conditions, the MATLAB code implemented the ode15s solver, recorded the period of the cycle of epidemics, and created pie charts for each pair of parameters with coloured sections to indicate the different cycle lengths observed for such pairings, dependent on the initial conditions. The simulations were run for a minimum of 500 years and solutions were tested to determine if the periodic solution had a length of $1-10$ years, or if it exceeded 10 years in length. The initial conditions tested in simulations are uniquely defined in each relevant figure. In order to test the period of epidemics, we recorded the maximum total population abundance observed over the course of one year, and repeated this for the 100 years preceding the maximum simulation length. We then compared the

```
% Bifurcation

% Set up default parameters
a=1;
b=2;
c=3;

% Set up initial conditions
S=90;
I=10;
R=0;
IC=[S,I,R];

% Set up bifurcation parameter
d=[0:0.001:1];

% Time conditions
MaxTime=500;

% Main iteration
for loop=1:length(d)
PAR=d(loop);
[t, pop]=ode15s(model,[0:MaxTime],IC,[a b c PAR]);
IC=[pop(end,1) pop(end,2) pop(end,3)];
Bif(loop,1:10)=interp1(t,pop(:,2),MaxTime-[0:9]);
semilogy(d(1:loop),Bif(1:loop,:));
set(gca,'XLim',[min(d) max(d)]);
end
```

Figure 1.5: Example Matlab code for drawing bifurcation diagrams.

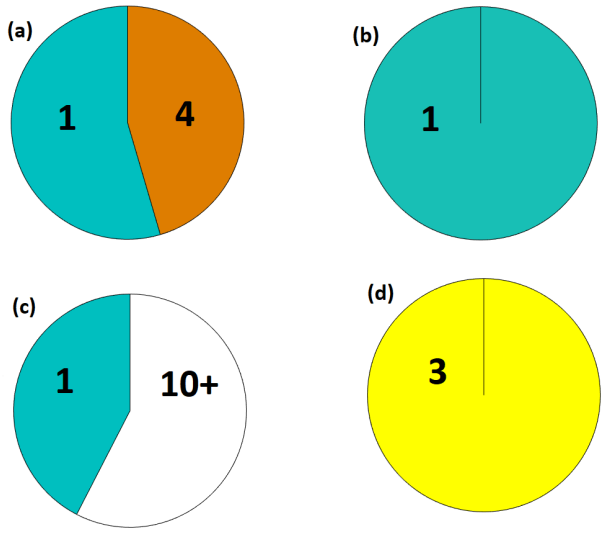

Figure 1.6: An example of pie charts displayed throughout the thesis. In (a) resulting dynamics for a particular pair of parameters are either annual, or repeating every four years. In (b) dynamics are always annual. In (c) we either have annual dynamics or dynamics repeating every 10 years or more, and in (d) dynamics repeat every three years for all initial conditions explored.

maximum abundance recorded in the first year (i.e. maximum time - 100), with the second year, and determined the percentage difference. In order to be classed as equivalent, the percentage error between values needed to be less than 2%. For example, if the difference between the maximum in year 1, and the maximum in year 2 was $> 2\%$, but the difference between years 1 and 3 was less than 2%, we recorded an epidemic cycle of length 2.

1.7.4 Fourier Spectra

Fourier spectra allow us to determine the dominant period of epidemics resulting from model simulations and will be shown throughout this thesis. To compute Fourier spectra, we used the Matlab (*MATLAB version R2018a*) function *fft*; a command which calculates the discrete Fourier transform of the resulting population dynamics, by using a fast Fourier transform algorithm. The aim of the computation is to find the frequency of the possible population dynamic cycles, where these cycles are buried in noisy data. The computation does not tell us the specific cycle length, but does indicate the dominant periods present for the model using certain parameter combinations. For the computation of Fourier spectra in this thesis, the Matlab code first creates a data set for the spectra, and in our case this is information about total population size through time. We run the code for 500 years in the first

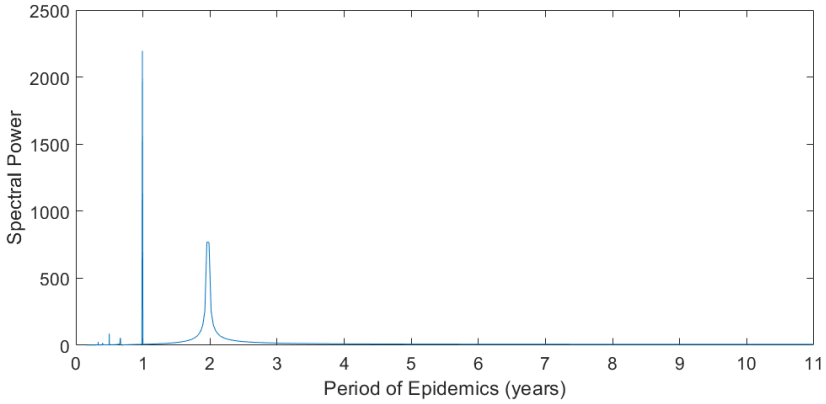

Figure 1.7: An example Fourier spectra indicating the dominant periodic cycles in a dynamic system. The underlying epidemic periods are either annual or biennial.

instance to remove transient dynamics, and then run the simulations for a further 1000 years, taking 12 equally-spaced samples per year for creation of the signal. Our code applies the Fourier transform, extracts the powers of frequencies and takes the inverse of these to obtain epidemic periods. An example Fourier spectra can be seen in figure 1.7. This plot shows an example of a Fourier spectra for a host-parasite system where dynamics are either dominated by annual or biennial underlying dynamics.

§ 1.8 Thesis Outline

In this thesis we explore the impact of multiple seasonal components acting on a host-parasite system, focussing on seasonality in birth rates and transmission. We consider host-parasite systems where disease can spread in different ways, and consider the effects of harvesting strategies on such systems.

In Chapter Two an SIR model with two seasonal components, one in birth and one in transmission, is formulated. We consider both a system where recovery from disease is not possible, and one where hosts can fully recover and gain lifelong immunity. In particular we explore the timing of the seasonal components, and how dynamics can change depending on the relative timing of the seasonal birth and the seasonal transmission.

In Chapter Three an additional transmission pathway is considered. Transmission is possible via direct contact, as in Chapter Two, and also available via an environmental reservoir of free-living infectious material. We formulate a model to incorporate both seasonality in birth and transmission, alongside an additional compartment to represent environmental transmission of disease. We explore how changing the seasonality impacts population and disease dynamics, and highlight the bi-stability of the system. We pay attention to how alternative initial conditions can affect dynamics and also how changing other parameters changes the system behaviour.

In Chapter Four seasonal harvesting strategies are introduced, and we incorporate these into the models from Chapter Two and Chapter Three. We specifically explore how the timing of harvesting a population is crucial in determining the disease cycle, and how small changes in harvest rate can alter dynamics dramatically, indicating bi-stability in the system. We note how increasing harvest rates can actually increase population numbers (a phenomenon we can link to a principle known as the "Healthy Herd Hypothesis"), and find harvest strategies that can maximise susceptible populations whilst minimising infection.

Chapter 2

How seasonal variations in birth and transmission rates impact population dynamics in a basic SIR model

§ 2.1 Introduction

Climate change, encompassing global warming, changes in ocean pH, air and water quality, humidity and precipitation patterns, is likely to exacerbate the current intricacy of relationships between hosts, parasites and transmission vectors (Altizer et al., 2013). Though not all host-parasite relationships will respond to warming in the same way, due to differences in range and location (also known as *climate envelope*), changes to the timings of our seasons as a result of global warming will impact the dynamics of populations and diseases (Sutherst, 2001; Kutz et al., 2005; McCarthy et al., 2001; Parmesan, 2006). We expect biological organisms to respond to changing environments, in particular by altering the timing of seasonally-dependent demographic processes. Two such time-varying processes are the species breeding schedule, and the timing of social gatherings.

Infectious diseases are ubiquitous in the natural world, and seasonality is well recognised as pivotal in determining disease dynamics (Soper, 1929). Understanding how infectious diseases can impact a host population is an important area of study as we endeavour to ensure species thrive in their natural environments, aiming to avoid population decline or indeed extinction. The dynamics of infectious diseases in wildlife populations is a well-studied area both in theory and in practice. Numerous studies have incorporated a form of seasonality into models of wildlife diseases, either in host birth rate (Roberts and Kao, 1998; White et al., 1999; Smith et al., 2008; Peel et al., 2014; Ferris and Best, 2018) or the transmission parameter.

The most common functional form for transmission seasonality is a sinusoidal

function. These have been incorporated into host macro-parasite models (White et al., 1996; Taylor et al., 2015) and host micro-parasite models (Ireland et al., 2004, 2007; Best, 2013). There are several reasons we might see a seasonal transmission rate in host-parasite relationships. For example, parasite abundance could be impacted by seasonal factors such as temperature and rainfall (Pascual and Dobson, 2005), or the host species could exhibit seasonal changes in immunity (Altizer et al., 2004; Laakkonen et al., 1999). In many natural populations, seasonal social behaviour will drive fluctuating transmission rates. For example, avian species exhibit seasonal behaviour in their migrations (Helm et al., 2006), and deer species in gathering for the breeding season (Lincoln, 1992).

Seasonality is likely to affect more than one trait in host-parasite relationships (Cable et al., 2017) since it is common for wildlife populations to exhibit separate breeding and social seasons (e.g. group migration), where the latter implies increased transmission rates due to elevated density of hosts in one area. Theoretical work on host-parasite dynamics using an SIR-type framework with one seasonal component is common, but very few studies with more than one seasonal element exist. We are aware of three such studies for wildlife systems (Swinton et al., 1998; Hosseini et al., 2004; Greenman and Pasour, 2011). We note here that multiple seasonal components have been considered in other frameworks, such as disease models for human populations (Dorélien et al., 2013) and predator-prey models in wildlife (Rinaldi and Muratori, 1993). Multiple seasonal components in an SIR model have shown different outcomes depending on the relative timing of seasonality. For harbour seals studied in Swinton et al. (1998), the seasonal processes of birth and transmission occur simultaneously, leading to a large annual fluctuation. On the other hand in Hosseini et al. (2004) where births and transmission are not synchronous, the seasonal components can each cause their own infection peak, resulting in a so-called *multi-annual* cycle. Greenman and Pasour (2011) further showed that two seasonal components, when out of phase, could lead to chaos in population dynamics. Given that many wildlife populations exhibit seasonal behaviours in both birth and aggregation (Altizer et al., 2006), we feel that both seasonal components should be incorporated into host-parasite predictive models.

In this work we explore how a seasonal host birth rate and a seasonal transmission parameter drive population and disease dynamics in a host-parasite system, and investigate how changes to the timing and amplitude of these processes alter dynamics. We introduce the model in 2.2, formulating the basic reproductive rate R_0 and the threshold for disease persistence. In 2.3.1 we explore the model dynamics in the absence of seasonality, and with only one seasonal component present before introducing both seasonal terms simultaneously. In 2.3.2 we investigate how changing the timing of birth and transmission impacts the population. By varying disease parameters in 2.3.3 we show how complex cycles can emerge, and then in 2.3.4 we show how recovery can stabilise dynamics. Finally in 2.4 we conclude our findings and discuss the results.

§ 2.2 The Model

Our model is based on those developed by Anderson and May (1981), with adaptations to consider both seasonal birth and transmission rates. The population dynamics of a host-parasite system are henceforth described by the following equations:

$$\frac{dS}{dt} = b(t)N - \beta(t)SI - (d + qN)S \tag{2.1}$$

$$\frac{dI}{dt} = \beta(t)SI - (\gamma + d + qN + \alpha)I \tag{2.2}$$

$$\frac{dR}{dt} = \gamma I - (d + qN)R \tag{2.3}$$

In this system, d represents the per capita natural death rate of individuals, α a disease-induced death rate (or virulence) and individuals are assumed to recover at per capita rate γ. The parameter q represents a density-dependent factor in the death rate, since it is assumed that increased competition between host population members will increase fatality, and the total population size is given by $N = S+I+R$.

Since we are concerned with the impact of a changing climate on the timing of our seasons we include time-dependent parameters in the model. It is assumed that when population members gather in groups, this results in an increased disease transmission (i.e. transmission is density-dependent), and that this can fluctuate throughout the course of a season depending on the social calendar of the species. We define $\beta(t) = \beta_0(1+\beta_1\cos(2\pi(t+\beta_2)))$ to be the varying transmission, where β_0 is the baseline transmission, β_1 the amplitude of seasonality and β_2 the timing of the transmission peak (i.e. the time of peak socialising). Similarly, the birth rate $b(t)$ is seasonal to represent a population with a particular breeding season. We define $b(t) = b_0(1 + b_1\cos(2\pi(t + b_2)))$, with b_0 the baseline birth rate, b_1 the amplitude of seasonality and b_2 the timing of the birth peak.

For the numerical simulations, Matlab (*MATLAB version R2018a*) software is used and the *ode15s* solver implemented (see section 1.7.1). We first consider a wildlife population with average lifespan of 1 year ($d = 1$), an average offspring per individual of 2 per year ($b_0 = 2$), and a disease from which it is not possible to recover ($\gamma = 0$). Infected individuals are subject to an increased per capita death rate due to disease virulence, and we define $\alpha = 7$. This means that the virulence of our disease decreases the lifespan of infected hosts to approximately 1.5 months, since the per capita death rate of infected members becomes $d + \alpha = 8$. The baseline transmission of the disease is assumed to be $\beta_0 = 1$. We assume first that neither birth or transmission are seasonal and hence set $b_1 = b_2 = \beta_1 = \beta_2 = 0$. When the seasonality is introduced, the default parameter set is as described by table 2.1. Using initial conditions with no seasonality included, dynamics settle to

Table 2.1: Initial parameter values used for double-seasonality model simulations. *initial population conditions unless otherwise stated.

Parameter	Description	Baseline
b_0	baseline birth rate	2
b_1	amplitude of birth	0.9
b_2	timing of birth peak	$\frac{1}{12}$
β_0	baseline transmission rate	1
β_1	amplitude of transmission	0.9
β_2	timing of transmission peak	$\frac{7}{12}$
d	natural death rate	1
α	disease-induced mortality	7
γ	recovery rate	0
q	density-dependent control	0.015
S_0	initial susceptible	90*
I_0	initial infected	10*
R_0	initial recovered	0*

a constant steady-state as anticipated. What we are most interested in however, is how dynamics change as we gradually introduce a seasonal transmission or a seasonal birth, and then the two combined.

§ 2.3 Results

To calculate R_0, we observe that the average time an infected member stays in their disease class is $d+\alpha+qN$ (in the absence of recovery), and the number of secondary infections produced is $\beta(t)N$. Assuming the entire population is disease-free, we thus define

$$R_0 = \frac{\beta(t)N^*}{d+\alpha+qN^*} \tag{2.4}$$

where N^* is the disease-free equilibrium.

The threshold level of the susceptible population which determines whether cases of disease will increase, happens when $\frac{dI}{dt} > 0$ (see section 1.3). That is, for this model,

$$\beta(t)S(t)I(t) - (d+\alpha+qN(t))I(t) > 0 \tag{2.5}$$

$$\beta(t)S(t) > d+\alpha+qN(t) \tag{2.6}$$

$$S > \frac{d+\alpha+qN(t)}{\beta(t)} \tag{2.7}$$

$$S > \frac{N(t)}{R_0}. \tag{2.8}$$

Since our transmission is a seasonally varying parameter, the threshold also varies with the seasonality. This threshold therefore allows us to work out, at any time t, whether disease will grow in the population.

2.3.1 Introducing seasonality

Figure 2.1 displays four bifurcation diagrams which allow us to explore how introducing seasonality in birth and transmission impacts disease dynamics (see section 1.7.2 for detail about this method). When periodically forced, SIR models can show oscillations which are integer multiples of the period of forcing; this is known as subharmonics. Since we introduce periodic forcing with a period of 1-year, we could anticipate any period of dynamics p with $p > 1 \in \mathbb{Z}$. Such subharmonics can move through period-doubling bifurcations (i.e. changes to the system result in dynamics doubling in length), and this can potentially lead to chaotic dynamics. When introducing seasonal transmission with no seasonal birth (figure 2.1a) we see this impact on population dynamics, i.e. we see a period-doubling bifurcation (Dietz, 1976; Aron and Schwartz, 1984) as subharmonics are produced from the introduction of a periodically-forced variable. Once β_1 is large enough, population dynamics after transient time settle to an oscillating steady-state where they repeat every two years. When we introduce seasonality in the birth, where no seasonality in the transmission rate exists (figure 2.1b), annual dynamics are dominant, however with fixed initial conditions we also see a small region of 6-year cycles, and small areas of 3-year and 12-year dynamics. For alternative starting values of S_0 and I_0, the dynamics can remain on an annual cycle (as shown by the blue line in figure 2.1b). This indicates bi-stability, i.e. there are multiple stable solutions where the outcome is dependent on the starting populations used. This highlights the importance of the initial population conditions in determining the population and disease pattern (Ireland et al., 2004) and confirms that we can obtain qualitatively different results for different initial conditions (Keeling and Rohani, 2008). The first two bifurcation diagrams suggest that seasonality only in transmission is more stable than when we consider seasonality only in the birth rate, since seasonal birth can induce cycles other than annual or biennial.

If we now assume high amplitude oscillations in birth ($b_1 = 0.9$) and vary β_1 we initially move through a period of chaos before dynamics become more regular (figure 2.1c). As b_1 is introduced into the model with fixed initial conditions and $\beta_1 = 0.9$ (figure 2.1d), dynamics move through a period of more complex dynamics before settling to a biennial cycle for higher values of b_1. The plot shows that a biennial cycle will exist throughout depending on varying initial conditions, seen by the blue lines in the figure; therefore we have another indication of bi-stability/multiple stable attractors when varying the value of b_1. From the plots displayed in figure 2.1 it appears that with the incorporation of two seasonal components we see a stabilising effect on the model (i.e. dynamics become more regular), with dynamics settling to a biennial cycle when both amplitudes b_1 and β_1 are larger.

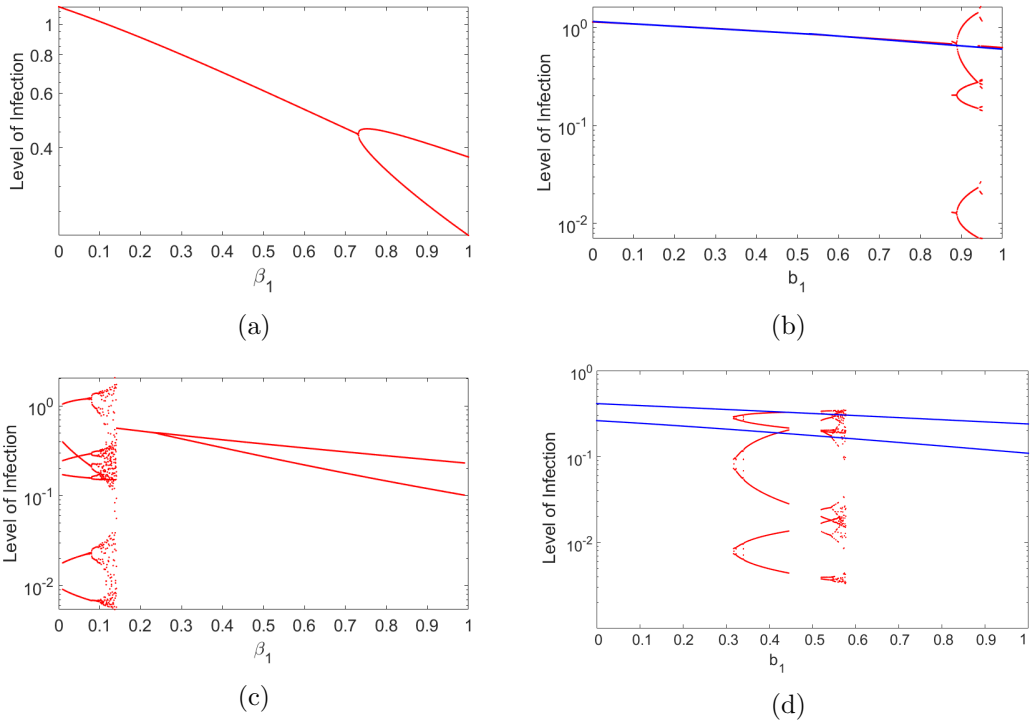

Figure 2.1: Bifurcation diagrams to show the changing dynamic behaviour when: (a) seasonality in transmission is gradually introduced into the model with no seasonality in birth. (b) seasonality in birth is gradually introduced into the model with no seasonality in transmission. (c) seasonality in transmission is gradually introduced to the model with seasonal birth amplitude $b_1 = 0.9$. (d) birth seasonality is introduced to the model when seasonal transmission has amplitude $\beta_1 = 0.9$. Note: y-axis scales are different for each figure. Blue lines indicate the existence of stable annual (b) or biennial (d) cycles independent of the parameter value.

These results are confirmed by figure 2.2a, where we display an array of pie charts (the first such plot of this kind can be found in Taylor et al. (2013), see section 1.7.3 for methodology) where every chart indicates which k-period cycles can occur for each pair of $b_1, \beta_1 \in [0 : 0.1 : 1]$ when computed for different starting conditions ($S_0, I_0 \in [10, 90], S_0 + I_0 = 100$). In general we see that as both b_1 and β_1 increase dynamics are more likely to be non-annual, and when removing both of the seasonal terms simultaneously, dynamics tend to repeat annually.

Though we notice that the inclusion of two seasonal terms has a partial stabilising affect on the dynamics, the amplitude of birth b_1 appears to have more influence on the resulting dynamics. With mid-high β_1 and low-mid b_1 we can obtain 3 or 6 year cycles, but then increasing b_1 results in dynamics on the more stable 2-year cycle. This suggests that the additional seasonality in birth can stabilise the disease dynamics. Whilst high b_1 produces more stable behaviour, high β_1 can still give 3/6/10+ year cycles. The natural frequency of the system (i.e. the frequency of the system in the absence of external forcing) is un-altered in these cases. This is because we are only considering changes to components of the periodic forcing, namely b_1 and β_1, hence these resulting dynamics observed in figure 2.2a must be due to the combination of the two seasonally forced functions. For other combinations of the seasonal amplitudes we observe instances of cycles exceeding 10 years in length. For example, when $0.6 \leq \beta_1 \leq 1$ and $b_1 = 0.6$, we see several possibilities for these 10+ year dynamics to unfold, suggesting possible chaotic behaviour. The array of dynamics we observe show that the same equilibrium is not always reached for a set parameter regime. The resultant dynamics depend on the initial conditions as there are multiple stable attractors and the specified initial conditions set the behaviour seen. Such bi-stable behaviour suggests that this general result, that increasing amplitudes stabilise dynamics, will not always hold. Indeed, for an alternative parameter set we can see different dynamics (figure 2.2b). Increasing the virulence to $\alpha = 8$ and the baseline transmission coefficient to $\beta_0 = 1.5$, we see a wider range of possible cycles. The general pattern remains as b_1 and β_1 are varied between 0 and 1 as we see dynamics moving from annual, to biennial with increasing amplitudes.

Fourier spectra allow us to determine the dominant period of the epidemics. To compute the spectra, we used the Matlab function *fft* (see section 1.7.4). Figure 2.3 shows how changing parameter values can result in different epidemic cycles. The model with baseline parameters as specified by table 2.1, and the model with seasonality only in transmission (figures 2.3a and 2.3b) show very similar likelihoods of different dominant epidemic cycles. For seasonality in birth only, however, the Fourier spectra indicates that different epidemic cycles are likely (figure 2.3c), with triennial dynamics dominating the spectrum. These results are concomitant with the bifurcations displayed in figure 2.1, as the Fourier spectra provide a snapshot of some of the dynamics observed. Figure 2.3 also confirms that a seasonal birth rate in the absence of seasonal transmission, for our particular parameter set described by table 2.1, can be more complex than the converse.

(a) The resulting k-period cycles when varying b_1 and β_1 for different sets of initial conditions ($S_0, I_0 \in [10, 90]$, $S_0 + I_0 = 100$) and other parameters as defined in table 2.1.

(b) The resulting k-period cycles when varying b_1 and β_1 for different sets of initial conditions ($S_0, I_0 \in [10, 90]$, $S_0 + I_0 = 100$) and: $b_0 = 2$, $b_2 = 1/12$, $\beta_0 = 1.5$, $\beta_2 = 7/12$, $d = 1$, $\alpha = 8$, $q = 0.015$.

Figure 2.2

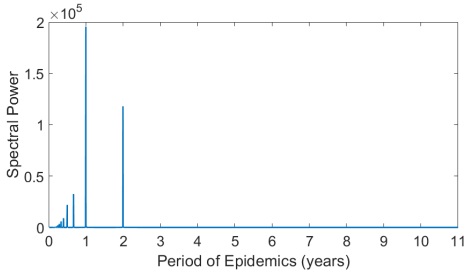

(a) $\beta_1 = 0.9, b_1 = 0.9$

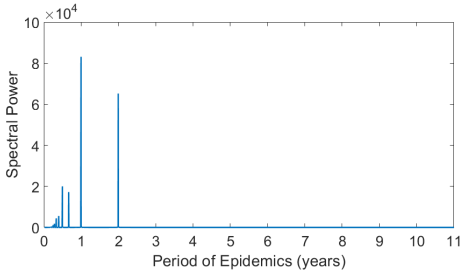

(b) $\beta_1 = 0.9, b_1 = 0$

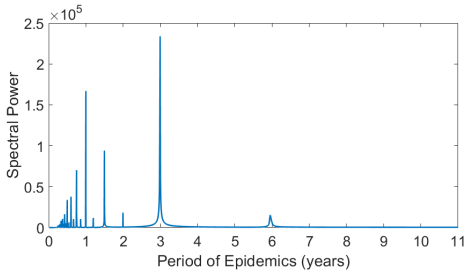

(c) $\beta_1 = 0, b_1 = 0.9$

Figure 2.3: Fourier spectra for different sets of initial conditions. (a) baseline parameters as in table 2.1. (b) seasonal transmission only; $\beta_1 = 0.9, b_1 = 0$. (c) only birth seasonal; $\beta_1 = 0, b_1 = 0.9$.

2.3.2 Timing of seasonal events

To explore how varying the timing of our seasons impacts population and disease dynamics, we consider bifurcation diagrams with b_2 and β_2 as the control parameters. Since b_2 and β_2 can vary within our defined season length of 1-year, we allow b_2, $\beta_2 \in [0, 1)$, where a season peaking at time 0 is the same as the season peaking at time 1. Figure 2.4a shows dynamics moving between 1 and 2-year cycles as the peak of births is varied across a one-year period. Similarly, figure 2.4b shows the changes for varying β_2. In both circumstances we see that disease dynamics occur annually, or every other year. From figure 2.4a is it clear that when births peak between approximately $0.5 - 4.5$ months prior to transmission (the timing of which is indicated by the vertical line), population and disease dynamics are regulated to an annual cycle hence the dynamics are most stable if reproduction peaks just before transmission. This is re-iterated by figure 2.4b, as the most stable dynamics are observed when transmission peaks $0.5 - 4.5$ months after birth, equivalent to our previous observation. We see from figure 2.5a that behaviour switches primarily between annual and biennial cycles for any initial conditions, however there are other regimes present including some instances of more complex 10+ year behaviour depending on the timing of birth and transmission. Clearly, the interplay of b_2 and β_2 is important for determining the disease cycle, but we can also note from this figure that the timings of b_2 and β_2 are not interchangeable. This is because our plot is not symmetric; i.e. the dynamics resulting from $b_2 = 0/12, \beta_2 = 1/12$ (always an annual cycle) are not the same as those when $b_2 = 1/12, \beta_2 = 0/12$ (always biennial). Hence, we must include the possibility for both births and transmission to vary in their timing. Despite some alternative dynamics present due to changes in initial population abundances, this plot again shows that the most stable behaviour (annual cycles) occur when births peak slightly before transmission.

We know that 2-year (biennial) cycles usually emerge when, after a peak in the transmission rate, the population of susceptible members is too low and has not recovered before the occurrence of another epidemic (i.e. it is below the threshold level of susceptible population members required for disease outbreak, see 2.2) (Keeling and Rohani, 2008). In our model, when the surge in births occurs just before an epidemic happens, the susceptible population is suitably high enough that the basic reproductive rate is greater than 1, leading to the more stable dynamics we observe. Figure 2.5b shows the population dynamics after transient time for the model with parameters as in table 2.1 and the threshold level of susceptible population members required for disease outbreak. The plot is in agreement with what we expect; when the abundance of susceptibles (green line) is greater than the threshold (blue line) we see a rise in the infection level (red dashed line). Due to the high amplitude of the transmission β, there are periods when the level of susceptibles is required to be very high for a disease outbreak. These periods correspond to when the transmission rate is at/around its lowest values since it is much harder for an epidemic to occur in these instances. Thus high amplitude oscillations in transmission rate

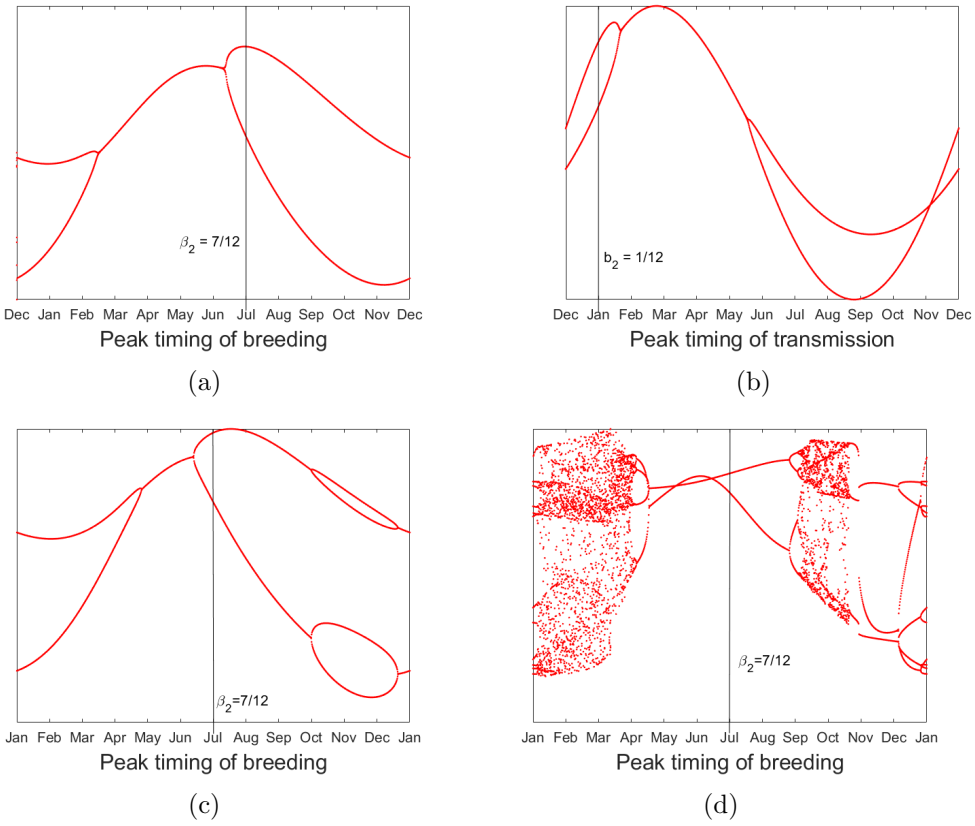

Figure 2.4: Bifurcation diagrams indicating the period of disease cycles when b_2 and β_2 are varied in different situations. In (a) and (b), initial conditions are as in table 2.1. In (c) we consider the impact of high transmission and in (d) high virulence for varying values of b_2. The vertical lines highlight the value of β_2 in (a), (c), (d) and of b_2 in (b).

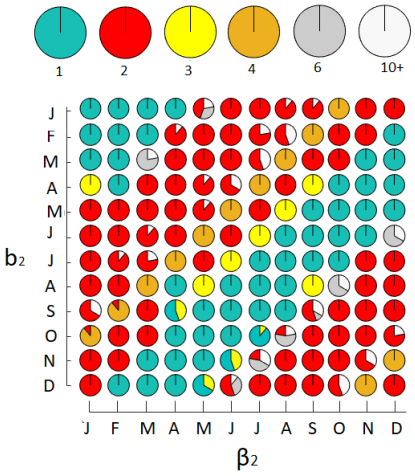

(a)

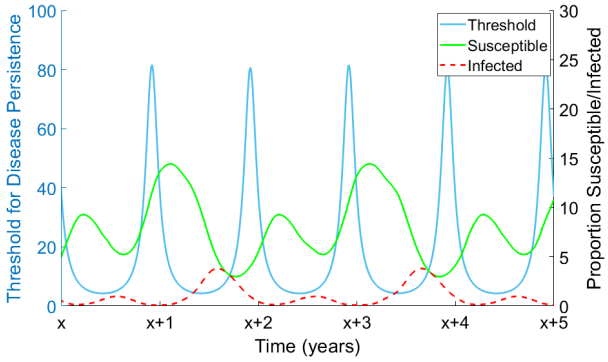

(b)

Figure 2.5: (a) the resulting k-period cycles when varying b_2 and β_2 for different sets of initial conditions ($S_0, I_0 \in [10, 90]$, $S_0 + I_0 = 100$) and other parameters as defined in table 2.1. Blue indicates annual cycles, red shows two-year, yellow three-year, orange four-year, grey six-year and white depicts 10+ year dynamics. (b) threshold level of susceptible population members required for disease outbreak (blue), plotted with the number of susceptible (green) and infected (red) members in the current population where parameters are defined as in table 2.1.

lead to slower growth of epidemics and therefore longer period cycles.

For other parameter regimes we see results consistent with the finding that a birth peak shortly before a transmission peak has the most stabilising effect on the population dynamics. For example, in a system with higher transmission rate or a system with high virulence, we see the same broad dynamic patterns (figures 2.4c and 2.4d). The bifurcation in figure 2.4c considers a much higher baseline transmission rate of $\beta_0 = 4$, with other parameters as in table 2.1. Here we see a similar pattern to those observed in figures 2.4a and 2.4b. Despite the evident chaos displayed in some areas of figure 2.4d, it is clear that dynamics are predominantly most stable when births peak before the transmission. This is seen by the region of 2-year cycles for b_1 in mid-April to mid-August. The parameters for this plot included an increased virulence and a decreased death rate ($\alpha = 12$ and $d = 0.1$) and kept other parameters as previous. Hence, these figures indicate that when moving to parameter regimes which result in more complex dynamics, the system still remains most stable when birth peaks shortly before transmission. Therefore, we are confident that the timing of the two seasonal components in relation to each other has an important role in determining the population dynamics.

2.3.3 Varying Disease Parameters

In figure 2.6 we see that for smaller α and β_0 values, population dynamics follow an annual cycle only. However as the two parameters are increased the dynamics become increasingly less-stable, where highest values of α and β_0 display the possibility of 10+ year dynamics. In between the extremes, a variety of possible dynamics are recorded. For example, when $\alpha = 6.5$ and $\beta_0 = 1$ we detect bi-stability, either seeing biennial dynamics or a cycle exceeding 10 years depending on initial numbers of susceptible and infected population members. Figure 2.6 depicts this situation by showing how population dynamics are settled in a 2-year regime, but then disruption by an external change at time x (indicated by the vertical blue line) such as an extreme weather event, culling, or hunting, leads to an instant switch to a much more complex regime. This sudden change in population and disease dynamics is the consequence of the bi-stable solution of the system. The dramatic change we see, in this case caused by a 10% "cull"of the population, would be significant in the study and application of this theory to real-world systems. For example, such removal of individuals could upset the ratio of male-female population members, and hence impact the reproductive capacity of the population (Acevedo-Whitehouse and Duffus, 2009). Successive events of this nature could ultimately lead to the collapse of a population, causing local, regional or national extinction (Thomas et al., 2004).

2.3.4 Recovery

If the host is able to recover from infection and gain life-long immunity, we need to consider this in our model. Using baseline parameters as in table 2.1, with $S_0 = 90$, $I_0 = 10$, $R = 0$, we produce a bifurcation diagram to indicate how increasing values of γ (the per capita recovery rate) influence the dynamics of disease (figure 2.7). We can see that, as γ increases, dynamics move from a biennial to an annual pattern, hence recovery has a stabilising effect on dynamics. We acknowledge here that two lines in the bifurcation appear to cross paths, but can confirm that this point remains a biennial cycle. The appearance of the crossing paths is due to the time points at which we sample dynamics and draw the path.

Amplitude of Birth and Transmission

With a recovery rate of $\gamma = 2$, we re-evaluated the impact of changing the amplitude of the seasons on the population and disease dynamics. Figure 2.8 shows a similar pattern of dynamics to the results shown in figure 2.2a, where increasing amplitudes tend to lead from annual to biennial dynamics, but we now see no instances of higher-period epidemics; i.e. no instances where dynamics repeat more often than two years. We can see that dynamics are still dependent on initial conditions, as there are two cases where dynamics are shown to be either annual or biennial, depending on the values of S_0 and I_0. The higher the value of $b_1 + \beta_1$, the more likely dynamics are to

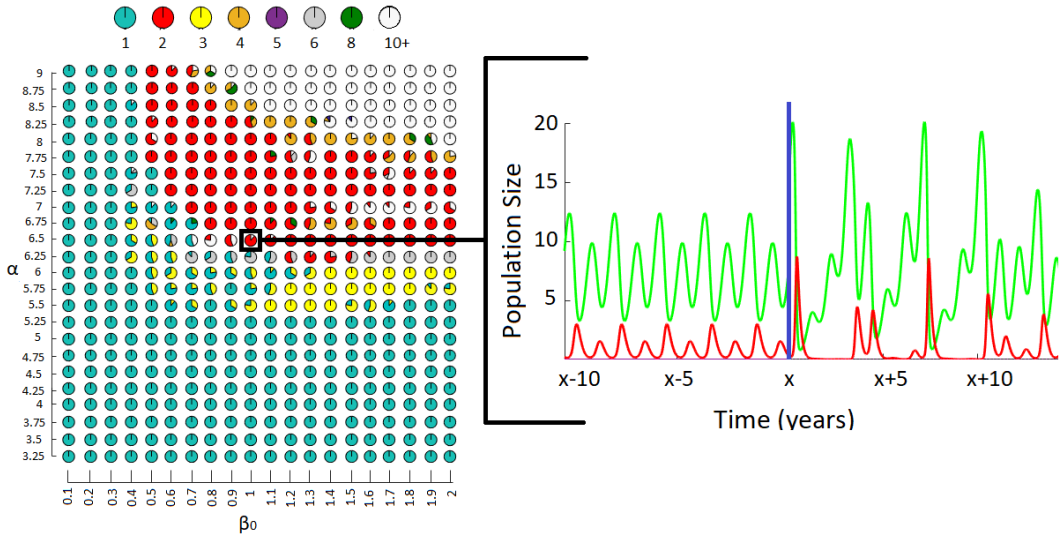

Figure 2.6: The resulting k-period cycles when varying α and β_0 for different sets of initial conditions ($S_0, I_0 \in [10, 90]$, $S_0 + I_0 = 100$) and other parameters as defined in table 2.1, with bi-stability in population dynamics demonstrated by the occurrence of an external event where dynamics change from a biennial cycle to 10+ year dynamics. Blue indicates annual cycles, red shows two-year, yellow three-year, orange four-year, purple five-year, grey six-year, green eight-year and white depicts 10+ year dynamic behaviour.

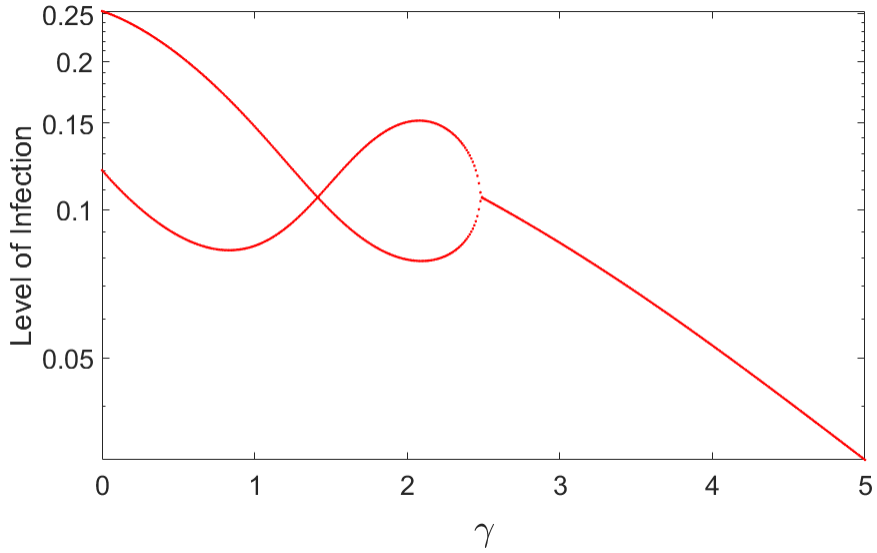

Figure 2.7: Bifurcation diagram to show how the introduction of recovery impacts disease dynamics, where other parameters are as table 2.1.

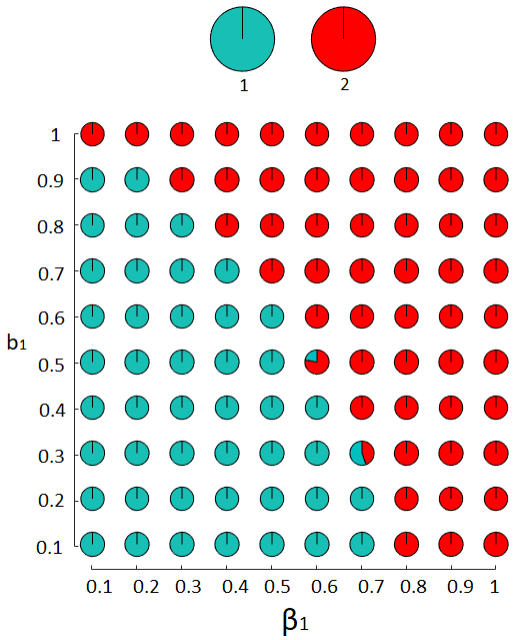

Figure 2.8: The resulting k-period cycles when varying b_1 and β_1 for different sets of initial conditions ($S_0, I_0 \in [10, 90]$, $S_0 + I_0 = 90, R0 = 0$) with $\gamma = 2$ and other parameters as defined in table 2.1. Blue indicates annual cycles and red shows two-year cycles.

be biennial rather than annual, as was shown similarly in figure 2.2a where larger $b_1 + \beta_1$ resulted in cycles of length greater than one year.

Timing of Birth and Transmission

In contrast to the wide variety of dynamics displayed by figure 2.5a, we see only annual and biennial patterns of disease in figure 2.9; another indication that the inclusion of recovery is helping to stabilise behaviour. However, despite this stabilisation by recovery, dynamics are still being driven by the relative timings of the birth and transmission seasons. We can clearly see that, again, annual dynamics occur when births peak shortly before the transmission, and biennial dynamics occur elsewhere.

We can explore this stabilising behaviour through Fourier spectra. In figure 2.10a we display Fourier spectra alongside a time-course of dynamics for the same set of parameter values (figure 2.10b). The parameters chosen to produce these plots were selected as figure 2.5a indicated that dynamics would be complex for this particular parameter set. Through the time-course we can see clearly that the population and disease dynamics are complex, with no pattern of recurring behaviour. This is

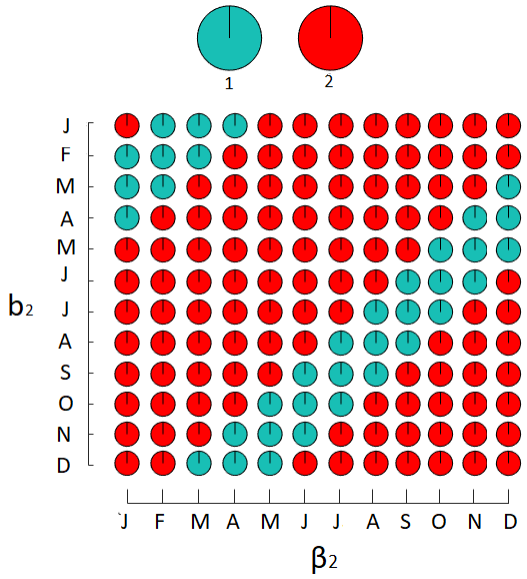

Figure 2.9: The resulting k-period cycles when varying b_2 and β_2 for different sets of initial conditions ($S_0, I_0 \in [10, 90]$, $S_0 + I_0 = 90, R0 = 0$) with $\gamma = 2$ and other parameters as defined in table 2.1. Blue indicates annual cycles and red shows two-year cycles.

reflected in the Fourier spectra, where there are no definite signals showing integer-period dynamics displayed. The 'spikes 'in this plot are not smooth, indicating uncertainty in the dominant signals and likely complex behaviour. In contrast, figure 2.10c shows the dominant cycles through the Fourier spectra when recovery is introduced, at rate $\gamma = 2$, where other parameters are as above. There are clearly dominant integer-period cycles of 1 and 2 years in length, hence the inclusion of recovery has stabilised the noisy data.

Varying Other Parameters

We saw in section 2.3.3 that changing the virulence of infection, alongside the baseline transmission coefficient β_0 had substantial effects on disease dynamics, particularly for higher values of α and β_0. Through our study of the possible dynamics, displayed in figure 2.6, we saw that, depending on initial conditions, dynamics could repeat annually, biennially or on 3, 4, 5, 6, 8 or 10+ year cycles. The most complex dynamics were predominantly seen at the highest values of α, and annual dynamics were the only cycle observed for $\alpha < 5.5$. When re-drawing figure 2.6 with $\gamma = 2$ we see that dynamics are entirely on either annually repeating cycles or 2-year cycles (figure 2.11). The increase to the recovery rate has regulated our previously observed population dynamics to more stable regimes, where even the most complex

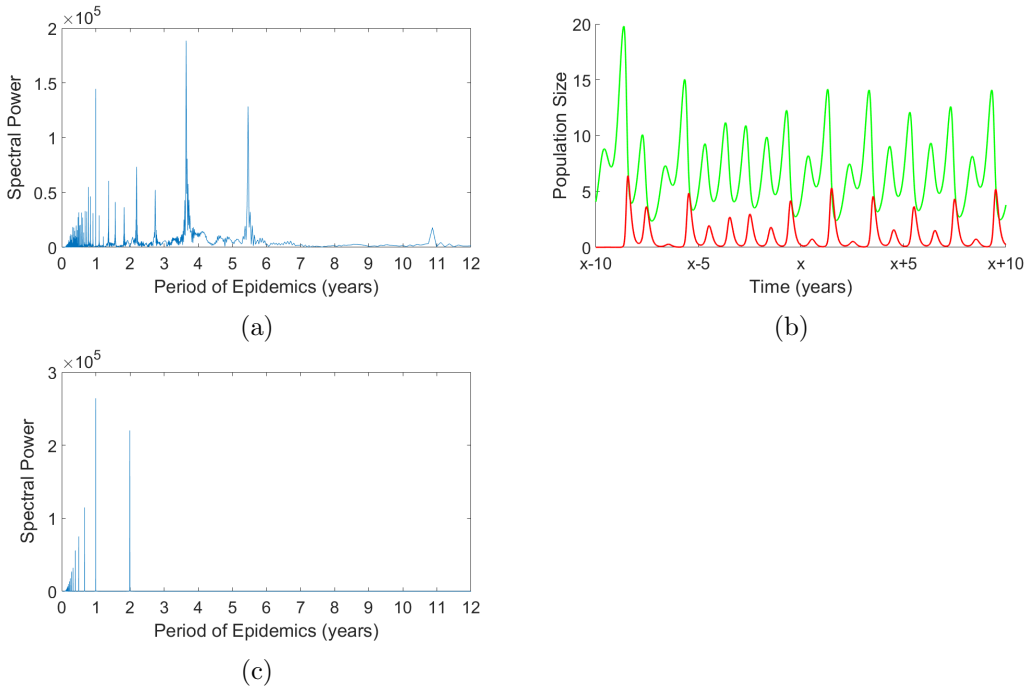

Figure 2.10: (a) Fourier spectra and (b) time-series data for disease dynamics when $\beta_0 = 1$, $\beta_1 = 0.9$, $\beta_2 = 8/12$, $\gamma = 0$, $b_0 = 2$, $b_1 = 0.9$, $b_2 = 11/12$, $d = 1$, $\alpha = 7$, $q = 0.015$, $S_0 = 30$, $I_0 = 70$, and $R0 = 0$. (c) Fourier spectra for the model with the above parameter values, where recovery is introduced at rate $\gamma = 2$.

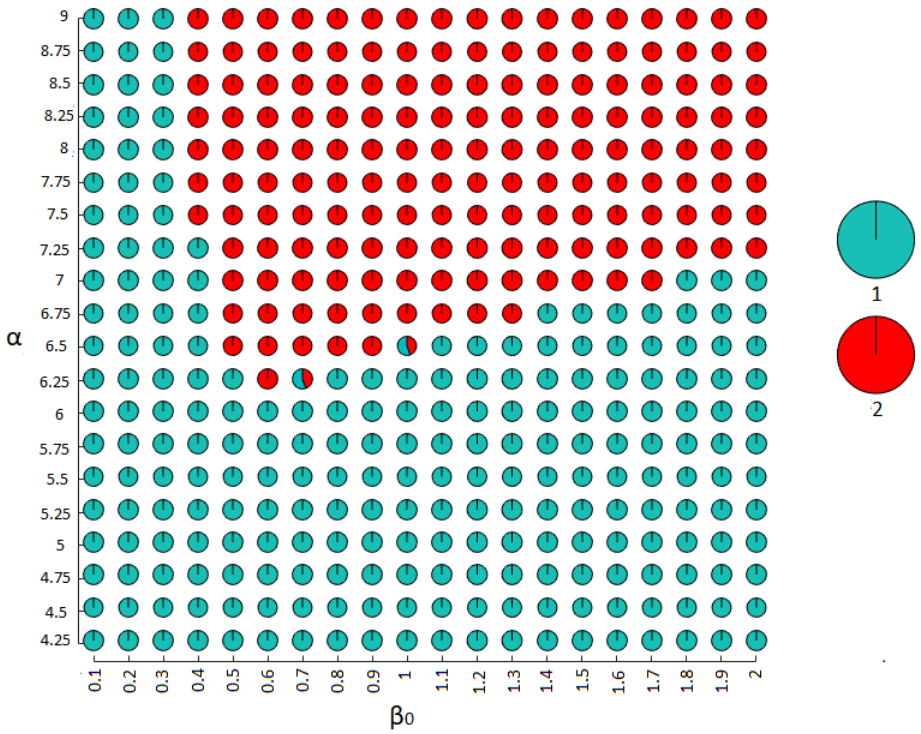

Figure 2.11: The resulting k-period cycles when varying α and β_0 for different sets of initial conditions ($S_0, I_0 \in [10, 90]$, $S_0 + I_0 = 100, R = 0$) with $\gamma = 2$ and other parameters as defined in table 2.1. Blue indicates annual cycles and red shows two-year cycles.

dynamics are now biennial. We notice that now, dynamics are always annual for $\alpha < 6.25$. Therefore, the minimum virulence value for which more complex dynamics can occur has increased (from 5.5 to 6.25), and we hence explore larger values of virulence to check for more complex dynamics beyond the values previously explored. A bifurcation diagram for α (figure 2.12a) using baseline parameters as in table 2.1, with $\gamma = 2$, indicates that we will observe more complex dynamics for more virulent diseases when the host is able to recover. We see that, for $\alpha \geq 11$, it is possible for population dynamics to repeat every four years via two period-doubling bifurcations, and subsequent doubling leads to 8-year dynamics, and then chaotic behaviour. For $\alpha > 13$ dynamics become more stable again, settling into a 3-year cycle. A further bifurcation, figure 2.12b where $\alpha > 15$, shows us how the dynamics can additionally change as the virulence increases. The 3-year cycles undergo period-doubling bifurcations to 6-year dynamics, and subsequently we again observe chaotic dynamics before the population eventually goes to extinction when $\alpha > 21$.

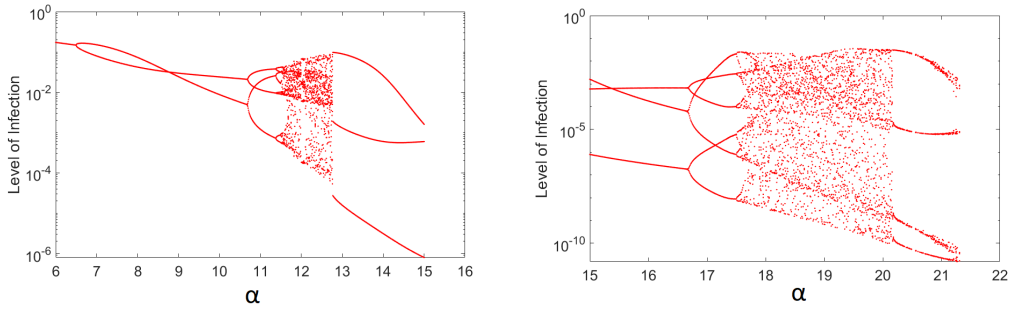

(a) (b)

Figure 2.12: Bifurcation diagrams to show the changing disease cycles as α is varied with recovery $\gamma = 2$ and parameters otherwise as in table 2.1.

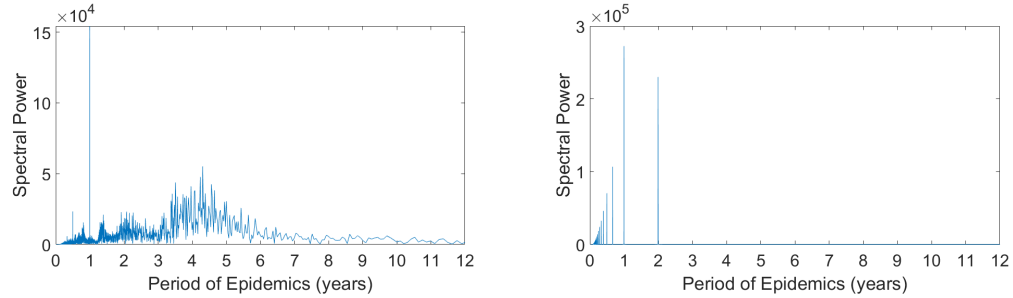

(a) (b)

Figure 2.13: Fourier spectra when $\beta_0 = 1.5$, $\beta_1 = 0.9$, $\beta_2 = 7/12$, $b_0 = 2$, $b_1 = 0.9$, $b_2 = 1/12$, $d = 1$, $\alpha = 8.5$, $q = 0.015$, $S_0 = 90$, $I_0 = 10$, and $R0 = 0$, where in (a) $\gamma = 0$ and (b) $\gamma = 2$.

We can again compare two Fourier spectra to show the difference recovery can make to complex dynamics. In figure 2.13 we can see the difference in dominant dynamics through the two Fourier spectra displayed. In figure 2.13a the data is extremely noisy, whereas in figure 2.13b the dominant cycles are annual and biennial. Figure 2.6 shows that dynamics should be unpredictable (10+ years in length) for the parameter set used and using the same parameters, with $\gamma = 2$, figure 2.11 indicates biennial dynamics. Hence, our results have been confirmed through the Fourier spectra.

§ 2.4 Discussion

In this work we explored the impact of seasonality in two life-history traits, birth and transmission, on a host-parasite system. Our results indicate that the relative timing of the two seasonal traits is crucial to the resulting dynamics, with dynamics

stabilising when births peak shortly before transmission. The relative amplitudes of the two fluctuating terms also has an important effect, with dynamics often being partially stabilised when both seasonal components have high amplitudes. We also found bi-stability between different cycle lengths to be a common outcome, and observed multiple stable attractors, meaning dynamics can switch to an alternative regime quickly.

Seasonality in wildlife host-parasite systems is ubiquitous, and as climate change alters the timing of our seasons, it is imperative to incorporate this into our predictive models (Altizer et al., 2006). We found that the relative timing of birth and transmission peaks determined switching between more and less complex cycles, where the occurrence of annual dynamics when births peaked just before transmission was consistently observed, with more complex, even chaotic, dynamics elsewhere. We found that simultaneous breeding and social peaks, in the majority of cases, did not lead to annual patterns. We demonstrated that our occurrence of annual dynamics for certain seasonal combinations is due to the fact that when births peak just before a disease outbreak, the susceptible population is replenished, raising the value of the basic reproductive rate allowing the next epidemic to occur. In contrast, when the birth rate peaks at other points in the year, the susceptible population is too low when the transmission rate increases, and a sustained disease outbreak is not possible until a future year when the population has sufficiently recovered (Keeling and Rohani, 2008). This is a reminder that R_0 depends on host demography as well as parasite traits. We may, therefore, predict that any changes to the timing of breeding or population gathering could have significant effects on the dynamics of particular populations.

Though we have discussed that our seasonal transmission is a result of social gathering, it is important to remember that variation in transmission rates can occur for other reasons. For example, temperature and rainfall aid transmission of vectored diseases (Lindgren et al., 2000), and species with ephemeral resources may aggregate around food sources when supplies are scarce (Páez et al., 2018). While we have assumed here that the two seasonal terms are independent, they may be part of the same biological process. For example, a population may gather together for a breeding season which would in turn increase transmission due to its density dependence. However, the spike in birth will only happen some time after this gathering (i.e. due to gestation periods). In this case the gestation period would be the key driver of the dynamics. We see that with a transmission peak before births occur, dynamics are more likely to be more complex, so this timing of seasonal forcing must as closely as possible represent the population being studied in order to gather realistic predictions.

We also explored how changing the amplitude of the seasonal breeding and transmission terms would impact the dynamics. When both amplitudes are small, dynamics remained annually repeating. Upon introducing larger variation in the seasonal forcing, complexity initially increases, however at high amplitudes in both birth and

transmission the system tended to settle to biennial dynamics. This generalises the result from Dorélien et al. (2013) that high seasonality in both terms leads to more stable dynamics when the events are timed differently in the year. The most complex behaviour we observed occurred at intermediate amplitudes of both breeding and transmission. This complexity occurs as a result of emerging 3/6/12-year cycles. In general however, the pattern is of 1/2-year dynamics. Therefore, depending on how strongly seasonal the breeding and/or transmission of a population is can determine how stable their population dynamics are.

We investigated how other epidemiological parameters, particularly α and β_0, impacted the dynamics and saw that increasing both led to a higher chance of more complex dynamics occurring, i.e. highly infectious fast-killing diseases are more likely to lead to chaotic dynamics. Both α and β_0 are closely tied to the threshold for disease persistence ($S > \frac{d+\alpha+qN}{\beta(t)}$). As the virulence α increases, the threshold will increase, and therefore it becomes less likely that the susceptible population will surpass this required level for disease outbreak. On the other hand, large baseline transmission β_0 means that our threshold is reduced, and it will thus fluctuate with smaller amplitude. Once the susceptible population has built high enough a large outbreak of disease occurs, but due to the high virulence it is rapidly diminished and consequently the susceptible population falls. However, since the threshold is smaller, the susceptible population has the opportunity to surpass the threshold level and hence cause more infection. The inter-play of these two parameters on which the threshold depends thus results in complex behaviour which is hard to predict, causing uncertainty in the time that epidemic outbreaks will occur. Depending on initial conditions and parameter values, there are instances of bi-stability which indicate that we have multiple stable attractors. As we demonstrated, this can lead to significant changes in the nature of the population dynamics if a sudden external change occurs. We note that, for the more complex behaviour to be observed, we require at least one of b_1 or β_1 to be high. This is in agreement with results from Keeling and Rohani (2008). The results hence show that the more deadly a disease, the more likely we are to be uncertain about population dynamics. This finding could be useful for informing management strategies of populations and help to regulate host-parasite interactions.

The inclusion of recovery in the model consistently stabilised population dynamics, often resulting in either annual or biennial dynamics when considered. We showed that, for varying amplitudes of birth (b_1) and transmission (β_1), higher values were more likely to show biennial dynamics. The results again showed the existence of bistable solutions, since dynamics were able to be either annual or biennial for a fixed parameter set, depending on the initial values of susceptible and infected population members. When varying the timing of our seasonal parameters, we found that population dynamics remained to be driven by the timings of birth and transmission, though these dynamics were stabilised to either annual or biennial cycles. When births peaked approximately $1-4$ months before transmission, we

again observed the most stable dynamics (annual repeats), with biennial dynamics elsewhere. Fourier spectra showed the difference in dominant cycles for certain parameter combinations. With no recovery, the Fourier spectra showed highly complex/noisy data with no dominant cycles, whilst with recovery, dynamics were clearly either annual or biennial shown by the strong infection peaks in the spectra. Rising virulences (α), and larger baseline transmission (β_0) led to more complex dynamics than the converse, though again we only observed biennial dynamics as the most complex cycle. The results here also confirmed the possibility of bi-stability in the model, since for certain parameter sets, dynamics could either be annual or biennial depending on initial population conditions. With recovery rate $\gamma = 2$, dynamics were shown to always be annual for $\alpha \leq 6$ regardless of the value of β_0. This is in contrast to our previous work with no recovery, where dynamics were always annual only for $\alpha \leq 5.25$. Hence, recovery allows for a greater disease virulence before dynamics become more complex; this is due to the fact that recovery induces removal of individuals from the infected class before death and/or virulence can act upon those population members. With this in mind, we explored larger values of virulence α to determine if recovery still regulated dynamics. We found that, for $\alpha \geq 11$, it was possible for population and disease dynamics to change to more complex cycles, showing that complex behaviour is still possible when a population is able to recover from the disease being studied. Overall, we found that recovery means population dynamics are more likely to be stable. This will aid decision making processes for population management since dynamics are more predictable and far less likely to switch behaviour rapidly. Although complex behaviour is possible, it is much less frequent and dynamics are predominantly between annual and biennial dynamics only.

In this study we made a number of assumptions that should be tested in future work. A clear question is whether the results found here would remain if seasonality instead occurred in different traits. We chose the two most obvious forms of seasonal behaviour, breeding and transmission, but we may also expect mortality and virulence to show seasonal trends, depending on the particular host-parasite system being studied. Based on our work, we suggest that timing will again be key due to the impact on the susceptible density and the basic reproductive ratio. Here we used a baseline SIR model but many variations to this model exist, as described in Anderson and May (1981). For example, we may wish to consider systems where there is a free-living parasite stage, or the impact of a latent period to the dynamics. These will both induce a delay in the infection process which may then have important consequences to the relative timing of seasonal traits. We may also want to consider alternative functions to represent our seasonally varying processes, such as in Hosseini et al. (2004) where the authors developed a square-wave function for seasonal birth. Such functions give the seasonality an 'on/off 'form. For a function with this structure, the seasonal parameter is fixed at 0 for a portion of the year, and then 'turned-on 'to some value at the required time-point. For example, if we

know our population breeds only in the months of June and July, we could fix $b_0 = 0$ for January-May and August-December, and fix $b_0 = x$, where x is the appropriate birth rate, for June and July. Our choice of function would be dependent on the system we want to study.

Our work indicates that a host-parasite system which is affected by seasonally changing components can be highly complex, highlighting the need to include appropriate seasonal terms and use relevant parameter values in models of host-parasites relationships to obtain biologically meaningful results. Changes to seasons impact population dynamics, and with the increasing threat of a changing climate, we need to continue to study how it can and will shape the future of our wildlife populations and their diseases.

Chapter 3

How environmental transmission and seasonal variations impact population dynamics using a compartmental disease model

§ 3.1 Introduction

The environment can play a large role in the transmission of disease; through contaminated food and water sources, excreted materials and decaying matter, infection can spread to susceptible members of a population. Environmental transmission is thus important to include in models of host-parasite relationships and has been considered appropriate for several specific wildlife diseases. These include: chronic wasting disease (CWD) (Miller et al., 2006), avian influenza (Breban et al., 2009), bovine spongiform encephalopathy (BSE) (Anderson et al., 1996), and rabbit haemorrhagic disease (RHD) (Henning et al., 2005). Theoretical work and models with environmental (also coined *indirect*) transmission are less common in literature, even though this form of transmission has been determined as being important for many types of diseases, such as prions, bacteria, macro-parasites and pathogenic viruses (Lange et al., 2016). Hence, for numerous populations and their contractable diseases, we should consider that parasite transmission can occur through the environment, as well as directly from host-host (Caley et al., 2009; Almberg et al., 2011; Lange et al., 2016).

Different pathogens will behave in the environment in different ways. For example, BSE in cattle can multiply in soil, but other diseases will remain dormant. Some diseases, such as the prion CWD, can persist in the environment for long periods,

whilst others will not survive for an extended period outside of their host (Almberg et al., 2011; Blackburn et al., 2019). Persistence of infectious material in the environment will also be dependent on conditions such as temperature and precipitation (Blackburn et al., 2019). Therefore global changes in climate, or other factors, will impact environmental transmission routes. In turn this has the potential to change host-parasite relationships (Al-Shorbaji et al., 2015).

Prion diseases have received considerable attention in work on host-parasite relationships with environmental transmission; they can persist in the environment for long periods, sometimes out-living their host species (Georgsson et al., 2006; Wiggins, 2009; Sharp and Pastor, 2011). It is common for prion diseases to maintain themselves for such extended periods in ground conditions (e.g. soil), though they can also live in shared food resources, decaying carcasses and excreted materials (Miller et al., 2004). In the case of CWD, transmission can occur both directly and indirectly (Vasilyeva et al., 2015). However, prion diseases are typically transmitted through the ingestion of infectious material (indirect), rather than directly from host-host (Miller et al., 2004; Georgsson et al., 2006; Wiggins, 2009). Miller et al. (2006) demonstrated how important the environment is in the transmission of CWD through the formulation and analysis of several SI-type models, where the SI model with indirect transmission most appropriately represented the empirical data available for their comparison work. However, despite recognition that the ungulate populations able to contract CWD display seasonal patterns in both breeding and aggregation (Sharp and Pastor, 2011; Vasilyeva et al., 2015), Miller et al. (2006) do not consider this. As stated in chapter 2, we believe the inclusion of seasonally varying rates to be extremely important in accurately investigating and representing host-parasite dynamics.

Another example of a disease for which a typical SIR model is not sufficient to represent observed dynamics is Avian Influenza. It is necessary to include an environmental transmission path in order to ensure predictive models are representative of empirical results (Breban et al., 2009). In addition, the seasonal breeding and migratory behaviours should be considered in modelling this host-parasite relationship. In a stochastic model of these host-parasite dynamics in ducks, Breban et al. (2009) find that even when environmental transmission is small, it plays a clear role in determining disease dynamics. The persistence of the disease is mostly dependent on the existence of the indirect transmission path however, and this has further been shown by Sauvage et al. (2003); Rohani et al. (2009); Almberg et al. (2011). This is due to the interaction of the direct and environmental transmission routes. In the model, the environmental disease reservoir is dependent on the infected population abundance, which in turn depends on the direct transmission of disease from susceptible members. Therefore, the environmental pool is created from seasonal intra-species interactions in this case. However in an $SEIR$-type model developed by Al-Shorbaji et al. (2015) including environmental transmission, but without seasonality, the direct transmission path played a bigger role in disease

outbreaks than the indirect transmission route. This could be due to the size of the host population determining how much the environmental transmission drives disease dynamics (Breban et al., 2009).

In this chapter we formulate a new SIR-type model to investigate disease dynamics in a population subject to seasonality in birth and direct host-host transmission. Additionally, it will be possible for susceptible members to contract disease from an environmental reservoir of disease via an indirect transmission process, not considered seasonal. In 3.2 we introduce our new model, the parameters, seasonal components and define the threshold level for disease outbreak. In 3.3 we explore the impact of having only one seasonal term in the model (3.3.1), and then how two seasonal terms change the dynamics (3.3.2). We then consider alternative initial conditions in 3.3.3, the timing of our seasonal events in 3.3.4 and varying disease parameters in 3.3.5. Finally in 3.4, we discuss our results and their implications.

§ 3.2 The Model

Our model is based on that in chapter 2, with adaptations to consider environmental transmission of disease. The population dynamics of a host-parasite system are henceforth described by the following equations:

$$\frac{dS}{dt} = b(t)N - \beta(t)SI - (d + qN)S - \delta SD \tag{3.1}$$

$$\frac{dI}{dt} = \beta(t)SI + \delta SD - (d + qN + \alpha)I \tag{3.2}$$

$$\frac{dD}{dt} = (d + qN + \alpha)I + \epsilon I - uD \tag{3.3}$$

In this system, d represents the per capita natural death rate of individuals and α a disease-induced death rate (or virulence). The parameter q represents a density-dependent factor in the death rate, since it is assumed that increased competition between host population members will increase fatality. The total population size is given by $N = S + I$, as we assume that recovery is not possible (i.e. the disease is fatal).

We introduce an additional disease class, D, representing an environmental reservoir of diseased material. The matter within this class is produced by a proportion of living infected members (representing excreted material), and the deceased infected population. Matter within the class exists in the environment for a specified time only. The transmission of decaying matter to susceptible individuals relies on contacts, with new infection occurring with parameter δ. Such contacts could involve susceptible members being near a diseased carcass, or ingesting disease prions via excreted material, for example. A proportion ϵ of the decay pool is produced from living infected population members (excretion of infectious material), and since decaying material stays infectious for a specified time it has a per capita removal rate, in this case u. We define this avenue of transmission to be an *indirect* pathway, since

infection arises as a consequence of environment-host contacts, rather than host-host contacts. This indirect transmission parameter δ is considered constant throughout this chapter, but could be an additional seasonal parameter in advancements.

We assume that a greater group size results in an increased host-host disease transmission (i.e. direct transmission is density-dependent), where the gathering of a group could be due to several natural processes for example migration, feeding or hibernation. We define $\beta(t) = \beta_0(1+\beta_1\cos(2\pi(t+\beta_2)))$ to be the varying transmission rate where β_0 is the baseline transmission rate, β_1 the amplitude of seasonality and β_2 the timing of the transmission peak (i.e. the time of peak socialising). The birth rate $b(t)$ is also considered to be seasonal to represent a population with a particular breeding season. We define $b(t) = b_0(1 + b_1\cos(2\pi(t + b_2)))$, with b_0 the baseline birth rate, b_1 the amplitude of seasonality and b_2 the timing of the birth peak.

Following the method of Van Den Driessche (2017), we can compute the basic reproductive ratio. The complete R_0 is the sum of the respective R_0 values from the direct transmission pathway, and the indirect transmission pathway. For the direct transmission component of R_0, we have

$$\frac{\beta(t)N}{d+\alpha+qN}$$

and for the indirect transmission (following R_0 calculations in Anderson and May (1981); Sharp and Pastor (2011)), we have

$$\frac{\delta(d+qN+\alpha+\epsilon)N}{u(d+\alpha+qN)}.$$

Therefore, the basic reproductive ratio for our model is

$$R_0 = \frac{N(\beta(t)u + \delta(d+qN+\alpha+\epsilon)}{u(d+\alpha+qN)} \tag{3.4}$$

where N is at the disease-free equilibrium.

The threshold level of susceptible individuals which determines if an outbreak of disease will occur, or if the disease will die-back, happens when $\frac{dI}{dt} > 0$ (as described in section 1.3). That is,

$$\beta(t)S(t)I(t) + \delta S(t)D(t) - (d+\alpha+qN(t))I(t) > 0 \tag{3.5}$$

$$\beta(t)S(t)I(t) + \delta S(t)D(t) > (d+\alpha+qN(t))I(t) \tag{3.6}$$

$$S(t) > \frac{(d+\alpha+qN(t))I(t)}{\beta(t)I(t)+\delta D(t)}. \tag{3.7}$$

$$\tag{3.8}$$

3.2.1 Cyclic behaviour of the underlying model

An interesting and important point of note for a model of this form is the possibility that the underlying dynamics (i.e. the model in the absence of seasonality) can cycle rather than settle to a stable equilibrium. This phenomenon was described by model G in Anderson and May (1981). The authors explain how S, I and D can oscillate, and the form that the stable limit cycle takes (i.e. the amplitude and period) is dependent on the parameter values used in model simulations. In Anderson and May (1981), this cyclic behaviour is more likely to occur for high-strength pathogens (high α) where the infectious stage lasts for a long time (small u).

Our defined model is highly complex, where it is difficult to perform algebraic analysis, even in the absence of seasonality. We therefore use numerical simulation methods to assess the behaviour of our host-parasite system.

§ 3.3 Results

For the numerical simulations, Matlab software (*MATLAB version R2018a*) is used and the ode15s solver implemented, as in chapter 2. For simulation purposes and to provide a reference point, we fix a default set of parameter values (table 3.1). The breeding rate of the population has a baseline of $b_0 = 2$ offspring per year, and the baseline transmission is $\beta_0 = 1$. Both seasonal parameters have amplitude $b_1 = \beta_1 = 0.9$, where births peak in month 1 ($b_2 = 1/12$) and transmission in month 7 ($\beta_2 = 7/12$). The death rate of the population is one-year ($d = 1$), and the virulence is $\alpha = 7$. This means that the average lifespan of a susceptible individual is 1 year, but infected members have a reduced lifespan of 1.5 months, since $d+\alpha = 1+7 = 8$. We take these parameter values for consistency, since these were the baseline values used in chapter 2. Decaying matter is able to stay infectious for a period of 6 months, and excreted material enters this class with rate $\epsilon = 12$. Susceptible population members can pick up disease from the decaying matter at rate $\delta = 0.1$. A summary of all baseline parameter values can be found in table 3.1.

In the absence of seasonality, $b_1 = \beta_1 = 0$, population and disease dynamics oscillate to an equilibrium state (figure 3.1) where numbers of susceptible and infected population members remain constant. Since we earlier explained the possibility of cyclic behaviour in an unforced environmental transmission model, we note that this fixed equilibrium is specific to our defined baseline parameter set (see table 3.1). With the inclusion of seasonal forcing however, dynamics display a wide range of behaviours.

3.3.1 Single Seasonal Forcing

Seasonal Birth

Without seasonal transmission ($\beta_1 = 0$), simulation of the model with other parameters as specified in table 3.1 shows dynamics repeating every three years. With

Table 3.1: Initial parameter values. *initial population conditions, unless otherwise stated.

Parameter	Description	Baseline
b_0	baseline birth rate	2
b_1	amplitude of birth	0.9
b_2	timing of birth peak	$\frac{1}{12}$
β_0	baseline transmission rate	1
β_1	amplitude of transmission	0.9
β_2	timing of transmission peak	$\frac{7}{12}$
d	natural death rate	1
α	disease-induced mortality	7
q	density-dependent control	0.015
δ	transmission rate from environment	0.1
ϵ	excretion rate	12
u	death rate of decaying matter	6
S_0	initial susceptible	90*
I_0	initial infected	5*
D_0	initial decaying	5*

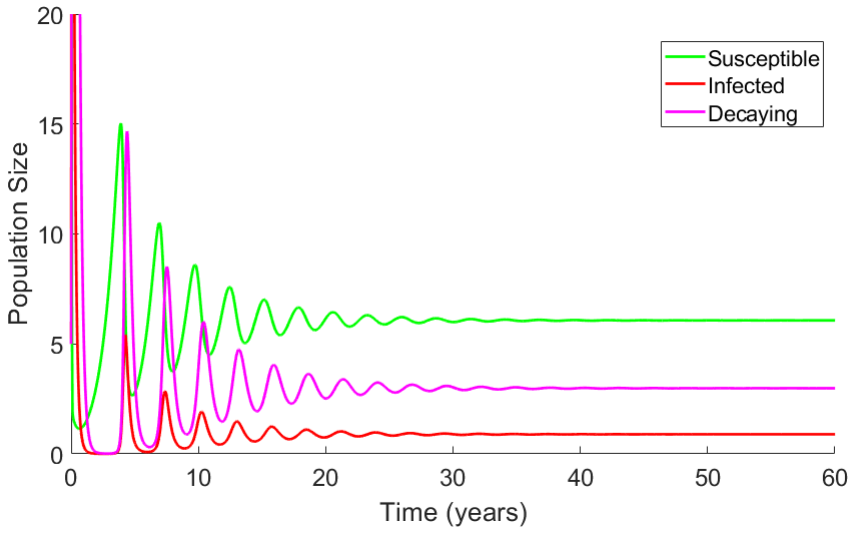

Figure 3.1: Oscillation of dynamics to a stable equilibrium for the model in the absence of seasonality, where parameter values are as defined in table 3.1 with $b_1 = \beta_1 = 0$.

alternative values of b_0 and b_1 however, we can additionally observe annual, biennial and four-year cycles (see figure 3.2). The occurrence of epidemics is dependent on the values of b_0 and b_1, and these also assert the prevalence of disease. Figure 3.2 shows a surface map to indicate the changing prevalence of infection for $10,000$ different pairings of b_0 and b_1, with contour lines to indicate the period of epidemics. We set $1.5 \leq b_0 \leq 5$ and $0 \leq b_1 \leq 1$ with parameter values sampled at regular intervals. The infection level presented is the largest prevalence observed during the disease cycle. It is clear from this plot that, when behaviour switches from one cycle to another, this impacts the maximum prevalence of disease seen within the population during a cycle, with longer cycle lengths tending to lead to higher maximum prevalences. We must note here that the occurrence of three-year cycles is fairly uncommon, yet our initial conditions and parameter values lead us to this cycle. Further analysis showed us that the cycle length can also be dependent on initial conditions, with bi-stability and multiple-stable attractors existing. The default parameter values taken are carried over from chapter 2, with the new additions of δ, ϵ and u estimated from different sources (Williams et al., 2002; Miller et al., 2006; Potapov et al., 2016). We recognise the rarity of the three-year cycle, and have described the reasoning for its occurrence here.

Seasonal Transmission

Omitting seasonal forcing in the birth rate but incorporating seasonality in transmission sees infections peak either annually or triennially (figure 3.3). Here we sample $10,000$ pairs of β_0 and β_1 values at regular intervals, with $0 \leq \beta_0 \leq 4.5$ and $0 \leq \beta_1 \leq 1$. The values of β_0 and β_1 determine the disease pattern observed with the largest explored values of both always resulting in triennial dynamics. There is an additional window of three-year cycles occurring for high β_1 and mid β_0. Higher maximum prevalences are only associated with non-annual dynamics; this is due to the way in which population abundances change through time in relation to the threshold for infection outbreak. As described in section 1.3, the number of susceptible population members must surpass a certain threshold for an outbreak of infection to occur. Figure 3.4 shows the thresholds for each possible cycle, with 3.4a highlighting a threshold for annual dynamics and 3.4b a threshold for triennial infection dynamics. From these plots we can see that when the susceptible population numbers (green line) move above the threshold (blue line) the number of infected population members (red line) increases, and when susceptible members dip below this threshold, we see a decrease in the infection.

3.3.2 Two Seasonal Terms

We now explore the population and disease dynamics when both birth and direct host-host transmission are considered seasonal. We assume $b_1 = \beta_1 = 0.9$ and $b_2 = 1/12$, $\beta_2 = 7/12$. Performing simulations for transient time (1000 years to

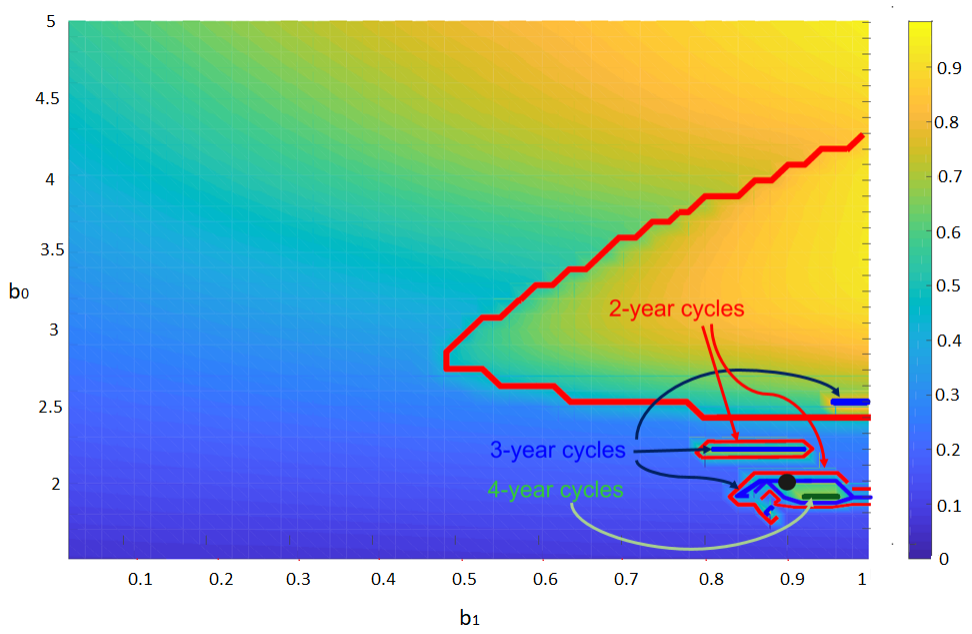

Figure 3.2: Surface map to indicate the maximum prevalence of infection observed during a disease cycle when varying the values of baseline birth rate b_0 and amplitude of the seasonal birth b_1 with no seasonality in transmission. Low prevalence is indicted by dark blue, and high prevalence by yellow. Contour lines indicate regions of different period epidemics, where inside the red lines dynamics are biennial, in the blue line dynamics are triennial and on the green line dynamics repeat every four years. The black dot indicates our baseline parameter values (on a three-year cycle).

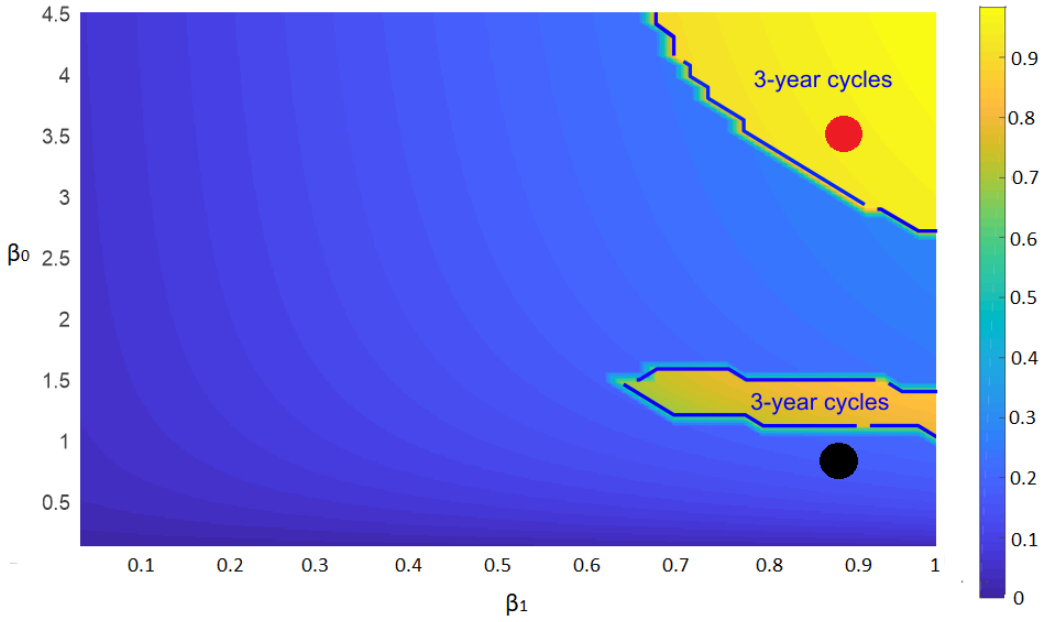

Figure 3.3: Surface map to indicate the prevalence of infection when varying the values of baseline transmission rate β_0 and its amplitude β_1 with no seasonality in birth. Contour lines indicate regions of different period epidemics, where inside the blue line dynamics are triennial and otherwise annual. The black dot indicates our baseline parameter values (on an annual cycle) and the red dot relates to the proceeding figure.

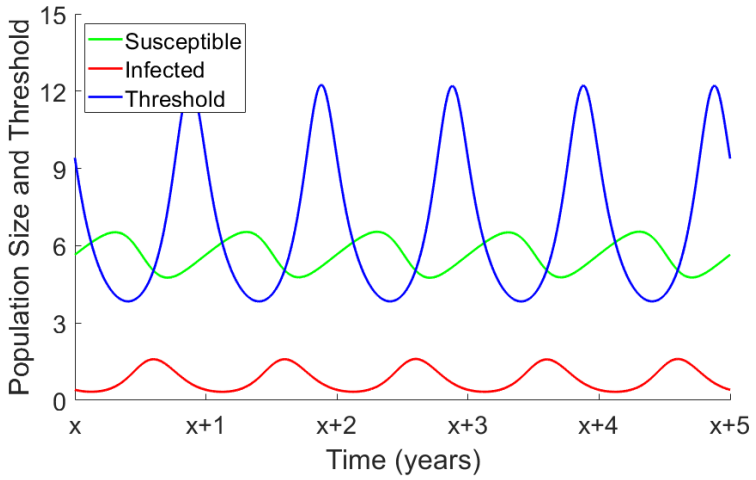

(a)

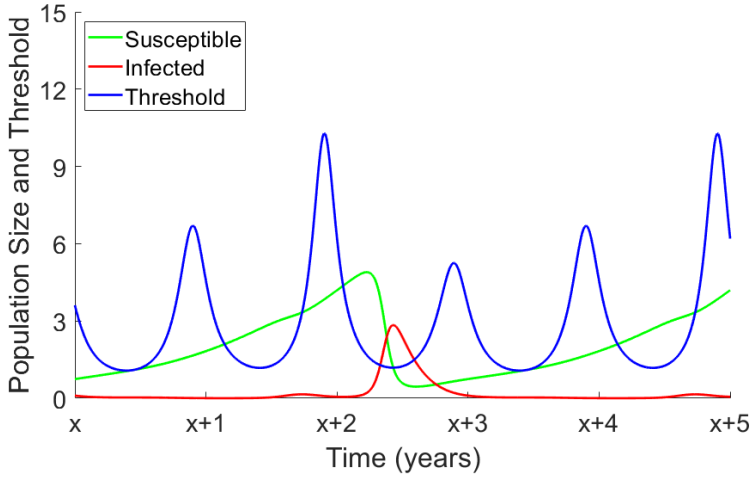

(b)

Figure 3.4: Threshold level of the susceptible population needed for a disease outbreak to occur. In (a), baseline parameters are implemented with $b_1 = 0$ (see black dot on figure 3.3). In (b), $\beta_0 = 3.5$, $b_1 = 0$ and other parameters use baseline values as defined in table 3.1 (see red dot on figure 3.3).

ensure dynamics have reached a steady-state), with fixed initial conditions $S_0 = 90$, $I_0 = 5$, $D_0 = 5$ and parameters as in table 3.1, population and disease dynamics settle to a cycle repeating every three years. Infection (and hence decaying material) breaks out in the population once the number of susceptible members is sufficiently high, at which point this number declines before rebuilding again. The threshold number of susceptible members required for infection to increase in the population (equation (3.8)) is calculated and plotted as a function of time in figure 3.5 alongside the dynamics of susceptible and infectious individuals. To plot the threshold, we use the output vectors of $S(t)$ and $I(t)$ from the *ode15s* MATLAB simulation, create vectors of the same length for each parameter necessary to compute the threshold (see equation (3.8)), and code the threshold equation into MATLAB in order to plot the figure depicted (figure 3.5). We see again that when the number of susceptible individuals surpasses the threshold line, infection levels begin to increase. Once the number of un-infected hosts declines, dipping under the threshold, we infection begins to decline.

As baseline rates and seasonal amplitudes had specific impacts on population dynamics in the model with single seasonality, we explore how changing these rates $(\beta_0, \beta_1, b_0, b_1)$ impact the dynamics under dual-seasonality. We show the different epidemic periods that occur as a result of altering b_1 and β_1 in figure 3.6. We sample $10,000$ parameter pairs, taking values at regular intervals with $0 \leq b_1 \leq 1$ and $0 \leq \beta_1 \leq 1$ and fix initial conditions as above ($S_0 = 90$, $I_0 = 5$, $D_0 = 5$). Cycle lengths are calculated using the same method as when computing pie diagrams (see section 1.7.3). The surface plot indicates that both amplitudes impact the overall dynamics. We see that non-annual dynamics occur only when $b_1 > 0.6$ (therefore annual dynamics only for any β_1 with $b_1 < 0.6$). Increasing β_1 at high amplitudes of birth impacts resulting infection periods also, as we see decreased stability for increasing β_1, with indication of a 9 year cycle. For a surface plot of b_0 vs β_0 (figure 3.7, where parameter values are sampled at regular intervals as previously described) we see that dynamics are more varied, often switching from annual to triennial with small changes in parameter values. Both b_0 and β_0 appear to have an impact on the resulting epidemic periods, where larger values of baseline birth rates settle epidemics to either annual or biennial cycles, and smaller values make dynamics less predictable. Changing the baseline transmission β_0 at lower baseline birth rates alters the period of disease cycles more readily; we observe rapid switching between different cycles with 6, 8 and 10+ year dynamics recorded for several parameter combinations. These more complex cycles and switching behaviours are also clearly seen as we vary both β_0 and β_1 simultaneously. Figure 3.8 shows us how biennial dynamics dominate with high amplitudes and relatively high baseline transmission, and how annual dynamics prevail for any amplitude when baseline transmission is small. It is the change in β_0 that perhaps has the most profound impact on determining the period of epidemics, a result in line with those observed in figure 3.7. We sampled $10,000$ parameter pairs, again taking values at regular

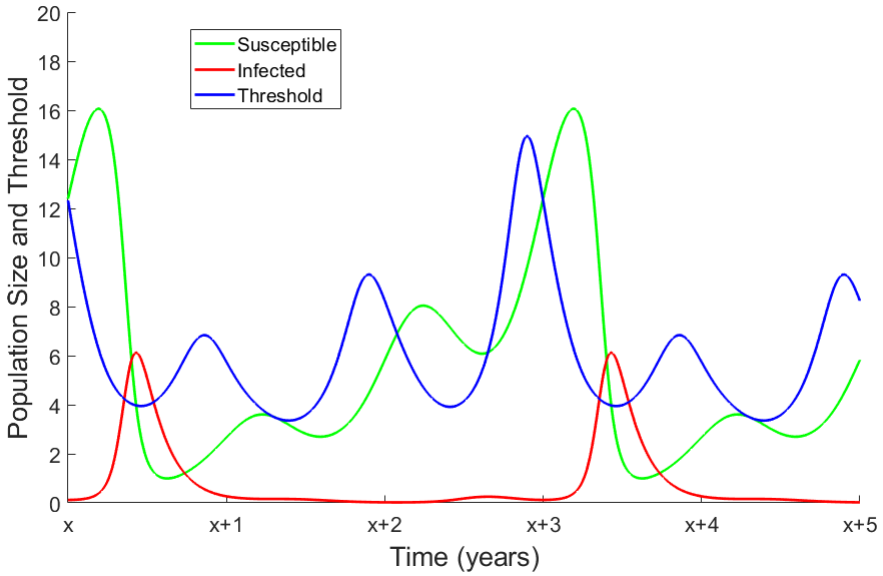

Figure 3.5: The level of susceptible population members needed (blue line) to cause infection to rise in the total population, where parameter values are those in table 3.1.

intervals. Bifurcations for each of $\beta_0, \beta_1, b_0, b_1$ show how these parameters can individually change the period of epidemics. As shown in figure 3.9, we observe annual, biennial, triennial and six-year cycles, and these are in agreement with our surface plots. These bifurcations show that we have multiple stable attractors as dynamics jump from one state to another when using fixed initial conditions (figures (b) and (d)), and this is explored further in the proceeding sections. With this, we can be confident that initial conditions are important for determining these disease cycles, as the dynamics observed represent certain basins of attraction for the set initial conditions used.

The variation in observed epidemic periods as a result of changes to $\beta_0, \beta_1, b_0, b_1$ with both terms seasonal is more wide-ranging than results obtained in section 3.3.1. For example we now see epidemic cycles greater than 6 years in length, and particularly we note that highly unstable 10+ year dynamics are found for different combinations of baseline birth, b_0, and baseline transmission β_0.

3.3.3 Alternative Initial Conditions

Changing the initial proportions of susceptible and infected individuals, along with the amount of decaying matter, can alter the dynamics resulting from a simulation of the model. With different initial population conditions, though keeping the same baseline parameter values (given in table 3.1), we observe annual, three-year and

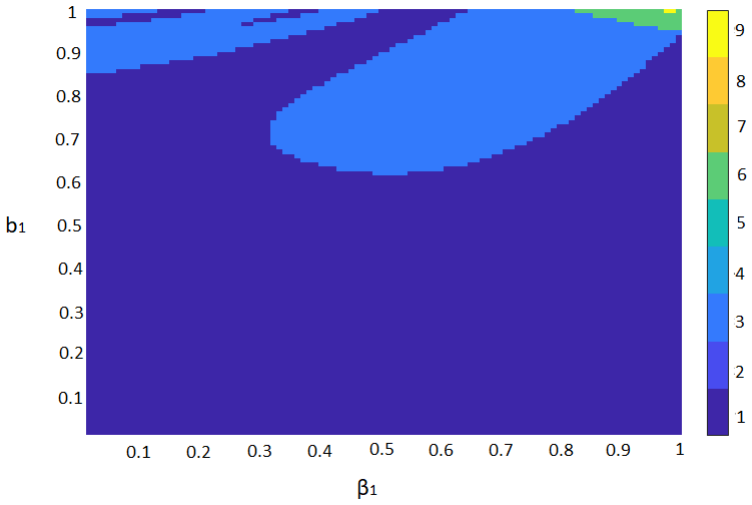

Figure 3.6: A surface plot to indicate how changing amplitudes of seasonality, b_1 and β_1, can impact the repeating dynamics of disease, where other parameter values are those in table 3.1. Different colours represent different periods of disease cycles.

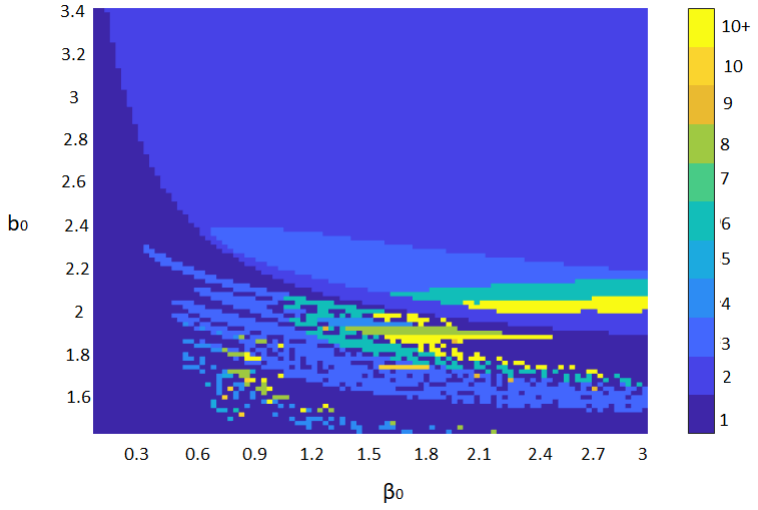

Figure 3.7: A surface plot to indicate how changing the baseline values of birth and transmission, b_0 and β_0, can impact the recurrence of epidemics, where other parameter values are those in table 3.1. Different colours represent different periods of disease cycles.

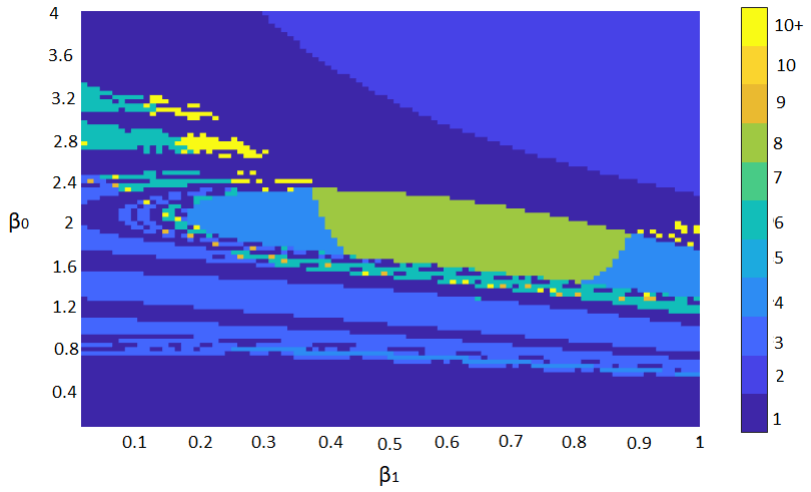

Figure 3.8: A surface plot to indicate how changing the baseline value of transmission and it's amplitude, β_0 and β_1, can impact the recurrence of epidemics. Different colours represent different periods of disease cycles.

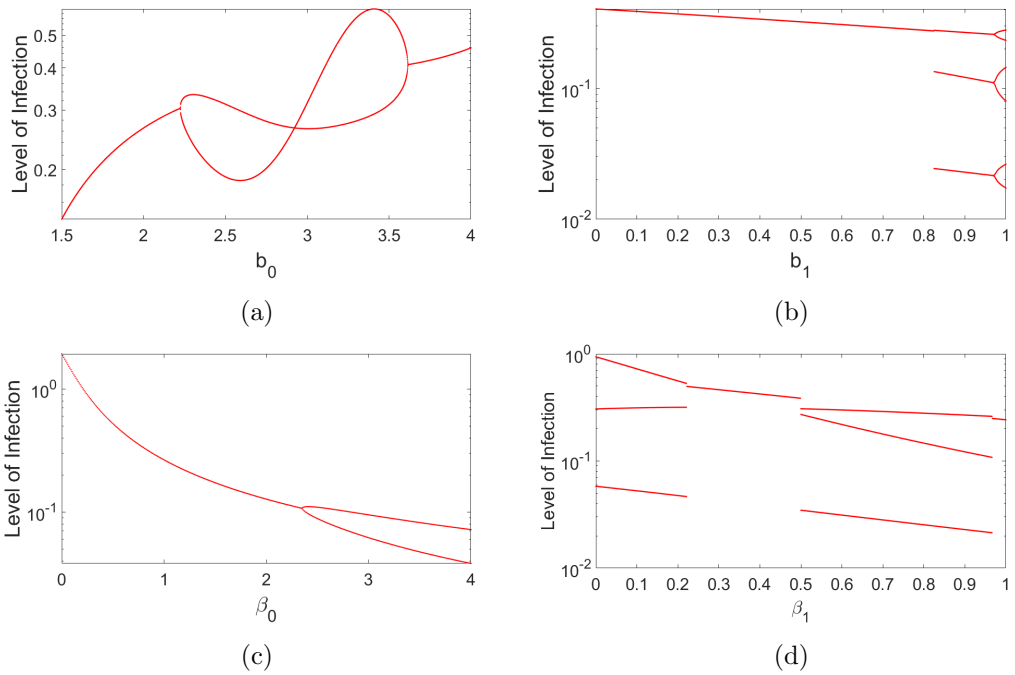

Figure 3.9: Bifurcations to show changing disease dynamics for varying values of b_0, b_1, β_0 and β_1, with other parameters as in table 3.1.

four-year disease cycles (figure 3.10), but interestingly biennial dynamics are never recorded for this particular parameter set. By changing the baseline parameter values, we can observe biennial dynamics, as was observed in figure 3.9. These plots therefore show that we have multiple stable attractors, each with its own basin of attraction (Keeling and Rohani, 2008) (i.e. sets of initial conditions S_0, I_0, D_0 which always result in the particular dynamic). In figure 3.10, we show the occurrence of epidemics for pairs of $S_0, I_0 \in 100$, and four different values of D_0. There is a clear pattern of recurring behaviour, and it is particularly noticeable that initially high numbers of both susceptible and infected population members will result in triennial dynamics. Fourier spectra help to highlight the elevated likelihood of observing triennial epidemic dynamics. The Matlab function fft is used to compute the discrete Fourier transform (DFT), a technique to change our time domain signal to its equivalent frequency domain signal. In figure 3.11 we see the occurrences of different disease cycles with initial conditions as in table 3.1. This spectrum confirms our observations in the surface plots (figure 3.10) that triennial epidemics are the most often occurring.

3.3.4 Timing of seasonal events

As we saw in chapter 2 the timing of the peaks and troughs of seasonal breeding and transmission within the specified one-year period can drive the dynamics of the epidemic cycles. Altering the timing of the peak for one of the demographic processes helps us to explore the different dynamics that could be produced. A bifurcation diagram is a good visual tool for this. Figure 3.12 shows how varying the timing of birth (b_2) will lead to different periods of epidemics when $\beta_2 = \frac{7}{12}$, and we can clearly see that the timings have a large impact on the occurrence of disease outbreaks. This bifurcation also highlights the importance of the initial population conditions, since it is clear that we switch between multiple stable attractors, and there is an annual cycle underlying throughout (blue line in figure 3.12). Notably, the incidence of epidemics is most stable when births peak $0.5 - 5.5$ months prior to the transmission peak, or when births peak $2.5 - 5$ months after the transmission. This can be explained by considering how rising numbers of susceptible population members (due to new births) and increasing transmission rates (more susceptible members becoming infected) interact, along with the threshold numbers required for an epidemic (described in section 1.3). This result is concomitant with those in chapter 2. We see again that the most stable behaviour occurs for births happening shortly before the peak in transmission.

In figure 3.13 we can see how the seasonal birth and transmission rates, separated by a period of 6 months, and the threshold, interact to result in outbreaks of infection. It takes time for the number of susceptible population members to build high enough above the threshold to cause disease outbreak, and once high enough we observe the epidemic. Due to the simultaneous decrease in birth rate and increasing transmission rates as the number of susceptible reaches its peak, we see a sharp de-

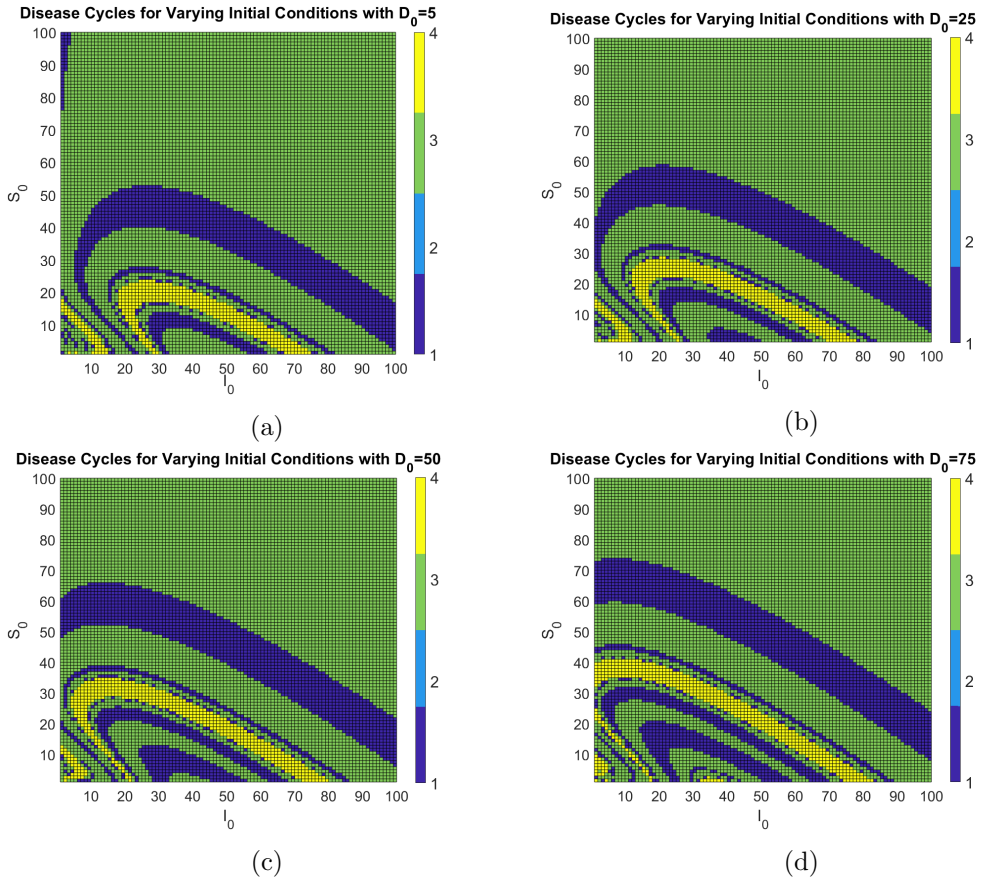

Figure 3.10: Surface plots indicating the period of epidemics for different population starting conditions, with all other parameters as in table 3.1.

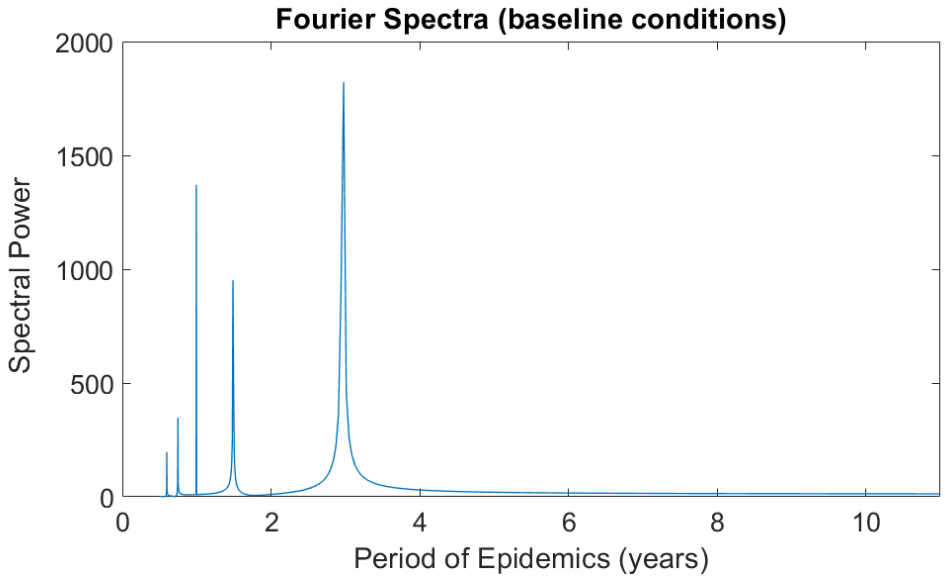

Figure 3.11: Fourier spectra highlighting the dominant epidemic periods for the model using baseline parameters as specified in table 3.1.

cline in the number susceptible and hence the rise in infection. This increase to the infected population, alongside the subsequent decreasing transmission rate assists the growth of the threshold;

$$S > \frac{(d + \alpha + qN)I}{\beta(t)I + \delta D}.$$

From this, we can see that the level of susceptibles required for disease to persist will increase when $\beta(t)$ decreases. We also note here the recurring pattern of the threshold we observe in figure 3.13. The level builds gradually over a period of three-years, matching the dynamics of the population, since the threshold is dependent on both the population of infecteds, and the total population size. Following the increase to the threshold, it is then less likely that the number of susceptible members will be able to surpass the level despite the growing birth rate. We then do not see an increase in infection as susceptible numbers have not recovered sufficiently.

3.3.5 Varying Disease Parameters

Non-seasonal model parameters will also have an impact on population and disease dynamics if varied. In particular, we note that it can be possible for the underlying model to oscillate in the absence of seasonality, depending on parameter values.

In figure 3.14 we see that increasing the strength of disease (virulence, α) can have a large impact on the resulting dynamics. Whilst for all β_0 and $\alpha < 5$ we have only annual cycles, when $\alpha > 5$ there is a much wider range of possible epidemic

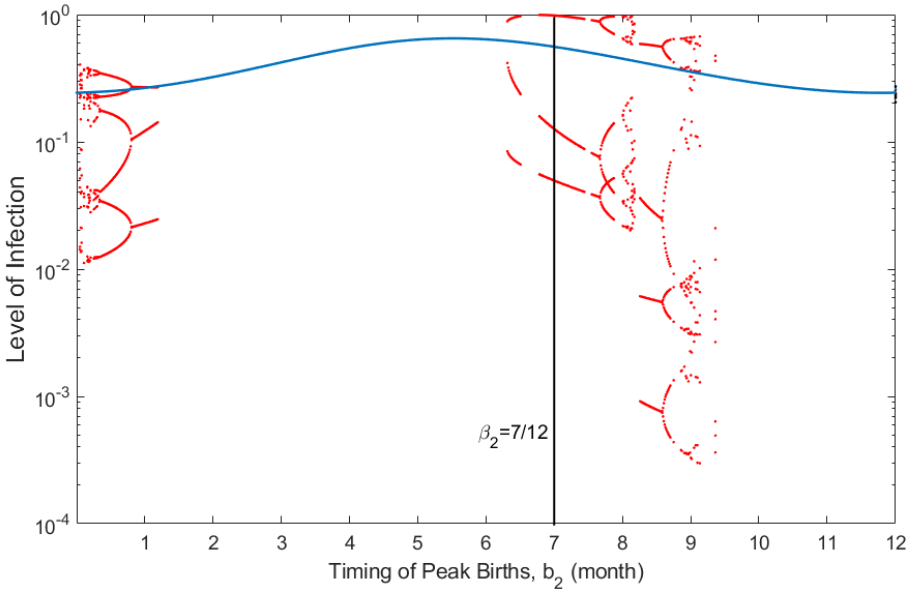

Figure 3.12: A bifurcation of parameter b_2 showing how changing the timing of seasonal birth can impact the period of disease outbreaks, with the dominant annual highlighted in blue. Parameter values used are those in table 3.1.

cycles, with the largest values of both resulting in the least stable 10+ year dynamics. Therefore, we are seeing that high virulence is driving more complex behaviour (a result we have seen in previous models, e.g. in chapter 2, section 2.3.3). We explored the behaviour of the unforced underlying model, and found that for all pairs of α and β_0, there were no occurrences of cyclic behaviour. Therefore, the patterns observed in figure 3.14 are not impacted by underlying cycling. The surface plot is computed for $10,000$ pairs of parameter values, taken at regularly spaced intervals with $0 \leq \beta_0 \leq 5$ and $0 \leq \alpha \leq 10$. We note here that the other parameters are as in table 3.1.

The transmission rate governing the indirect transmission of diseased material from the environment to living susceptible members, δ, and the excretion rate of infectious material from living infected members into the decaying class, ϵ, have some interesting interacting dynamics when we consider different combinations of the two parameters. Depending on the value of each of δ and ϵ we observe different disease dynamics, from annual to 10+ year patterns. Higher values of both tend to lead to more unstable dynamics (i.e. dynamics not repeating annually), though there are many other combinations displaying non-annual patterns. Figure 3.15 shows a surface plot to indicate how changing the values of δ and ϵ alters the occurrence of epidemics. We consider $10,000$ pairs of δ and ϵ, with $0 \leq \delta \leq 1$ and $0 \leq \epsilon \leq 20$, where values are taken at regular intervals. In addition, we explored the underlying

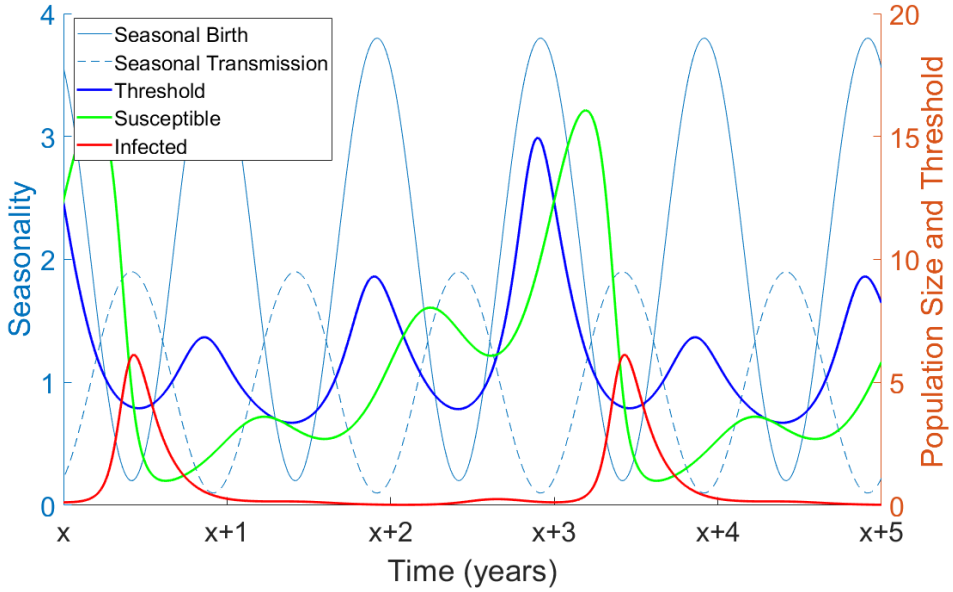

Figure 3.13: Population dynamics after transient time, with seasonal birth and transmission rates highlighted alongside the threshold of susceptible population members needed to infection to rise. Parameter values used are those in table 3.1.

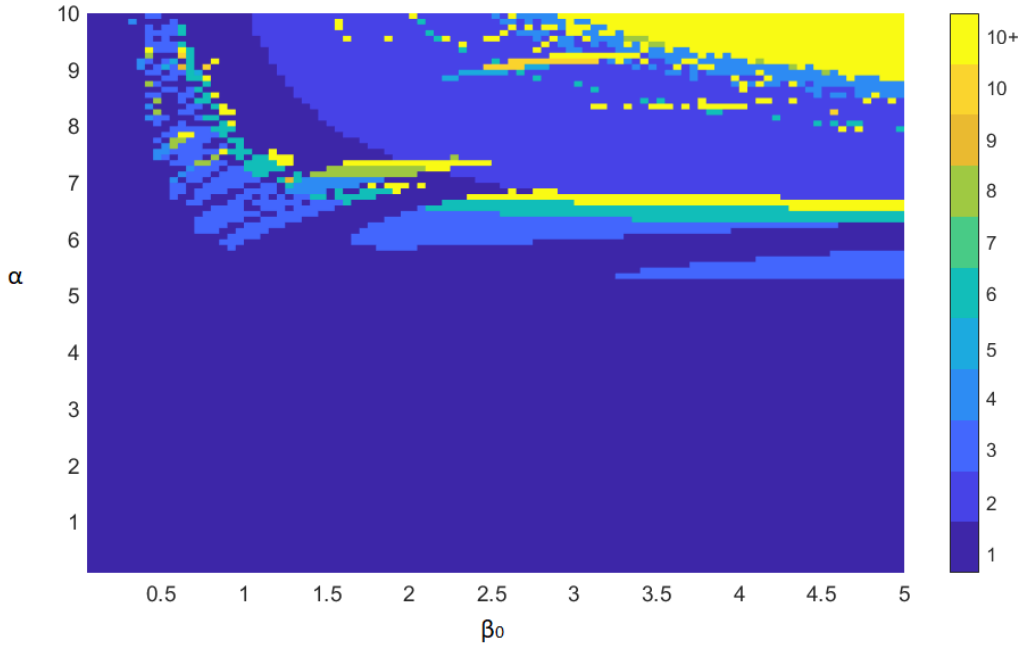

Figure 3.14: Surface plot to indicate how changing the values of α and β_0 can impact the cycles of disease epidemics, where other parameter values are those in table 3.1.

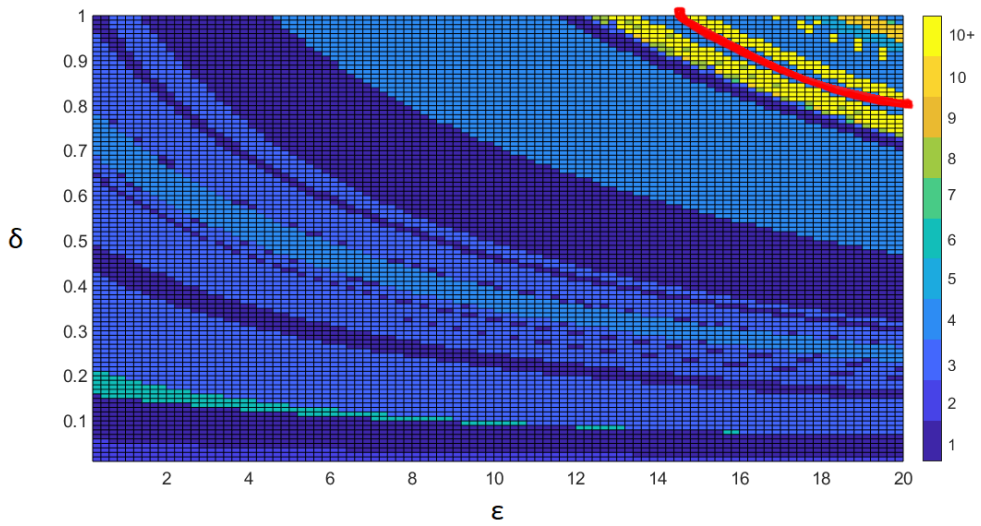

Figure 3.15: Surface plot to indicate how changing the values of δ and ϵ alters the occurrence of epidemics, where other parameter values are those in table 3.1. The red line separates the regions with and without oscillatory behaviour in the unforced model, where to the right of the line, unforced dynamics are cyclic.

dynamics in the absence of seasonality. Through exploring each pair of δ and ϵ, with $b_1 = \beta_1 = 0$, we find that increasing both δ and ϵ leads to cyclic dynamics in the unforced model. The behaviour is shown by the red line on the surface plot in figure 3.15, where to the right of the line, the unforced model displays oscillatory dynamics. Through further analysis, we determined that the cycles existing to the right of the red line do remain at integer periods, despite the underlying oscillatory (not necessarily integer period) dynamics.

Comparing our two transmission forms, δ and β_0, we also see varying behaviour depending on the specific combination of parameter values. We performed a simulation of the model, recording the length of the disease cycle for $10,000$ parameter pairings. The values of δ and β_0 are selected at regular intervals, where $0 \leq \delta \leq 1$ with step 0.01 and $0 \leq \beta_0 \leq 2$ with step 0.02. Using this, we created a histogram (figure 3.16) to display how often each disease cycle length occurs. In this we see that 1, 3 and 4 year cycles dominate, with a few occurrences of other cycle lengths. In figure 3.17, we see that we are more likely to observe the less predictable 10+ year dynamics for low values of the baseline transmission β_0 and high values of the transmission from decaying material δ. This figure also confirms our observations from the histogram as we see an abundance of 1, 3 and 4 year cycles. This is in contrast to results seen previously in chapter 2 section 2.3.1, where high values of β_0 were required for more complex dynamics to be observed. Therefore, there is an im-

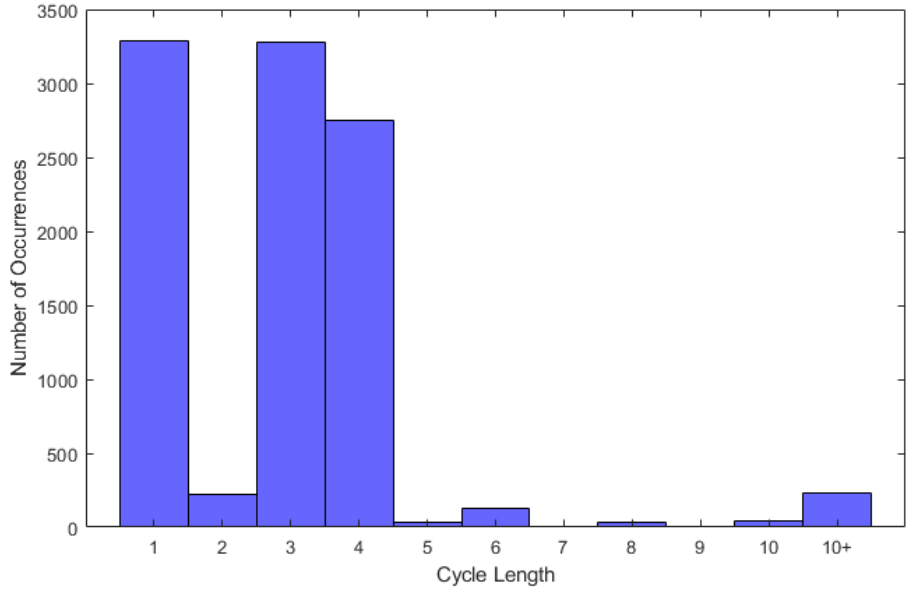

Figure 3.16: Histogram to display how many occurrences of each cycle length we observe for 10000 combinations of δ and β_0, where $0 \leq \delta \leq 1$ and $0 \leq \beta_0 \leq 2$ are sampled at regular intervals.

portant interplay between the two transmission types. In the absence of seasonality, it is possible that the underlying dynamics cycle. Shown in figure 3.17, we see the region where the non-forced model exhibits oscillatory behaviour. To the left of the red line (where we have high δ and low β_0), the unforced model cycles. We note that the occurrence of biennial cycles is rare. We might have anticipated period-doubling from annual to biennial to four-year cycles with changing transmission rates, however in this case we are therefore likely to have multiple stable attractors, where dynamics switch rapidly between different cycles. Again we explored the periods of the cycles existing in the region where underlying dynamics oscillate, and again found that cycles repeated at integer periods.

§ 3.4 Discussion

The ability for infectious materials to exist in the environment, and transmit to susceptible hosts is not an uncommon occurrence. For example, prion diseases such as chronic wasting disease can persist in the environment for a long time, even out-living their host (Sharp and Pastor, 2011; Almberg et al., 2011). Avian influenza is another disease with the ability to transmit through the environment, with the host species also exhibiting seasonal changes in their behaviour (Breban

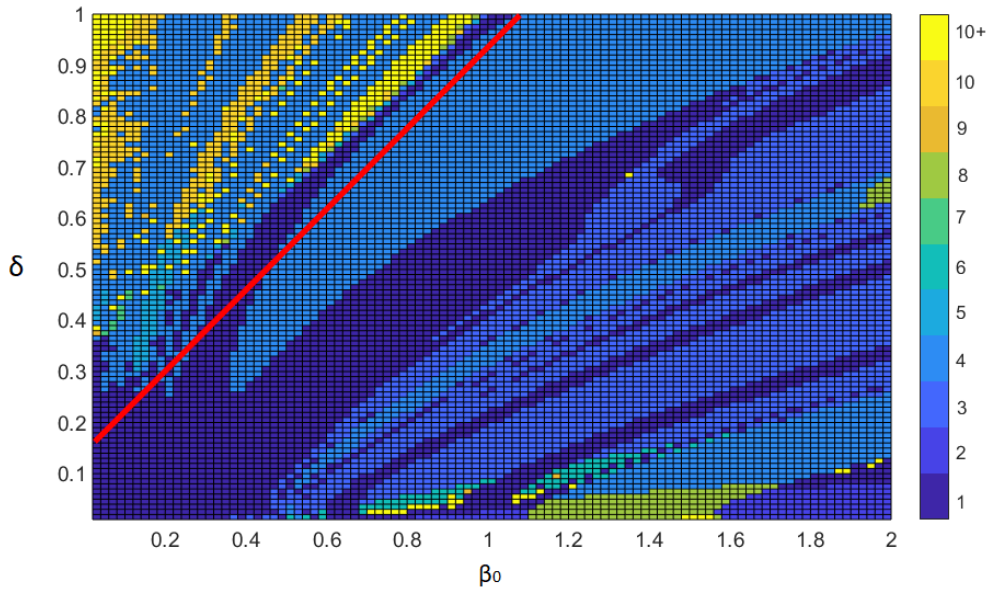

Figure 3.17: Surface plot to indicate how changing the values of δ and β_0 result in different disease cycle lengths. The red line separates the regions with and without oscillatory behaviour in the unforced model, where to the left of the line, unforced dynamics are cyclic.

et al., 2009). Seasonality in species behaviour, for example in the processes of birth and aggregation, is also common in many wildlife populations. However, theoretical work to date has rarely explored the combination of both environmental transmission and seasonal demography in hosts. Given the need to more accurately model host-parasite systems (Altizer et al., 2006), such an omission in literature needs addressing. The work in this chapter has explored how seasonal birth and transmission can impact a host-parasite relationship, where infection can transmit both directly and through the environment. We specifically explored how changes to the seasonal components, through magnitude, amplitude and timing, can impact dynamics. In addition, changes in other parameters were explored to understand how different host-parasite systems may behave.

The environment can play an important role in the transmission of disease from infected members of a population to those who remain susceptible, be it through shared food resources, excreted material, or decaying matter. This environmental transmission process, teamed with seasonality in birth and direct transmission routes, has not been considered in previous theoretical work, and in this chapter we have shown how the three processes interact to produce different population dynamics depending on parameter combinations. With this model, we have been able to explore the impact of seasonally varying processes on a host-parasite relationship where it is possible for disease to spread directly from host to host, or indirectly through the environment. We found results both in agreement with those from chapter 2, and some contrasting. For example, dynamics were most stable for births occurring in the months before the peak of transmission, as in chapter 2. However in contrast, increasing amplitudes of the seasonal components did not stabilise dynamics in this model. In addition, with the possibility of the underlying dynamics cycling in this model with indirect transmission, we found that lower values of baseline birth rate β_0 could lead to more complex dynamics, a result not seen in chapter 2. The existence of complex dynamics arising from small changes in parameter values means that to apply this model to biological systems, we need detailed information about the demographics of hosts, and of the behaviour of the disease.

It is well known that ungulate species, including mule deer, show seasonal patterns in both breeding and group behaviour (Lincoln, 1992; Bartmann et al., 1992; Williams and Miller, 2002). In the study by Miller et al. (2006), SIR-style models with indirect (environmental) transmission were found to be the best fit for data on chronic wasting disease in mule deer, however, their model did not consider the possibility of seasonally varying rates. Therefore, this is a clear example of an existing host-parasite system in the wild where our model would be suited to representing the relationship and behaviours of a population and the disease. With appropriate parameter values, and representations of seasonal processes, we could be able to enhance the results of Miller et al. (2006) by providing a model which considers seasonality in breeding and aggregation. Information about the host-parasite sys-

tem from empirical evidence would be necessary for finding appropriate parameter values, and our model outcomes could be compared to existing results.

Breban et al. (2009) used an SIR-style model with environmental transmission, direct transmission, migration and seasonal transmission dynamics to model avian influenza. The disease, showing recurring patterns of epidemics every $2-4$ years, was not sufficiently represented by a standard SIR model, but the inclusion of environmental transmission helped to more accurately describe dynamics. The model in this study was designed to match the specified system, showing the necessity for seasonally varying rates with indirect transmission pathways. Therefore, our model would be applicable to this type of host-pathogen system, where we could adapt the model as necessary to suit specific systems.

In chapter 2, and in Dorélien et al. (2013) for example, increasing the amplitudes of the seasonally varying processes stabilised dynamics when the seasonal events occurred at different times in the calendar year. For the model in this chapter, having incorporated an environmental transmission pathway, we obtain different results. The indirect transmission route and seasonality lead to more complex dynamics as amplitudes increase with the possibility of three, six-year or nine-year cycles depending on the amplitude values. In this case, therefore, the stability of the system is decreasing as amplitudes increase. The addition of environmental transmission to the model also plays a role in these patterns of dynamics. The indirect transmission and the presence of infectious material in an environmental reservoir means that the susceptible pool of members is reduced for an extended period after the initial disease epidemic, which makes an immediate repeat of disease less likely. The dynamics are in this case exacerbated by the increasing amplitude of seasonality, and dynamics become more complex as they increase. Again, as seen in chapter 2, we see that the strength of the seasonality of breeding and of transmission can determine the stability of population dynamics and disease cycles.

Given the ubiquity of seasonal processes in wildlife systems, and the impact that climate change is having on our seasons, the study of changes to the timing of seasons is important. We demonstrated the switching between stable cycles, and highly complex dynamics, depending on the timing of our seasonal processes. The most stable dynamics occurred when births peaked shortly before the main transmission season; this result is in line with our findings from the model in chapter 2. Also similarly to our previous model, we found that when breeding and transmission seasons were matched in time, dynamics were more complex. This behaviour can be explained by considering the threshold for disease outbreak, and the interactions between the seasonal birth and transmission processes. Rising birth rates lead to an influx of susceptible population members, which in turn will increase the infected population due to a greater abundance of hosts available for infection, raising the susceptible population above the threshold. If the possibility of transmission is also to rise following births, this cements the infection increase, regulating the dynamics. However, for different timing of births, it may not be possible for the susceptible

pool to be sufficiently replenished over the threshold for disease to break out in the population, meaning it is not possible for disease to increase. This is especially true for this model where environmental transmission, as explained above, lengthens the removal time of individuals from the population. This delay in an increase to the susceptible pool means that dynamics are less likely to be regulated to a more stable cycle, and this is further pronounced when the underlying dynamics of the model cycle. With the possibility for highly complex dynamics to occur depending on initial population conditions and the relative seasonal timings, we can thus conclude again that the timing of seasonal processes can significantly impact our population and disease dynamics.

In line with the results from chapter 2 section 2.3.3, high virulence and baseline transmission resulted in the most varied and complex dynamics observed. Thus again we see that a deadly and highly transmissible disease will cause more uncertainty in the population cycles. We can see why this occurs by considering the threshold for disease outbreak: $S(t) > \frac{(d+\alpha+qN(t))I(t)}{\beta(t)I(t)+\delta D(t)}$. Large virulence leads to a larger threshold, whilst rising transmission causes the threshold to decrease, and fluctuate with smaller amplitude. Complex behaviour results from the inter-play between these two parameters; the changing threshold makes dynamics hard to predict leading to uncertainty in outcomes. The results also suggested the existence of multiple-stability due to the rapid changes in dynamics for small changes in parameter values. Acknowledging that dynamics could be highly unpredictable for diseases with large transmissibility and virulence is important when the management of populations and disease needs to be considered. This is because any management should ensure that required targets are met (Wobeser, 2002), and dealing with highly-sensitive systems may require a very specific and detailed management approach. For endangered species where disease management would aim to save populations from extinction, knowledge and understanding of the host-parasite dynamics is even more imperative (Woodroffe, 1999; Millán et al., 2009).

As shown by Anderson and May (1981), the presence of an indirect transmission route can lead to cyclic dynamics in an unforced SIR-style model. This is due to the environmental transmission pathway inducing a delay in replenishment of susceptible members following an epidemic. In this model with both an indirect and a direct transmission path, governed by the parameters β_0 and δ, we saw that cyclic underlying dynamics occurred for higher values of δ with lower values of β_0. These underlying cyclic dynamics led to more complex cycles when seasonality was also incorporated into the model. This contrasts results found both previously in this chapter, and in chapter 2, where we have seen that dynamics are more complex with increasing β_0. We see here that increasing the environmental transmission parameter δ has a stronger influence on dynamics since we observe that low β_0 with rising δ led to the most complex behaviour. Therefore the presence of these underlying dynamics leads to the alternative pattern of behaviour (low baseline transmission leads to more complex dynamics) observed when seasonality is acting on the model,

and we see the strength of the environmental transmission in determining the pattern of disease.

One note from the analysis of this model is the rarity in occurrences of biennial dynamics. Period-doubling bifurcations can be common in seasonal models of host parasite relationships (Dietz, 1976; Aron and Schwartz, 1984), where annual dynamics give way to biennial dynamics, followed by four-year cycles as transmission rates are varied. With this in mind, we propose that our model contains multiple stable attractors, switching dynamics rapidly from one state to another, with biennial dynamics omitted. Further analysis in our work showed this existence, where initial population conditions were important for determining disease cycles.

Given the novel nature of this work, there is scope for progress both theoretically and empirically whereby advances could explore specific host-parasite systems, incorporating both our two seasonal components and the environmental reservoir of disease. They could involve age and/or space structure (e.g. see Valle et al. (2013); Getz et al. (2019)), recovery from disease, latency in infection and waning immunity, for example. In addition, host-parasite systems can have further complexity, with multiple hosts and multiple parasites where both direct and indirect transmission of disease can occur. Exploring the possibility of disease control is also an important area of study.

As climate changes begin to alter host-parasite relationships, exacerbating the prevalence of infections due to global warming, the need to model and predict management strategies for optimal disease and population control will become increasingly important. Using mathematical modelling techniques, we can help to alleviate the damaging consequences of a changing climate.

Chapter 4

How seasonal harvest impacts host-parasite dynamics with seasonality in birth and transmission

§ 4.1 Introduction

Mathematical models are a crucial tool in developing management strategies for infectious disease outbreaks, and their use in recent years has been increasing since we have seen outbreaks of new infections in both humans and wildlife (Wearing et al., 2005; Caley et al., 2009; Boyce et al., 2012; Porter et al., 2013; Kucharski et al., 2020). However, the need to recognise and acknowledge any underlying mechanisms of infectious diseases in wildlife populations is crucial before extensive control can be implemented (Gulland, 1995). Ideally field studies would coincide with theoretical modelling, but in the absence of practical observations and data collection, mechanistic models can sufficiently capture the behaviour of a host-parasite relationship and can aid understanding of how the system can be managed under seasonal control. In this work, we use mechanistic disease modelling to explore management strategies of infectious diseases.

Wildlife populations are frequently managed for human exploitation, where harvesting seasons are short, and performed at a specific time in order to achieve optimal yield whilst maintaining a sustainable population (Choisy and Rohani, 2006). Optimal strategies can be hard to find however, since the behaviour of species is predicted to fluctuate increasingly as extreme weather becomes more persistent due to climate change (Houghton et al., 2001), and wildlife populations are constantly adapting to their ever changing environment (May et al., 1978). In addition, different species will have different responses to the impacts of climate change; some populations for example, white-tailed deer, will benefit (Johnston and Schmitz, 1997), whilst others

such as polar bears will suffer (Stirling et al., 1999). Therefore, to find a successful harvest strategy, reliable knowledge of population dynamics is essential (Stokes, 2012). Finding management strategies which can be flexible and adaptable will be of significant importance in designing control strategies, and here we seek to explore changeable management processes.

Harvesting or management strategies do not exclusively occur for the benefit of the human population. Instead of focussing on a maximised yield, harvests may occur with the aim of controlling and/or eradicating disease. A prominent example of harvesting for disease control is the culling of badgers in the United Kingdom, as a suggested means of controlling Bovine Tuberculosis (TB) outbreaks in cattle/livestock (Donnelly et al., 2003b). Another example is the attempted control of fox rabies in Europe (Woodroffe et al., 2004). In designing programmes of management, the aim of the control is necessary in order to achieve desired outcomes.

Susceptible-Infected-Recovered (SIR) compartmental models are an important tool for exploring how populations and disease can be controlled together through management strategies. The incorporation of harvesting into SIR models to investigate optimal control strategies of wildlife populations has been well studied, with research efforts also including the study of populations with density-dependent constraints and those under a seasonal influence (Kokko and Lindström, 1998; Xu et al., 2005; Choisy and Rohani, 2006; Greenman and Pasour, 2011). Seasonally varying harvests are, by definition, adaptable. They can be manipulated to accommodate changes in species behaviour, and changes in environmental conditions (Boyce et al., 2012), for example by altering the timing of harvests or the magnitude of the management. Despite evidence that harvest timing can have substantial effects on dynamics (Cid et al., 2014), the result of varying timing of harvest has not been extensively studied. Depending on the time it is performed, harvest can lead to highly complex dynamics (Tang and Chen, 2004), or population extinction (Cid et al., 2014). In addition, since diverse environments are common for many species, imposing upon the dynamics of populations and infectious diseases within them, successful management of host-parasite relationships also relies on how such diversity impacts the population (Parratt et al., 2016). Therefore, studying seasonal processes in host-parasite relationships is vital as it will enhance knowledge on best practises for disease management (Fisman, 2007). In determining the most appropriate management strategies for different host-parasite systems, we must ensure decisions are led using accurate models of host-parasite relationships, particularly if the disease is widely distributed, highly pathogenic (Duke-Sylvester et al., 2011) and occurring in a complex environment. Managing diseases in wild populations can be difficult, where detailed knowledge of both the species and the pathogen is essential (Wobeser, 2002). Hence, an optimal control strategy can only be achieved if the host-parasite system is fully understood.

Since seasonality has long been recognised as important in determining population and disease dynamics (Soper, 1929), and seasonality affects multiple traits in

host-parasite relationships (Cable et al., 2017), we deem it important to consider multiple seasonal processes in our models. The inclusion of external periodic forcing into an SIR-type model, in addition to the possibility of seasonal harvest, will have an impact on the resulting dynamics. The interplay between forcing functions, in terms of both their timing and amplitude can excite changes (Greenman and Pasour, 2011). Such changes will also depend on the type of forcing, i.e. whether it is internal to the system (for example birth rates, transmission, death), or whether it is external (for example, human-initiated activities such as culling, or vaccination). Using multiple external forcing, we aim to more accurately represent host-parasite systems, and explore how they interact to produce different dynamics. We explored multiple internal forcing functions acting on host-parasite systems in chapters 2 and 3. In chapter 2 we explored a host-parasite system using an SIR model, and in chapter 3 we extended this to consider the possibility of environmental transmission. In this chapter, we add an external forcing function to our previously developed models to represent a harvest strategy.

The impact of seasonally harvesting in a host-parasite system with multiple other seasonal processes has not, to our knowledge, been investigated. Here we seek to determine how harvest strategies can be used to regulate a population with both seasonal births and seasonal transmission of an infectious disease, and explore other impacts that different harvest strategies can have on both the host population and the disease dynamics. We will aim to find a harvest strategy that maximises the population of susceptible members, minimises infection and produces a high yield. We explore variations of the classic SIR models developed by Anderson and May (1981). Our models are deterministic and in continuous-time, with seasonality in both the birth and transmission rates. We consider a population subject to density-dependent constraints in the death rate, and a disease from which it is not possible to recover. The host population is assumed to be well-mixed, that is, there is no age or sex structure considered. Harvest strategies come in the form of time-dependent functions, where we will particularly look at how the timing of harvest in relation to the seasonal births and transmission impacts disease dynamics.

§ 4.2 The Model

Our model is of an SI form; we are considering a population subject to a fatal infectious disease, appropriate for diseases such as Bovine Spongiform Encephalopathy (BSE) (Anderson et al., 1996), Chronic Wasting Disease (CWD) (Miller and Conner, 2005), and Transmissible Mink Encephalopathy (TME) (Imran and Mahmood, 2011). We define the system of ordinary differential equations depending on whether the harvest season is active or inactive. The equations governing our population dy-

namics are:

$$\frac{dS}{dt} = b(t)N - \beta(t)SI - (d + qN)S - h(t)S \tag{4.1}$$

$$\frac{dI}{dt} = \beta(t)SI - (d + qN + \alpha)I - h(t)I \tag{4.2}$$

where $h(t)$ defines the harvest season with

$$h(t) = \begin{cases} h_0 & \text{if } n.s < t < n.r, \\ 0 & \text{otherwise.} \end{cases} \tag{4.3}$$

The increase to the death rate caused by harvest during the defined period, which we will call for ease the *harvest rate*, is given by h_0, whilst s represents the start date of the harvest season, r the season end date and $n \in \mathbb{N}$ the year of harvest. This form of harvest can be described as a *constant effort* harvest. During the defined season individuals are removed with a constant rate, where larger populations will see greater removal as interactions between the hunter and the hunted are more likely. We could think of this harvest being performed by the same hunter sitting in the same place every day during the harvest season. In 4.1 and 4.2, $b(t)$ describes the seasonal birth rate, $\beta(t)$ the seasonal transmission (due to, for example, seasonal social gatherings), d the natural per capita death rate, α the disease-induced death rate (or virulence) and q our density-dependent crowding constraint on the death rate. We assume that it is not possible to target harvest only on infected population members, and thus the harvest strategy applies equally to both susceptible and infected individuals. The seasonal transmission rate is of the form:

$$\beta(t) = \beta_0(1 + \beta_1 \cos(2\pi(t + \beta_2))) \tag{4.4}$$

with β_0 the baseline transmission rate, β_1 the amplitude of seasonality and β_2 determining the timing of the cosine peak. Similarly, the birth rate $b(t)$ is seasonal and is of the form:

$$b(t) = b_0(1 + b_1 \cos(2\pi(t + b_2))) \tag{4.5}$$

with b_0 the baseline birth rate, b_1 the amplitude of seasonality and b_2 the timing of peak births.

The natural death rate of our population is assumed to have a density-dependent constraint acting upon it. Such increases to natural death rate can be a consequence of over-crowding in a population with perhaps competition for limited food resources, small sized areas in which to inhabit, or rivalries for attracting a mate. Inclusion of the density-dependent term in the death rate has been used in numerous studies of wildlife populations including those by Anderson and May (1981), Greenhalgh (1990) and Hosseini et al. (2004). Our transmission is considered to be direct; we rely upon contact between susceptible and infected population members for disease to spread. As we are considering the impact of harvest on a wildlife population, the transmission is density-dependent; as population size increases, so too

Table 4.1: Initial parameter values.

Parameter	Description	Baseline
b_0	baseline birth rate	2
b_1	amplitude of birth	0.9
b_2	timing of birth peak	$\frac{6}{12}$
β_0	baseline transmission rate	1
β_1	amplitude of transmission	0.9
β_2	timing of transmission peak	$\frac{11}{12}$
d	natural death rate	1
α	disease-induced mortality	7
q	density-dependent control	0.015
h_0	harvest factor	varying
s	start date of harvest	varying
r	end date of harvest	varying
S_0	initial susceptible	90
I_0	initial infected	10

does contact rates between population members. This assumes that the population is well-mixed, i.e. individuals are equally likely to interact with one another at any time during the year, be it during breeding, foraging, socialising etc..

To avoid additional complexity in the analysis we fix the birth and transmission seasons, and their rates. For this we assume breeding and social gatherings are out of phase, which is common for many free-ranging wildlife populations (see, for example, Altizer et al. (2004), Helm et al. (2006) and Gilg et al. (2012)) and fix $b_2 = 6/12$ and $\beta_2 = 11/12$ so that transmission peaks five months after the peak of births. This reflects newborns entering a population whilst the group is more spread out, with transmission rising as individuals start to gather more after breeding has taken place. In chapter 2, figure 2.5a indicates that no matter the initial population conditions, dynamics will repeat on a biannual cycle for the given set of initial parameter values. So although the dynamics are not the most stable, we do know that initial conditions will not change the cycle length in the absence of harvest. In this work we explore how changes in harvest strength and timing impact the population and disease dynamics. We will make changes to the start and end dates of the harvest season, and alter the abundance of the population harvested during such a season. As in previous work, numerical simulations are performed using Matlab (*MATLAB version R2018a*), and we implement the *ode15s* solver.

§ 4.3 Results

Assuming the population is not harvested at any time, dynamics of disease repeat every two years (figure 4.1a, confirming the result from figure 2.5a in section 2.3).

These biennial dynamics see a year with proportionally high numbers of infection one year, followed by a smaller infection level the year after.

4.3.1 Harvest Strength and Timing

To explore the impact of changing harvest strength, we fix parameters as in table 4.1 and set $s = 10/12$, $r = 12/12$ in the first instance, so that harvest coincides with the peak transmission time, i.e. when the population is gathered together more densely, making a harvest easier to perform. In figure 4.1 we can see the effect of different harvesting strengths on the population of susceptible and infected individuals. Since harvest is occurring when infected numbers are near their lowest values, and susceptible members near their highest, this harvest strategy is mostly removing susceptible individuals. We notice in the first instance that the strength of harvest determines the occurrence of epidemics; with no harvest we have biennial dynamics, yet when $h_0 \in [1, 3, 4, 5]$ (4.1b and 4.1d - 4.1f), dynamics of disease repeat annually. For $h_0 = 2$ (4.1c), dynamics repeat every three years where there are two years of low infection followed by a year with a larger outbreak, and when $h_0 = 6$ (4.1g) the whole population goes to extinction. This strategy therefore, if not performed correctly, could have a detrimental effect to a population since under or over harvesting could cause the dynamics to change to a non-annual cycle, or indeed eradicate the entire population. Additionally, we notice that the maximum number of infected individuals is similar when either we have no harvest, or when $h_0 = 2$. Having said this, harvesting at rate $h_0 = 2$ gives a higher number of susceptible individuals every third year than the maximum achieved with no harvesting. Therefore, although the strategy is less stable, being on a three-year cycle, we can observe greater numbers of healthy (susceptible) individuals in certain years.

A bifurcation diagram (figure 4.2a) shows the changes in disease cycles as h_0 is varied from 0 to 5. We can see regions close to $h_0 = 2$ and $h_0 = 3$ where dynamics become less-stable and can change the length of epidemic cycles (red line) with fixed initial conditions, but a mathematically stable annual cycle exists throughout (black line) despite the even more complex cycles that can emerge around $h_0 = 0.5 - 1$. Therefore these dynamics are clearly dependent on initial conditions as the bifurcation diagram shows that we have multiple stable attractors (we can switch from one regime to another very quickly depending on the initial conditions). An example of such a switch is shown in figure 4.2b, where an addition of 10 susceptible members to the population at time x alters dynamics from a stable annual cycle to a more complex cycle (eventually settling to a six-year regime), with harvesting performed at rate $h_0 = 1$. This helps to show the bi-stability in the model, whereby a small change in population size can lead to quite different dynamics. We note here that we explored other changes to the populations, and these also disrupted the stable annual cycle. For example, when removing 10% of the population, we see a change to a complex regime which settles back to an annual cycle after approximately 20 years. The addition of 5 susceptible members also caused the annual cycle to

alter, displaying complex dynamics for 25 years before settling back to an annual regime. In computing the bifurcation, we sampled dynamics at annual intervals. The figure suggests that the branches between $h_0 \approx 1.2$ and $h_0 \approx 1.75$ will join up, but we do not see these in the bifurcation due to the basin of attraction being very small, and the way in which we have sampled the dynamics. To show the possibility of these branches meeting, we tested alternative initial population conditions at harvesting rate $h_0 = 1.5$. Computing 99 iterations, with $S_0 + I_0 = 50$ and $S_0, I_0 \in [0.5 : 0.5 : 50]$, our pie chart displayed the existence of three-year disease cycles for certain sets of initial conditions (see figure 4.3). Therefore, this work suggests that non-integer combinations of initial population conditions are required for such dynamics to occur, and we have a small basin of attraction for these dynamics since they are not observed in the bifurcation diagram, where we sample only integer initial conditions.

Using these two plots, we can see the two benefits of keeping on an annual cycle; dynamics are predictable and infection is kept low. We explore the impact of changing initial population conditions in figure 4.4 where here we can see that dynamics can be dependent on the initial abundances of susceptible and infected individuals. The pie charts show the resulting periodic cycles after running the model for transient time using 100 different starting conditions, $S_0, I_0 \in [1, 99]$ with $S_0, I_0 \in \mathbb{Z}$ and $S_0 + I_0 = 100$. For $h_0 = 3$ and $h_0 = 4$, dynamics of disease will always be annual, regardless of the initial population conditions. However when $h_0 = 1$ or $h_0 = 2$, the initial abundances of susceptible and infected individuals determine the cycle observed. With $h_0 = 1$ dynamics either repeat annually or every six years, where the latter is the dominant cycle. When $h_0 = 2$, disease reoccurs either annually or every three years. In terms of management therefore, it would be advisable to steer clear of harvesting around certain values to avoid unintentionally changing the dynamics and it is imperative that initial population abundances are known. In general, though, as h_0 increases infection levels decrease, and from $h_0 = 6$ infection (and in fact the whole population) is eradicated.

To help visualise how increasing h_0 is impacting the population dynamics, we compare the strategies $h_0 = 1$ and $h_0 = 3$. In figure 4.5 we can see the population dynamics of susceptible individuals in 4.5a and infected members in 4.5b where parameters used are those in table 4.1. As the harvest season begins, the susceptible population has just reached its peak. The impact of h_0 is seen in the decline of susceptible members, where the increased strength of $h_0 = 3$ causes a sharper decline in the susceptible population than when $h_0 = 1$. This larger decline causes the abundance of susceptible members to be lower immediately at the end of the harvest season for $h_0 = 3$. This decrease in the size of the population will lead to a decrease in the death rate (due to our density dependent constraints, whereby death rate increases with a larger total population size). In addition, this smaller susceptible pool will produce fewer infections since the transmission rate is defined by βSI. Together, this means that a slower rate of decline is observed as infection builds from

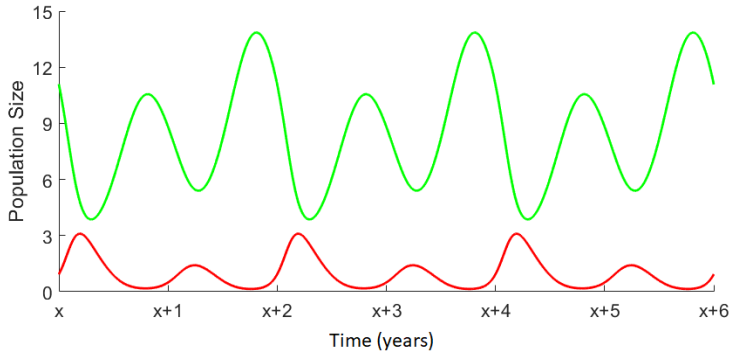

(a) $h_0 = 0$

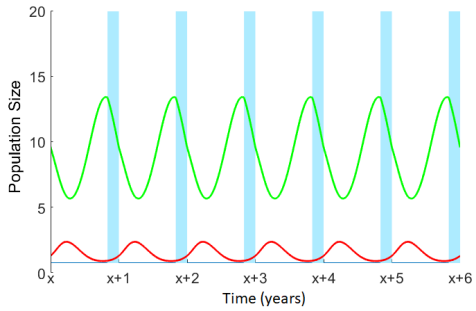

(b) $h_0 = 1$

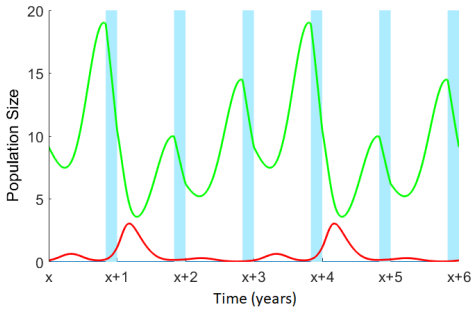

(c) $h_0 = 2$

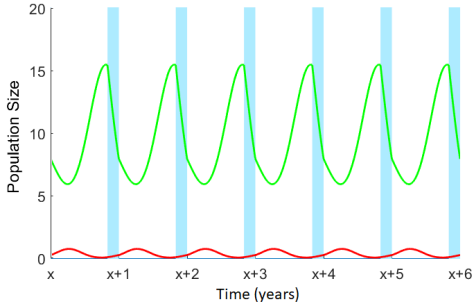

(d) $h_0 = 3$

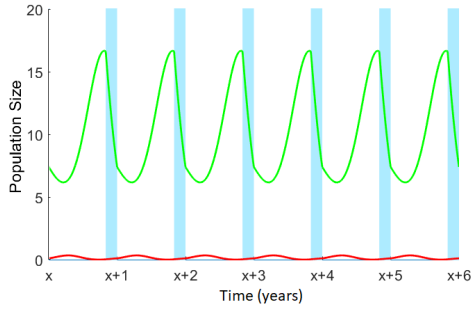

(e) $h_0 = 4$

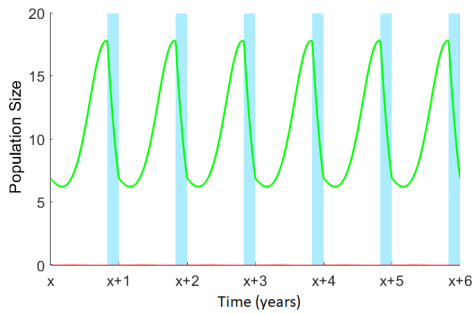

(f) $h_0 = 5$

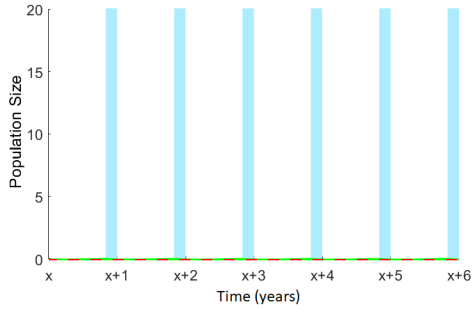

(g) $h_0 = 6$

Figure 4.1: Population dynamics of susceptible (solid green line) and infected (red dashed line) individuals under different harvesting strategies. The shaded regions indicate the timing of the two-month harvest season.

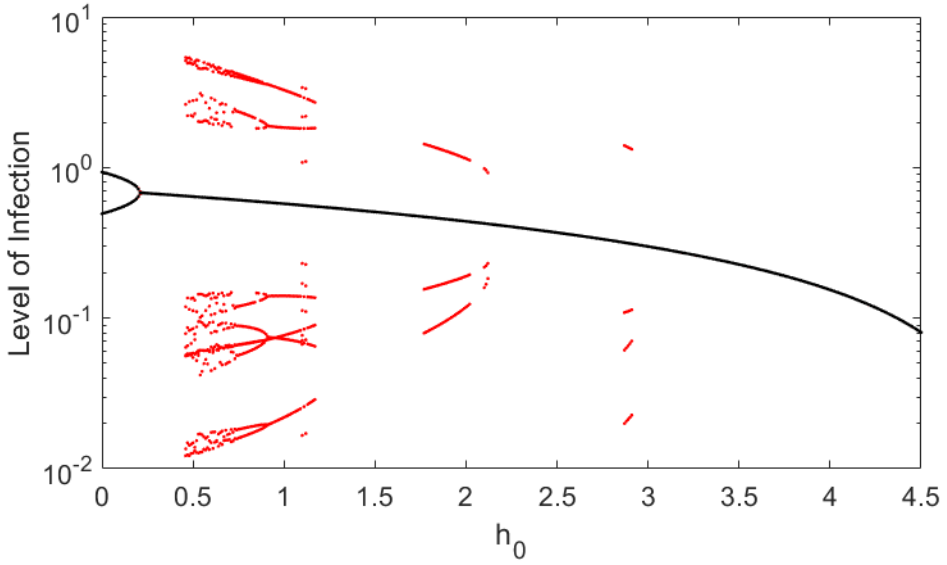

(a) Bifurcation diagram showing the different population cycles observed whilst varying h_0 when $s = 10/12, r = 12/12$. The black line shows the stable cycle existing throughout, whilst the red line shows the possibility of changing cycle lengths from multiple stable attractors.

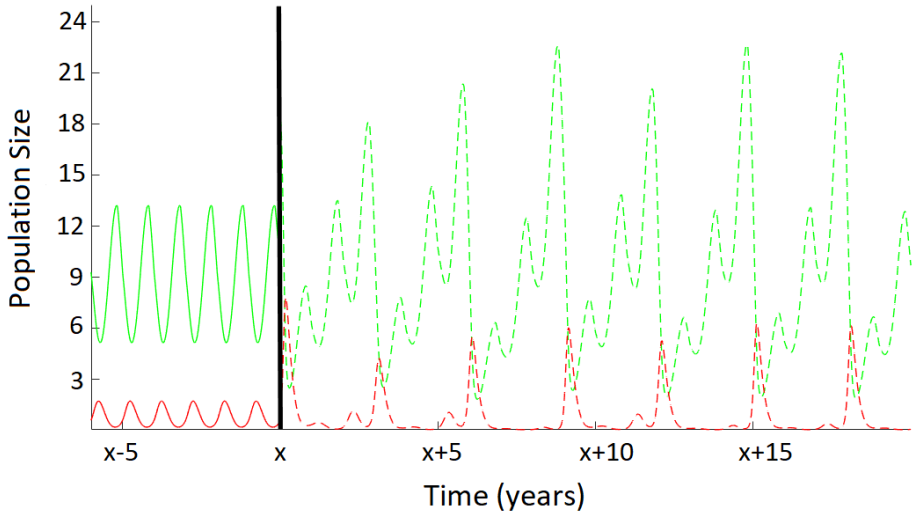

(b) How population dynamics can rapidly change as a result of adding 10 susceptible members into the population at time x, where $h_0 = 1$, $s = 10/12, r = 12/12$ and other parameters as in table 4.1. Green shows susceptible, and red infected, population members.

Figure 4.2

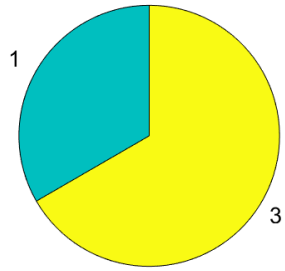

Figure 4.3: Pie chart to indicate the possibility of both annual and three-year cycles for different initial conditions $S_0 + I_0 = 50$ and $S_0, I_0 \in [0.5 : 0.5 : 50]$. Other parameters are as specified in table 4.1 with $h_0 = 1.5$, $s = 10/12$, $r = 12/12$.

the transmission season. Now the susceptible population is larger at its minimum value when $h_0 = 3$ compared with its minimum when $h_0 = 1$ due to this decrease in death rate. Hence when $h_0 = 3$ there are more susceptible members going into the breeding season, and thus as birth rate increases, the susceptible population builds to a greater abundance in the case of higher harvesting rates. In this case, it is also true that the lower numbers of infected individuals leads to a decreased reduction to the susceptible pool. In the infected population the harvest season begins as infection is rising; a consequence of both the maximised susceptible population and the increasing transmission rate. Stronger harvest, therefore, slows the growth rate of infection during the harvesting season leading to smaller numbers of infected members once the season has ended. This, along with the smaller abundance of susceptible members as explained above, means that when $h_0 = 3$ infection cannot rise as much as when $h_0 = 1$. Therefore the harvesting is both limiting infection in the population (figure 4.5b) whilst increasing the abundance of susceptible members (figure 4.5a).

4.3.2 Alternative Harvest Timing

Though harvesting at different times may be more complicated to perform as individuals are less densely populated, it is important to explore whether a different strategy could lead to more optimal results. Can performing harvesting at a different time lead to infection extinction with a lower harvesting rate? Can we maximise the proportion of susceptible members at any one time? We explore this below.

In figure 4.6 we present bifurcations for harvesting during different times of the year, where we have used initial conditions as specified in table 4.1. From the bifurcations we can see that our original strategy of harvesting during the peak transmission season (figure 4.2a) displays slightly more stable dynamics, indicated

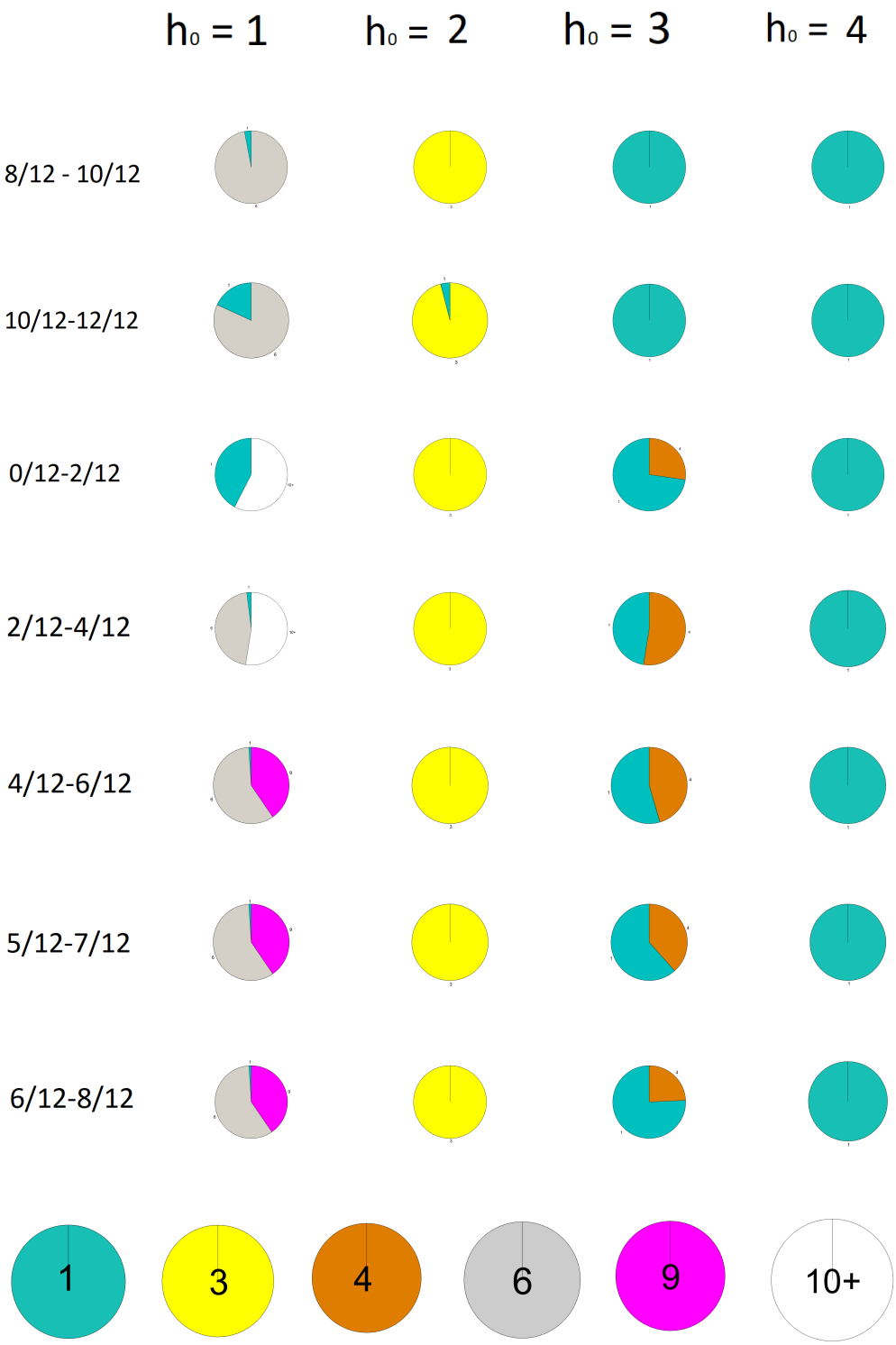

Figure 4.4: Pie charts indicating the likelihood of different dynamics for each of the harvesting strategies at the four harvest rates $h_0 = 1, 2, 3, 4$. The rows represent each simulated harvest strategy, where for example, $8/12 - 10/12$ indicates the harvest begins in month 8, and ends in month 10.

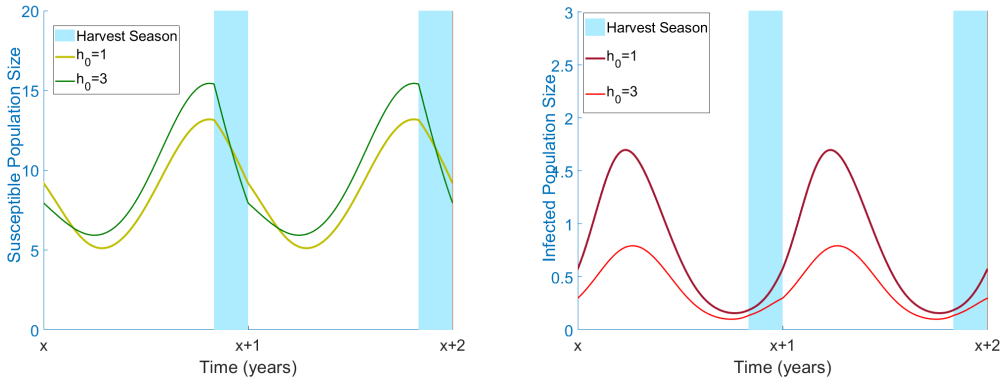

(a) (b)

Figure 4.5: Comparing the strategies of harvesting $h_0 = 1$ and $h_0 = 3$. In (a) we compare the susceptible populations and in (b) the infected populations.

by the smaller areas of chaotic and non-annual dynamics, whilst the new strategies presented show a wider range of possible dynamics, depending on initial conditions. We are most likely to alter dynamics to a highly complex, or even chaotic, cycle for a harvest from $s = 0/12$ to $r = 2/12$, or, $s = 2/12$ to $r = 4/12$, of which the latter time coincides with the peak infection levels in the system in the absence of harvest. We note here that *peak transmission* and *peak infection* should not be confused: *peak transmission* occurs at the value of β_2 where population members are gathered more closely together, and *peak infection* levels in the population occur later as a consequence of the peak transmission season increasing the likelihood of susceptible individuals becoming infected. The other harvesting strategies presented show largely similar dynamics, and all eventually eradicate the disease for higher values of h_0. The bifurcation diagrams show again that a stable one-year cycle exists throughout, so again we remind ourselves that dynamics are dependent on initial conditions. We also note here that varying the timing of harvest does not appear to have a significant impact on the quantitative elements of the model, i.e. infection levels are similar no matter when the harvest season occurs. It is the complexity of disease dynamics that display greater changes for the different harvesting seasons. We computed these bifurcations taking samples at yearly intervals. We also found the same results held for computations at six-month sampling intervals.

These findings are re-iterated by the pie charts shown in figure 4.4, where we show the likelihood of dynamics for each harvesting rate in each scenario where the occurring dynamics are dependent on the initial population conditions. As in chapter 2, the displayed pie charts indicate which k-period cycle occurs for different starting conditions. In this figure, there are 99 sets of initial conditions used in simulation, where $S_0, I_0 \in [1, 99], S_0 + I_0 = 100$ and $S_0, I_0 \in \mathbb{Z}$. Using these pie charts, we can see how the different harvesting strengths impact dynamics. For $h_0 = 2$ dynamics

are always triennial, no matter the initial conditions, and for $h_0 = 4$ the dynamics are always annually repeating. Thus in these cases, it is the harvest strength and it's potential interaction with other seasonal parameters that drive the behaviour of the system. When either $h_0 = 1$ or $h_0 = 3$ however, the initial population conditions have an impact on the resulting population dynamics observed. For $h_0 = 3$ we either observe annual or four-year cycles, though for harvesting from $s = 8/12$ to $r = 10/12$ dynamics are only ever annual. Our most complex observed behaviour occurs for the smaller harvesting rate of $h_0 = 1$. Depending on the timing of harvest and the initial population conditions, we can observe annual, six, and nine year cycles, and also cycles exceeding ten years in length. With this information in mind, it would be crucial to avoid harvest at and around this rate since it can cause dynamics to become highly complex. An example of these complex dynamics can occur for harvesting from $s = 2/12$ to $r = 4/12$ with rate $h_0 = 1$. In figure 4.7a we show a 20-year time-course, where it is clear that dynamics are not on a cycle of less than ten years in length, and by plotting the phase-plane of the $S - I$ dynamics (figure 4.7b), it is evident that our dynamics are repeating every 12 years. We note that these plots display a very strong three-year signal in the dynamics. Using a Fourier plot, we can show the strength of this triennial signal (figure 4.7c) and using this we can conclude that our dynamics are not quasi-periodic, since the strong signals occur at integer values, and that the triennial cycle is indeed dominant.

The results from the pie charts suggest that a higher harvesting rate of $h_0 = 4$ will be the most effective in controlling occurrence of dynamics, but it is imperative to ensure that this harvest rate also achieves our other aims (as outlined in section 4.1), principally minimising infection and maximising the number of susceptible individuals.

We now fix our initial conditions at $S_0 = 90$, $I_0 = 10$ and show in figure 4.8 the progression of how the maximum number of susceptible individuals and the maximum proportion of infected individuals changes as we increase the harvesting strength h_0 for the different times of harvesting. After running the model for transient time (in this case 1000 years, ensuring dynamics have settled to their equilibrium state), we record the maximum susceptible abundance and the maximum infected proportion during one further disease cycle. This allows us to observe how high the population numbers reach during the disease cycle, and what proportion of the population is infected at the peak of an outbreak. With this information, we can clearly see if harvest strength or timing, or a combination of the two, can help to reduce maximum infection levels and/or increase healthy population numbers. For $h_0 = 1$ the timing of harvest does not have a significant impact on what happens to the maximum proportion of infection within the population during a cycle, nor the maximum number of susceptible individuals observed in each disease cycle. This matches with our findings above, where the harvest strength did not impact dynamics, it was the initial conditions controlling the epidemic cycles and hence population numbers. Infection levels and maximum susceptible members do

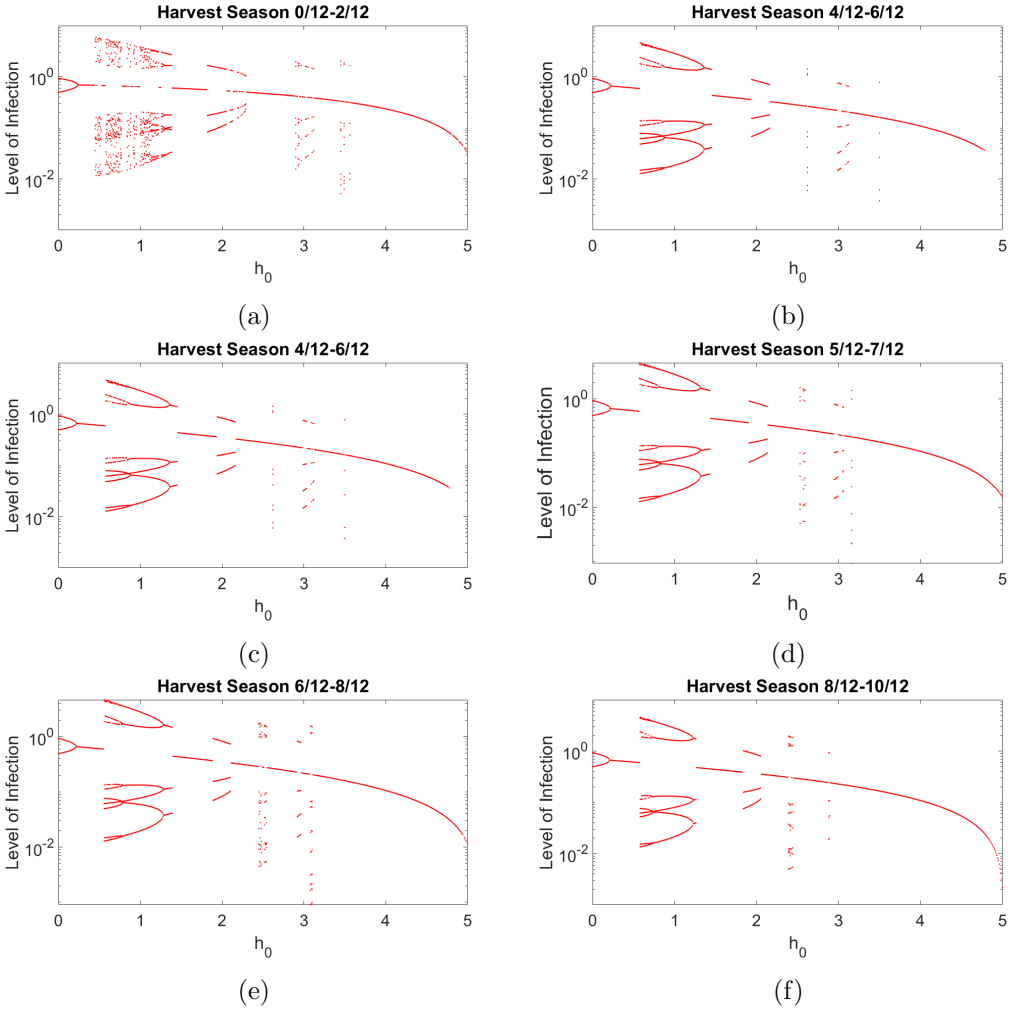

Figure 4.6: Bifurcations showing how changing h_0 impacts disease cycles for harvesting at different times during the year.

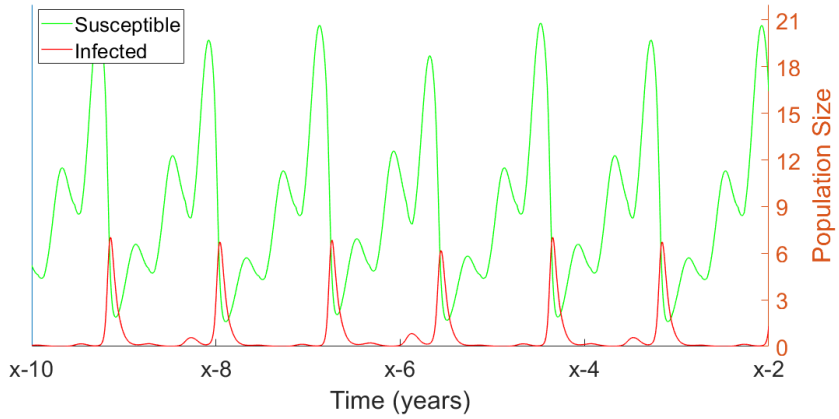

(a) Population dynamics after transient time for harvesting from $2/12 - 4/12$ at rate $h_0 = 1$.

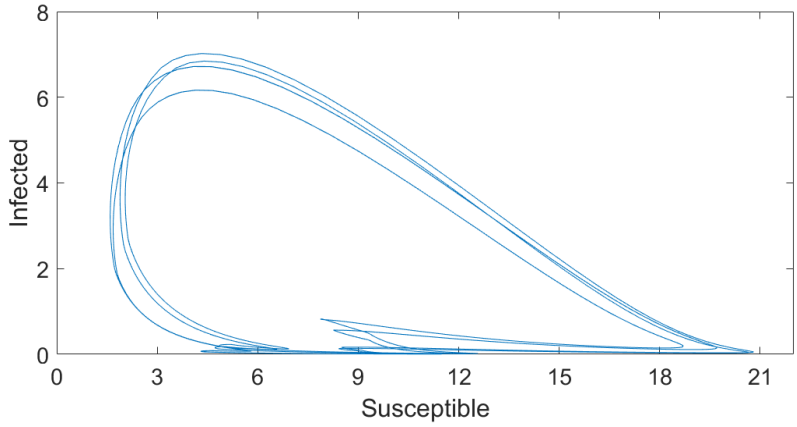

(b) Phase-plane for the dynamics of S and I.

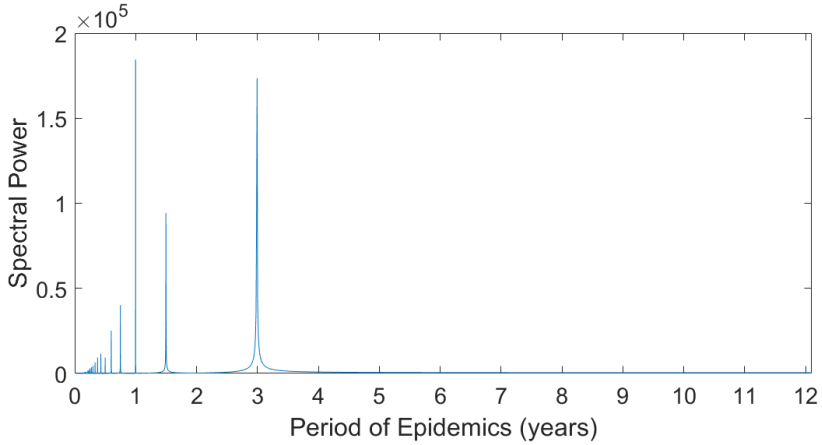

(c) Fourier signals indicating strength of different disease cycle lengths.

Figure 4.7

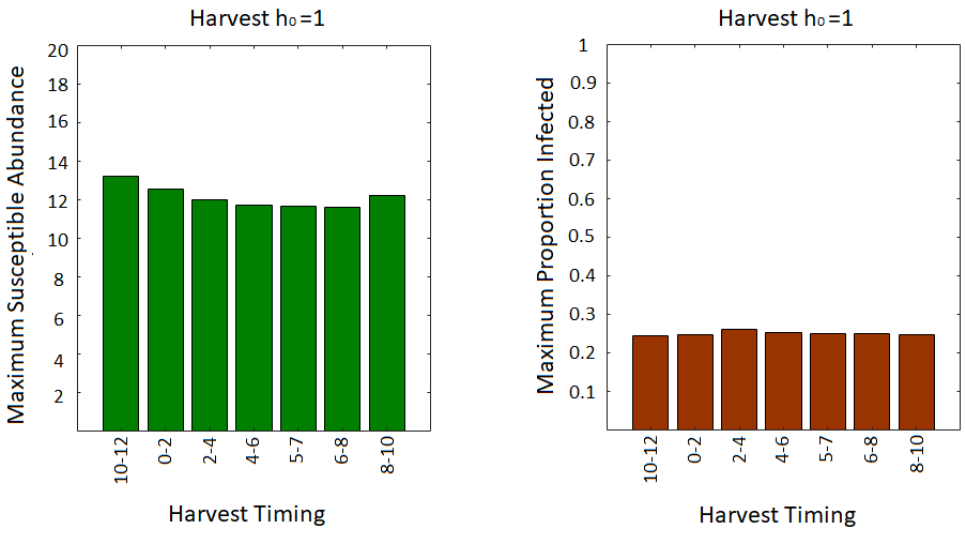
Harvest h₀ =1
Maximum Susceptible Abundance
20
18
16
14
12
10
8
6
4
2
10-12
0-2
2-4
4-6
5-7
6-8
8-10
Harvest Timing
Harvest h₀ =1
Maximum Proportion Infected
1
0.9
0.8
0.7
0.6
0.5
0.4
0.3
0.2
0.1
10-12
0-2
2-4
4-6
5-7
6-8
8-10
Harvest Timing

(a)

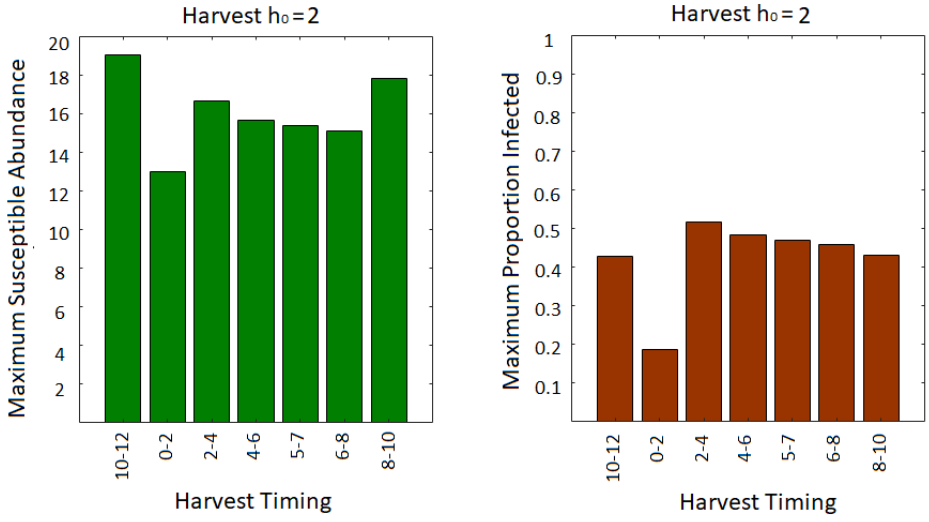
Harvest h₀ = 2
Maximum Susceptible Abundance
20
18
16
14
12
10
8
6
4
2
10-12
0-2
2-4
4-6
5-7
6-8
8-10
Harvest Timing
Harvest h₀ = 2
Maximum Proportion Infected
1
0.9
0.8
0.7
0.6
0.5
0.4
0.3
0.2
0.1
10-12
0-2
2-4
4-6
5-7
6-8
8-10
Harvest Timing

(b)

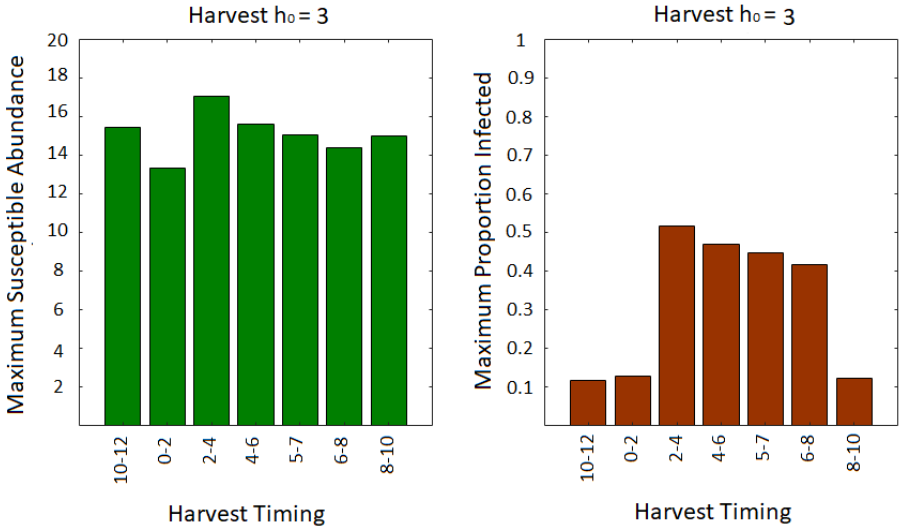
Harvest h₀ = 3
Maximum Susceptible Abundance
20
18
16
14
12
10
8
6
4
2
10-12
0-2
2-4
4-6
5-7
6-8
8-10
Harvest Timing
Harvest h₀ = 3
Maximum Proportion Infected
1
0.9
0.8
0.7
0.6
0.5
0.4
0.3
0.2
0.1
10-12
0-2
2-4
4-6
5-7
6-8
8-10
Harvest Timing

(c)

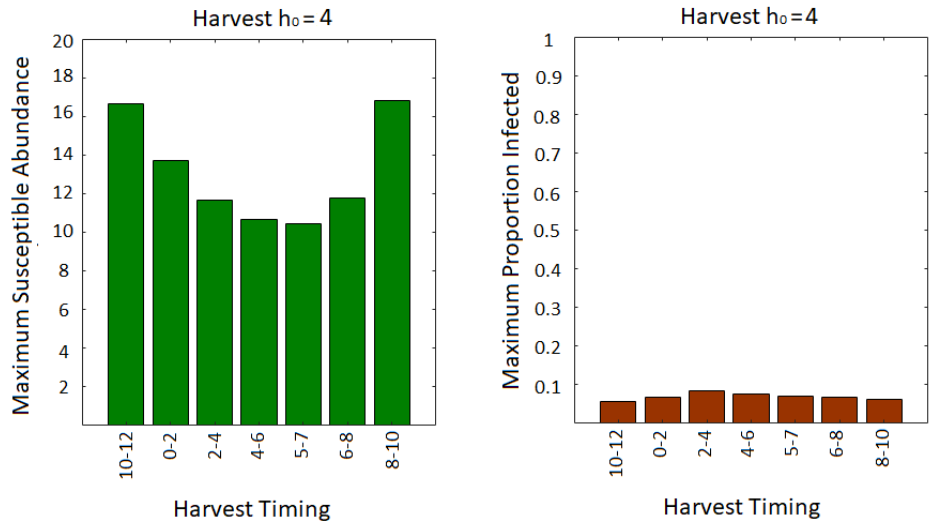
Harvest h₀ = 4
Maximum Susceptible Abundance
20
18
16
14
12
10
8
6
4
2
10-12
0-2
2-4
4-6
5-7
6-8
8-10
Harvest Timing
Harvest h₀ =4
Maximum Proportion Infected
1
0.9
0.8
0.7
0.6
0.5
0.4
0.3
0.2
0.1
10-12
0-2
2-4
4-6
5-7
6-8
8-10
Harvest Timing

(d)

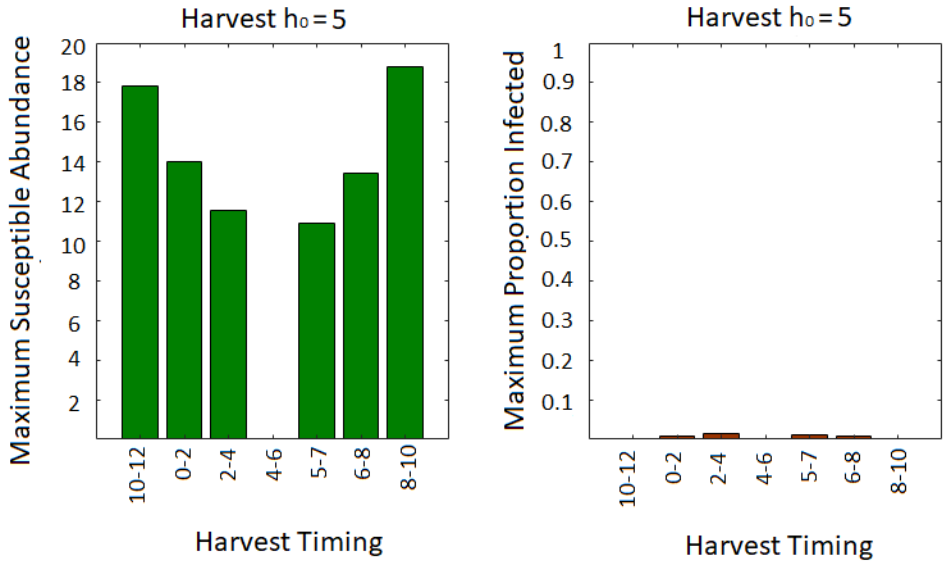

(e)

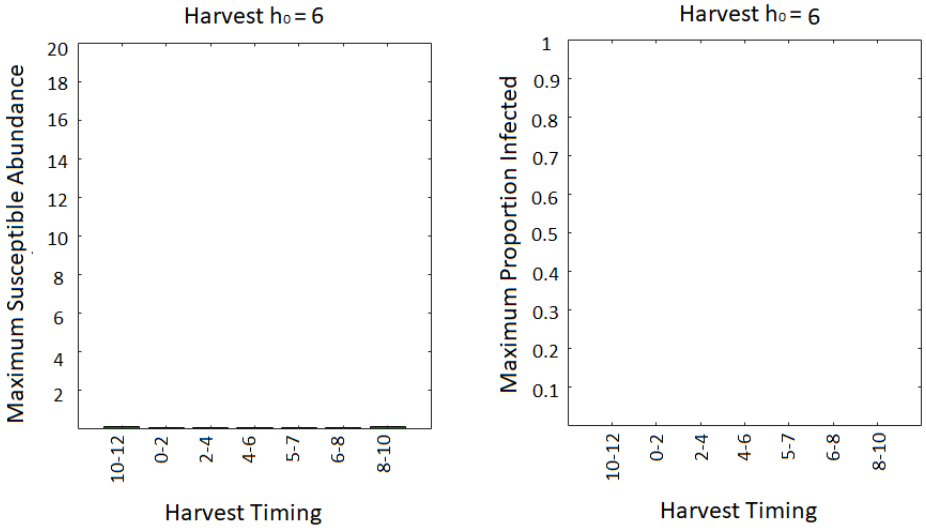

(f)

Figure 4.8: Maximum numbers of susceptible individuals, and the maximum proportion of the population infected, for different harvesting strengths and different timings of harvest. We record the maximum susceptible abundance and the maximum infected proportion during one disease cycle, once dynamics have settled to their equilibrium state.

not alter much when $h_0 = 2$, except for harvest timed between month 0 and month 2. Though this strategy decreases the infection, it also lowers the maximum abundance of susceptible members. When we have a harvesting strength of $h_0 = 3$ the abundance of susceptible members does not alter greatly between harvest timings, however the maximum infection proportion can significantly change depending on when harvesting occurs in the year. When harvesting from months $10-12$, $0-2$ and $8-10$ we are able to minimise infection in the population, making these strategies effective. Therefore, for these harvests with initial conditions $S_0 = 90$, $I_0 = 10$, we are in an annual regime, whilst for harvesting from $2-4$, $4-6$, $5-7$ and $6-8$ we are in a less stable four-year cycle as indicated is possible in figure 4.4. If $h_0 = 4$ all infection levels are low, meeting one of our principle aims. The maximum abundance of susceptible members changes depending on the timing of harvest, with months $10-12$ and $8-10$ giving us the highest number of these healthy individuals. We know that we are in an annual cycle here for all harvest strategies (figure 4.4), and so this confirms that the harvest rate $h_0 = 4$ is effective in meeting our management aims. The population dynamics when $h_0 = 5$ are significantly different depending on when the harvest occurs. The entire population is eradicated in harvesting between months $4-6$, whilst infection is lost and susceptible numbers are maximised when harvesting from months $8-10$ and $10-12$, making these ideal strategies. In the other cases we see good numbers of susceptible individuals and insignificant amounts of infection, making these also good strategies for meeting management aims. In all cases when $h_0 = 6$, both the susceptible and infected populations have been eradicated.

As identified in three of the six cases above, harvesting between months 8 and 10 appears to give effective results from the management whereby susceptible individuals are maximised and the infection proportion is minimised. This basic analysis suggests that harvesting shortly before the peak of transmission, therefore, could be as effective as harvesting during the peak transmission season. We note here that all simulations are carried out, in this case, for a fixed pair of initial population conditions. Therefore, having a detailed knowledge of population numbers is essential for performing an effective harvest.

4.3.3 Comparing Harvest Seasons $8-10$ and $10-12$

Figure 4.9 compares the susceptible and infected population levels for harvesting strength $h_0 = 3$ in the strategies where harvest occurs from months $8/12-10/12$ and $10/12-12/12$, again where we use the initial population conditions $S_0 = 90, I_0 = 10$. We must note here that these initial conditions ensure we stay on the more stable annual disease cycle when $h_0 = 1$, despite evidence from figure 4.4 that this is often not the case for this harvest scenario. In the first instance we can see clearly that the infected populations show very little difference in their dynamics and abundance. In the earlier harvesting scenario, the susceptible population undergoes removal whilst still building to its potential maximum following the peak birth season. The onset of

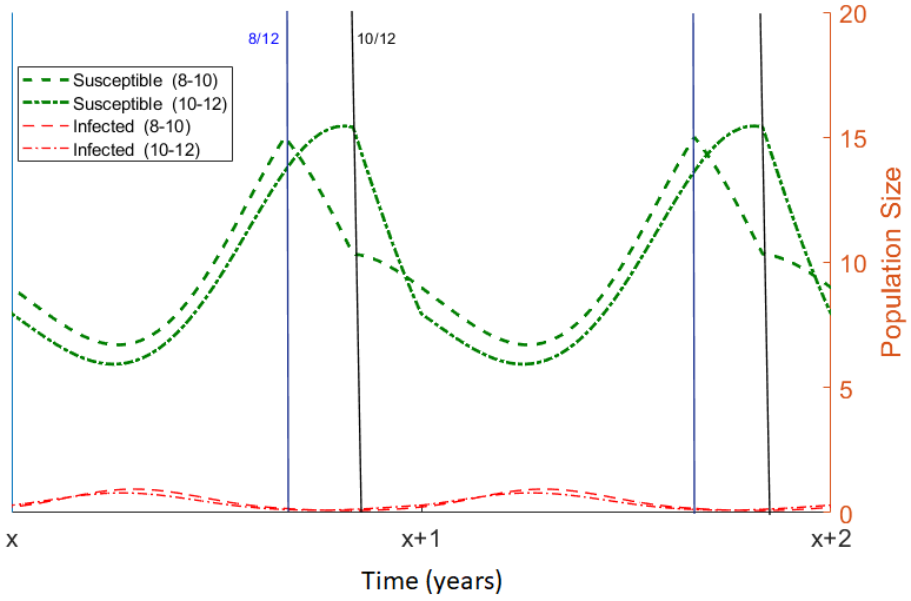

Figure 4.9: Comparing susceptible and individual population levels for harvesting strength $h_0 = 3$ when harvest is timed from $8/12 - 10/12$ and $10/12 - 12/12$ where the initial conditions used are those in table 4.1.

harvest leads to a decline in the number of susceptible individuals, which as described previously in section 4.3.1 will lead to a decrease in the death rate (due to density dependent constraints). The decline observed is not as sharp as that seen during the $10/12 - 12/12$ month harvest since transmission is still building during months $8 - 10$. These two factors mean a slower rate of decline in susceptible members is observed both during the harvest season and once the harvest season ends. This leads to a higher minimum susceptible population. However as harvest occurs before the susceptible numbers can reach their maximum, this value is slightly lower than that observed when harvest occurs from $10/12 - 12/12$. To further try to determine the more appropriate harvest strategy, we look at the numbers of the population that are harvested during each season. To do this, we created a 'harvested 'class, which counted the number of individuals removed due to the harvest parameters $h_0 S$ and $h_0 I$. We ran our simulation for transient time (1000 years) to ensure dynamics had reached a steady-state before counting the numbers harvested in the proceeding harvest season. In figure 4.10 we show the harvested population numbers in both the $8/12 - 10/12$ and $10/12 - 12/12$ month harvests for the five harvesting strengths $h_0 = 1, 2, 3, 4, 5$. As the harvest rate h_0 increases, the harvested population abundance increases at an approximately linear rate. We can see that harvesting from $8/12 - 10/12$ gives us a slightly higher yield in all cases, though the difference is again not significant. With these results in mind, it does not appear to matter significantly which harvest strategy, in terms of timing, would be best to take. From the results in figures 4.4, 4.8 and 4.10, a harvest rate of $h_0 = 4$ will give the best results in terms of minimising infection whilst maximising susceptible population numbers. If the harvest rate can be kept at $h_0 = 4$ to ensure the populations do not go to extinction or enter an alternative disease cycle, the decision on harvest timing may need to be made based on other factors such as resource availability or the seasonal environmental conditions.

4.3.4 Changing the length of the harvest season

We initially fixed a two-month window for our harvest season, so we now explore how a different approach in season length could impact dynamics of disease in the population. Exploring a season length of four months, we see that lower harvesting rates can be as effective as our higher harvesting rates from a two-month harvest season. When harvesting from $s = 8/12$ to $r = 12/12$, a rate of $h_0 = 2.5$ gives a maximum susceptible abundance of 17 individuals, and the harvest yields 11 individuals from the population over the course of the harvest season (see figure 4.11). This is similar to harvesting at rate $h_0 = 5$ for the two-month strategies $s = 8/12, r = 10/12$ and $s = 10/12, r = 12/12$. The result shows that, for this set of parameter values and initial conditions, we can double the season length and half the harvest rate for similar yield to be achieved. With the fixed harvest rate of $h_0 = 2.5$, comparing the four-month strategy to our $8 - 10$ and $10 - 12$ strategies explored in section 4.3.3 shows a marked improvement in yield and maximum numbers of susceptible

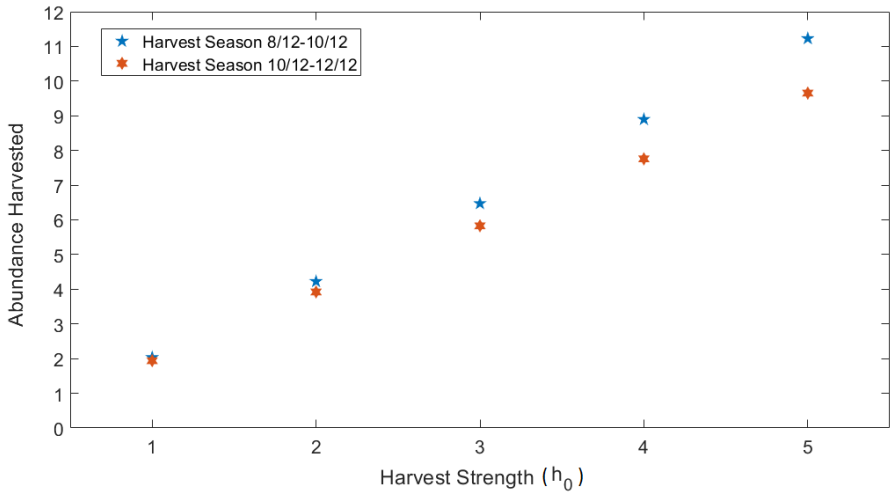

Figure 4.10: Comparing the numbers of population members harvested for different harvest rates when harvest is timed from $8/12 - 10/12$ and $10/12 - 12/12$ where the initial conditions used are those in table 4.1. Harvested numbers are counted over one season after dynamics have reached a steady-state.

population members, and we also observe a decline in infection levels. Figure 4.12 shows the comparison, highlighting how the four-month strategy compares to the two-month counterparts. Whilst there is little difference in the maximum susceptible abundance observed, both the maximum infected proportion and abundance harvested are more desirable for the longer harvest season as infection is eradicated and yield is high. A bifurcation diagram for the harvest rate h_0 in the four-month harvest season shows the possibility of alternative disease cycles (figure 4.13). Similarly to those bifurcations in figures 4.2a and 4.6f, figure 4.13 shows a consistent annual cycle is present with, though depending on initial conditions we may observe alternative dynamics, indicating the bi-stability of the system. These alternative dynamics are further noted by the pie charts in figure 4.14, where we show the different disease cycles observed for $h_0 = 0.5, 1, 1.5, 2$. Similarly to the results in 4.3.2, larger values of h_0 lead to the most stable dynamics with both $h_0 = 1.5$ and $h_0 = 2$ always giving annually repeating dynamics. Thus the harvest rate h_0 is dominant in controlling the disease cycle.

§ 4.4 Model with Environmental Transmission

In certain wildlife-disease systems, the omission of environmental transmission in models of host-parasite dynamics can lead to failing management strategies (Lange et al., 2016). With environmental transmission, controlling diseases can become more complicated. Removal of infectious material from the environment is likely

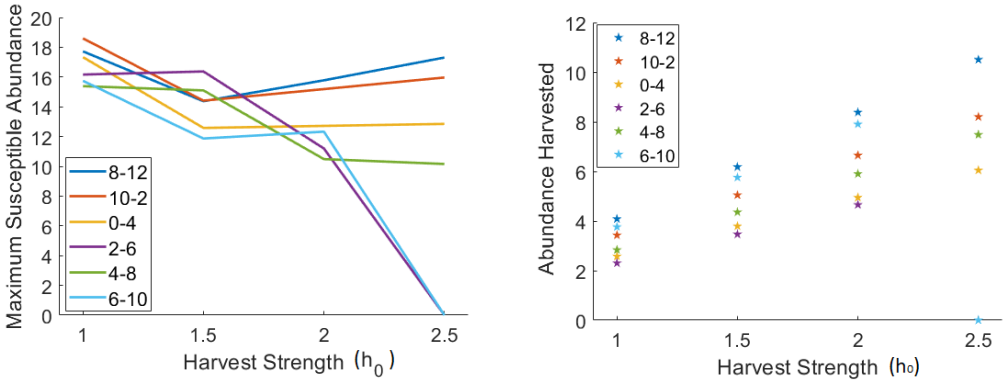

(a) (b)

Figure 4.11: (a) maximum susceptible abundance and (b) abundance harvested, for six different four-month harvesting strategies.

to be resource heavy and labour intensive, in both determining the existence of environmental infectious material, and performing its removal (Breban et al., 2009; Rohani et al., 2009). In this section we seek to investigate management strategies in a model where disease is able to pass to susceptible hosts through indirect environmental transmission, as well as directly from host-host.

Our model here is an adaptation of that used in chapter 3, where we have included a harvesting season. Our system is modelled by the following equations:

$$\frac{dS}{dt} = b(t)N - \beta(t)SI - (d + qN)S - \delta SD - h(t)S \tag{4.6}$$

$$\frac{dI}{dt} = \beta(t)SI + \delta SD - (d + qN + \alpha)I - h(t)I \tag{4.7}$$

$$\frac{dD}{dt} = (d + qN + \alpha)I + \epsilon I - uD \tag{4.8}$$

where $h(t)$ defines the harvest season with

$$h(t) = \begin{cases} h_0 & \text{if } n.s < t < n.r, \\ 0 & \text{otherwise.} \end{cases} \tag{4.9}$$

Parameters are as described in section 4.2 with the following additions: D represents an environmental reservoir of diseased material which includes the deceased infected population, and a proportion ϵ of living infected members (from excreted material). Susceptible individuals contract disease from the decay pool by direct contacts, with new infection occurring with parameter δ. Decaying material only stays infectious for a specified time, and is removed at rate u. In table 4.2 we give the baseline parameters rates used in the analysis. As in previous work, the numerical simulations are performed using Matlab (*MATLAB version R2018a*) with implementation of the *ode15s* solver.

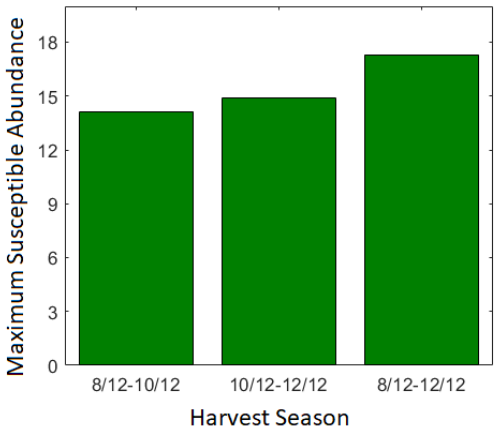

(a)

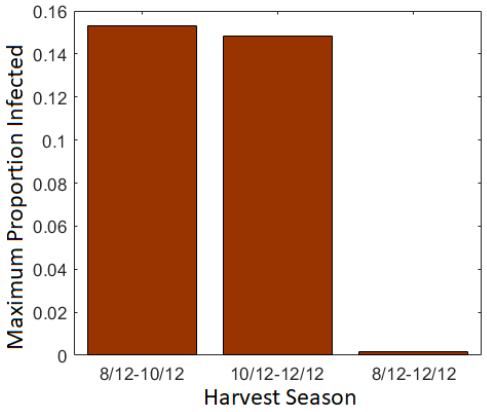

(b)

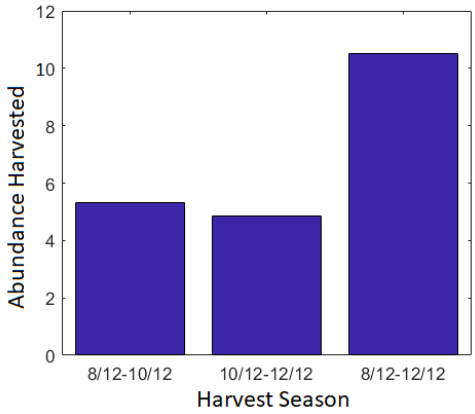

(c)

Figure 4.12: Comparing the different harvest seasons $8/12 - 10/12$, $10/12 - 12/12$ and $8/12 - 12/12$ when $h_0 = 2.5$. (a) maximum susceptible abundance, (b) maximum infected proportion and (c) abundance harvested.

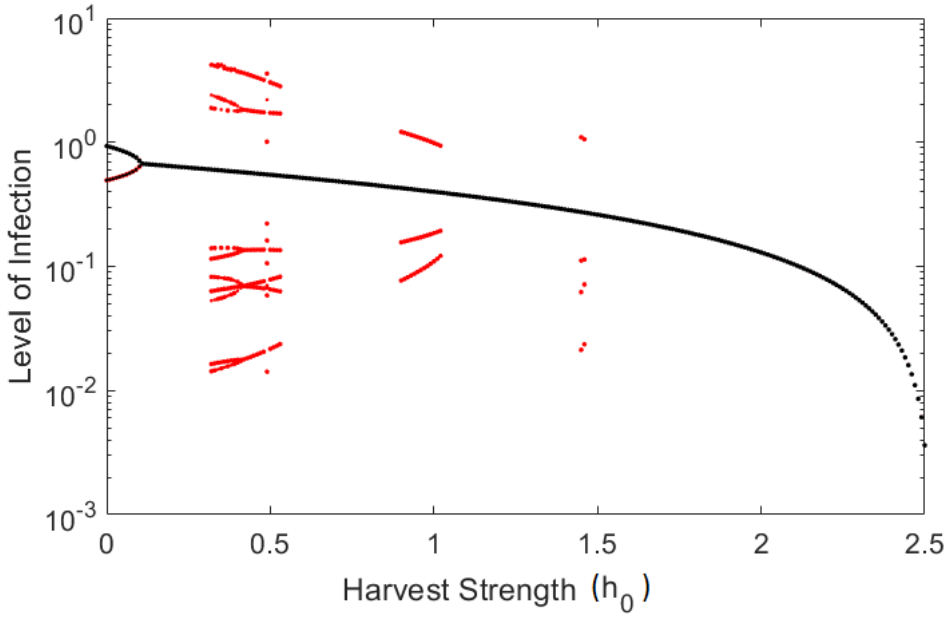

Figure 4.13: Bifurcation diagram indicating the changing disease cycles as h_0 is varied from 0-2.5, where initial conditions are specified in table 4.1.

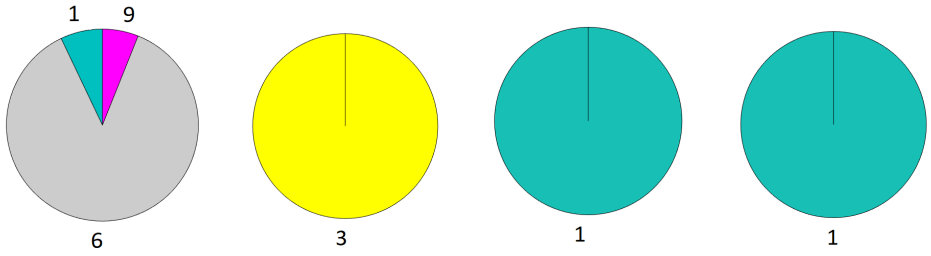

(a) (b) (c) (d)

Figure 4.14: Pie charts indicating the recurrence of disease for the longer harvest season $s = 8/12$, $r = 12/12$ in four harvesting strengths $h_0 = 0.5, 1, 1.5, 2$. Cycle lengths are indicated by colours; see figure 4.4 for colour key.

Table 4.2: Initial parameter values.

Parameter	Description	Baseline
b_0	baseline birth rate	2
b_1	amplitude of birth	0.9
b_2	timing of birth peak	$\frac{6}{12}$
β_0	baseline transmission rate	1
β_1	amplitude of transmission	0.9
β_2	timing of transmission peak	$\frac{11}{12}$
d	natural death rate	1
α	disease-induced mortality	7
q	density-dependent control	0.015
δ	transmission rate from environment	0.1
ϵ	excretion rate	12
u	death rate of decaying matter	6
h_0	harvest rate	varying
s	start date of harvest	varying
r	end date of harvest	varying

4.4.1 Results

In the absence of harvest, population dynamics repeat every three years, as seen in chapter 3, section 3.3. Figure 4.15 shows us the population and disease dynamics over a period of six years and with this we can see the triennial pattern where a larger disease outbreak occurs once every three years. We note that this applies for our specified set of parameter values and initial conditions, where other values could give alternative results. In addition, we must note that we have chosen the same values as in chapter 3, section 3.3, where the underlying model does not produce cyclic dynamics in the absence of seasonality. Therefore it is important to consider that the results definitely hold for this specific case only.

With the introduction of harvest, we can easily control disease outbreaks in effective ways. Assuming the two-month harvest season occurs during the peak transmission season ($s = 10/12$, $r = 12/12$), harvest rate does not need to be high for population dynamics to regulate to an annual cycle. Indeed, a harvest rate of $h_0 = 1$ leads to annual dynamics with a fairly low infection level upon outbreak (figure 4.16a). Increasing the harvesting rate to $h_0 = 5$ leads to the almost eradication of disease (figure 4.16b), and in figure 4.17 we can see that increasing the harvest rate both increases the susceptible population abundance and decreases the infection within the population, until we reach $h_0 = 6$ where the entire population has died. We must note again here that these results hold for the fixed set of parameter values used, and could change for alternative values.

A bifurcation diagram using fixed initial conditions (figure 4.18) of the dynamics

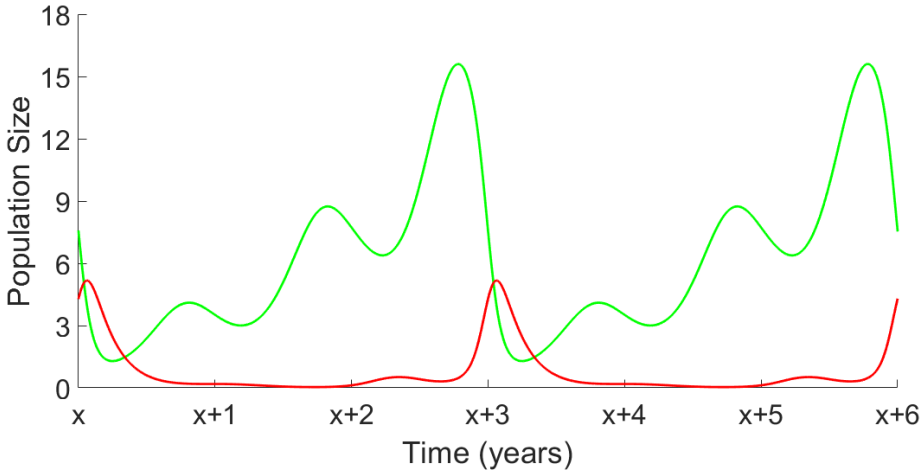

Figure 4.15: Population dynamics in the absence of seasonal harvesting with parameters as defined in table 4.2 over a six-year period.

as h_0 is varied from $0-5$ highlights our findings. We can see that a very small harvest leads to annual dynamics, and there is only a small region between $h_0 = 1$ and $h_0 = 2$ where the disease cycle changes; in this instance to a four-year cycle. The dynamics, therefore, remain fairly stable using this harvest strategy and we can achieve our aim to reduce infection whilst maintaining the susceptible population. This reflects our findings from chapter 3 in that, this $SIRD$ model with dual seasonality is in general more stable than the model from chapter 2. It is important to note here that we have used a fixed set of initial conditions for commencing the simulation; $S_0 = 90, I_0 = 5, D0 = 5$. We explored other initial conditions, and did not find any alternative disease cycles for integer values of h_0. For example, we computed the bifurcation diagram using extrapolated initial conditions (values dependent on the results of previous simulations), and additionally explored pie diagrams which showed only one-year cycles. Hence, we are confident in the dominance of this one-year cycle.

Similarly to section 4.3.2, we explore if other harvesting strategies can result in higher susceptible population numbers and lower infection levels with smaller harvesting rates. We explore harvesting strengths $h_0 = 2-5$ and in figure 4.19 results are displayed. We can see that for $h_0 = 3-5$ the strategies with $s = 8/12, r = 10/12$ and $s = 10/12, r = 12/12$ lead to the highest numbers of susceptible individuals at their maximum whilst also displaying low levels of infection. This is in-line with our results from section 4.3.2 with both strategies appearing equally effective in disease and population management. We see different results when $h_0 = 2$ (figure 4.19a). For our fixed set of parameter values, and initial population conditions, harvesting from months $0-2$ and $2-4$ give the highest numbers of susceptible

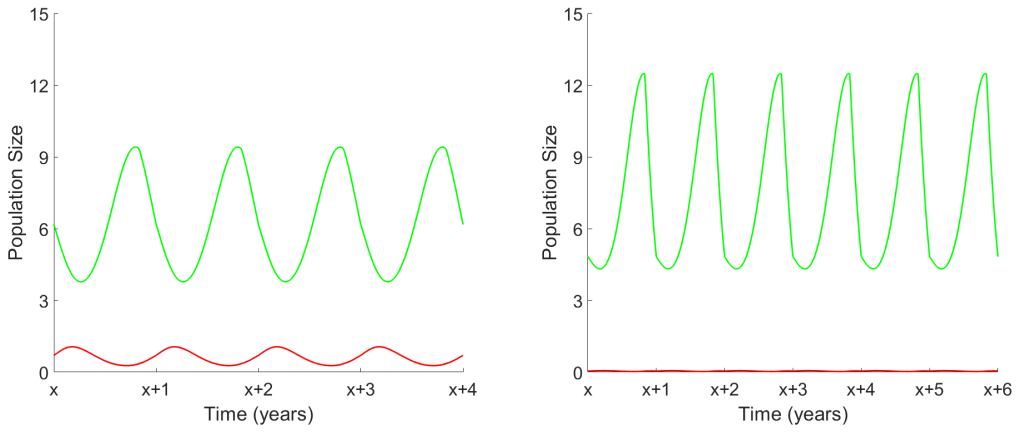

(a) (b)

Figure 4.16: Proportions of susceptible and infected individuals when (a) $h_0 = 1$, and (b) $h_0 = 5$ for $s = 10/12$ and $r = 12/12$.

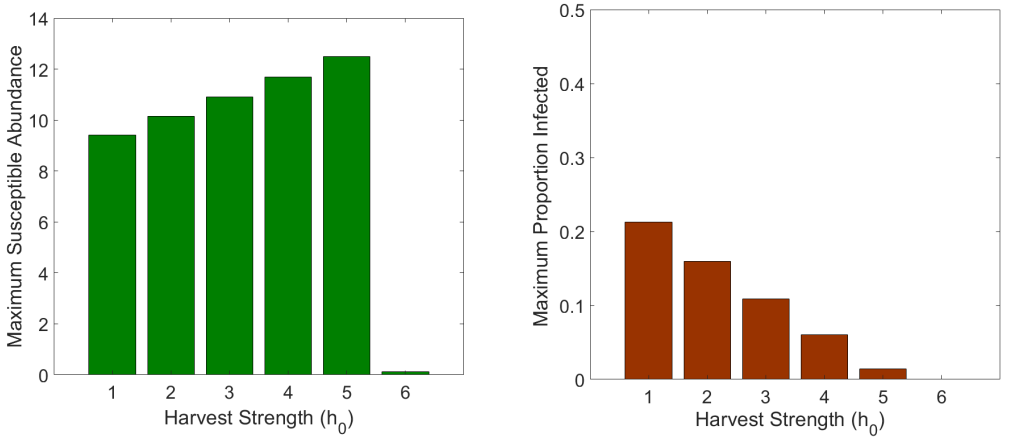

(a) (b)

Figure 4.17: (a) the maximum number of susceptible population members, and (b) the maximum proportion of infected individuals, for five different harvesting strengths when $s = 10/12$ and $r = 12/12$.

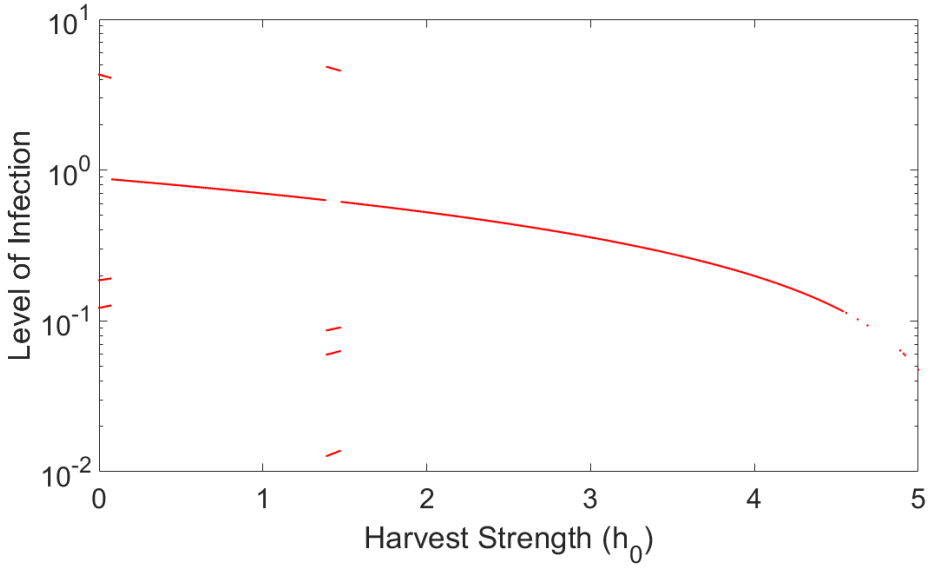

Figure 4.18: Bifurcation diagram of h_0 showing the changing disease cycle lengths when harvest occurs from $s = 10/12$ to $r = 12/12$, where initial conditions are specified in table 4.2.

population members. However, it must be noted that these cases also result in high maximum proportions of infection. This is due to the dynamics being in a non-annual cycle. We can check this through bifurcation diagrams of h_0 for each of the harvest strategies with $s = 0/12, r = 2/12$ and $s = 2/12, r = 4/12$. Figure 4.20 shows that when $h_0 = 2$ in both cases we do have dynamics on a non-annual cycle for our initial conditions specified in table 4.2, with these dynamics repeating every four years. These strategies are therefore less stable, and since infection can reach high levels every four years, they do not meet our aims despite also having high maximum numbers of susceptible members in the population. Thus again we see that harvesting just before, or during, the peak transmission season is likely to produce the best possible results from a population harvest.

4.4.2 Comparing harvest seasons 8/12-10/12 and 10/12-12/12.

As with the model in section 4.2, harvesting timed at either $s = 8/12, r = 10/12$ or $s = 10/12, r = 12/12$ appear to give the best results in terms of maximising the susceptible population and minimising infection. It is difficult to assert which method would be the most effective from our analysis conducted above, and so we look into the abundances of the population harvested during each season. Figure 4.21 shows the harvested population abundances for four different harvesting strengths $h_0 = 1, 2, 3, 4, 5$ in both of the harvest seasons $s = 8/12, r = 10/12$

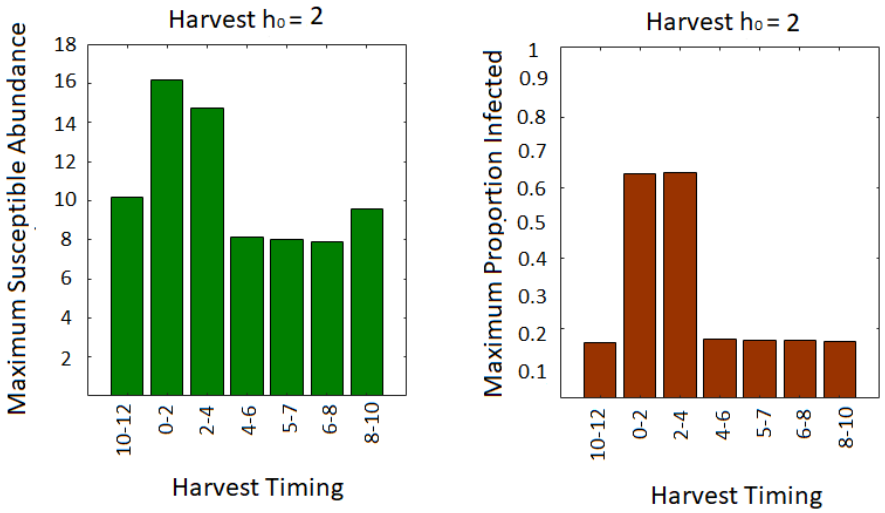
Harvest h₀ = 2
Maximum Susceptible Abundance
18
16
14
12
10
8
6
4
2
10-12
0-2
2-4
4-6
5-7
6-8
8-10
Harvest Timing
Harvest h₀ = 2
Maximum Proportion Infected
1
0.9
0.8
0.7
0.6
0.5
0.4
0.3
0.2
0.1
10-12
0-2
2-4
4-6
5-7
6-8
8-10
Harvest Timing

(a)

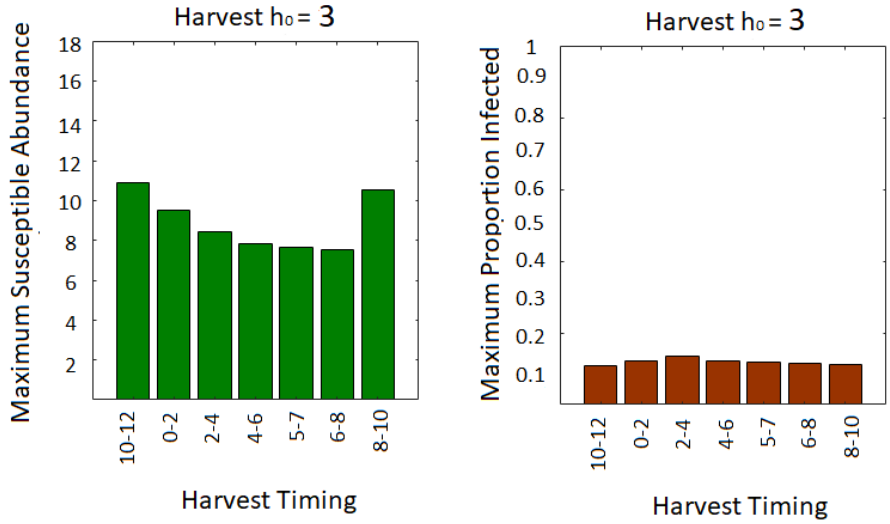
Harvest h₀ = 3
Maximum Susceptible Abundance
18
16
14
12
10
8
6
4
2
10-12
0-2
2-4
4-6
5-7
6-8
8-10
Harvest Timing
Harvest h₀ = 3
Maximum Proportion Infected
1
0.9
0.8
0.7
0.6
0.5
0.4
0.3
0.2
0.1
10-12
0-2
2-4
4-6
5-7
6-8
8-10
Harvest Timing

(b)

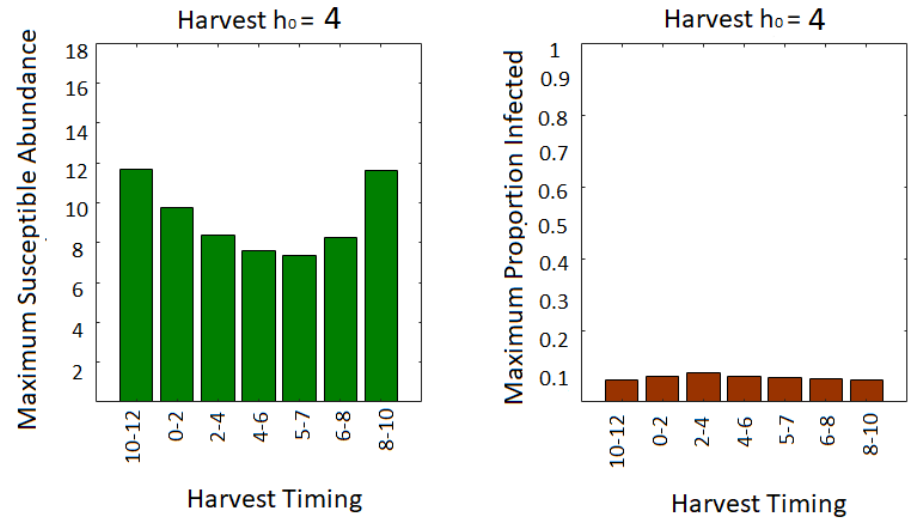

(c)

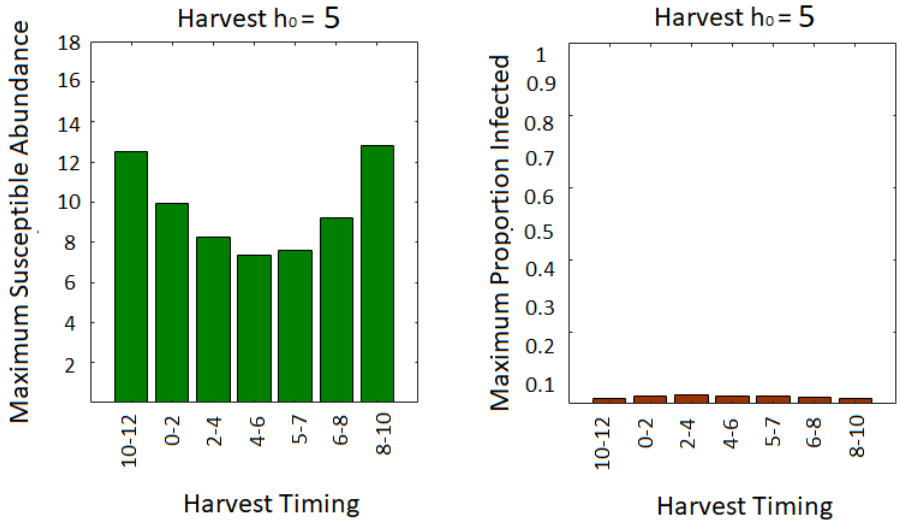

(d)

Figure 4.19: Maximum numbers of susceptible individuals and the maximum proportion of infection in the population for different harvesting strengths and different timings of harvest.

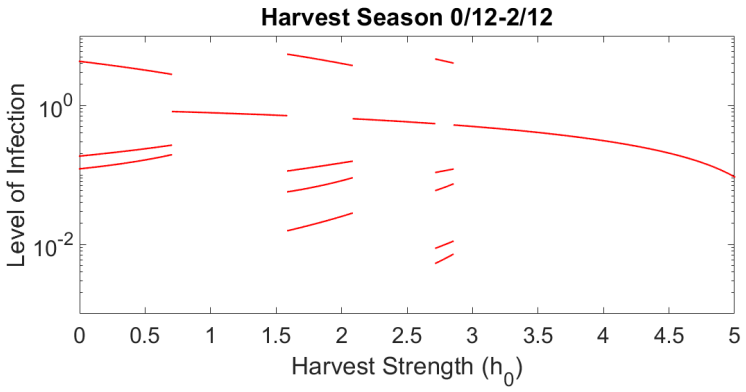

(a)

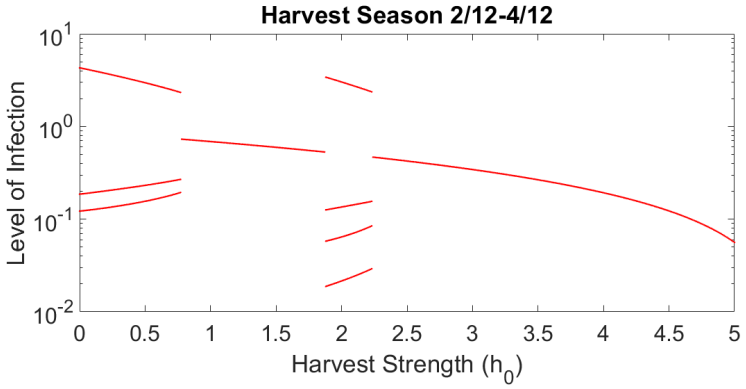

(b)

Figure 4.20: Bifurcation diagrams of h_0 for the harvesting strategies with seasons (a) $s = 0/12, r = 2/12$ and (b) $s = 2/12, r = 4/12$ with other parameter values as in table 4.2.

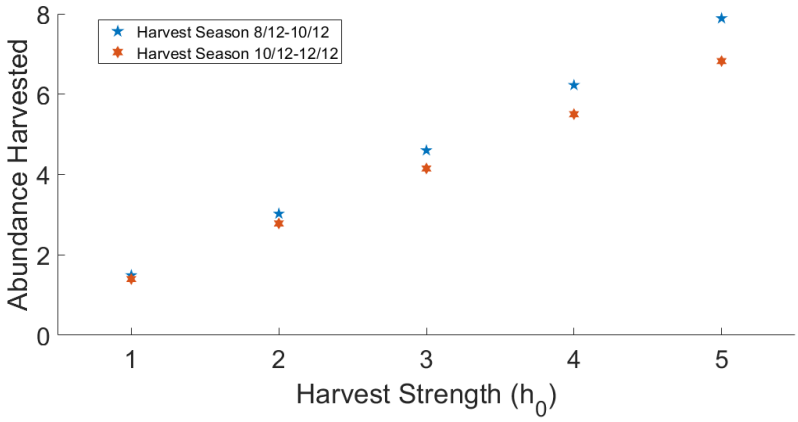

Figure 4.21: Comparing the numbers of population members harvested for different harvest strengths when harvest is timed from $8/12 - 10/12$ and $10/12 - 12/12$.

and $s = 10/12, r = 12/12$. From this we can see that, as in 4.3.3, harvesting from $8/12 - 10/12$ results in a slightly higher yield compared with harvesting at $10/12 - 12/12$. The differences in yield increase as h_0 increases, but we still cannot say that these are significantly different to make a big impact on deciding which method would be most suitable to implement. We can say that either method would be more effective than any other timing of harvest, and that an exact decision may need to be based on other factors such as environmental conditions, costs and availability of resources.

4.4.3 Increasing the length of the harvest season.

As in 4.3.4 we look at extending the length of the harvest season. We see again that a longer season with smaller harvest rate can produce similar results (in terms of maximising the susceptible populations and harvested yield) as a shorter season with a higher harvest. With the two-month season $s = 10/12, r = 12/12$, the maximum susceptible population with a harvest rate of 5 is approximately 13 individuals, and the yield harvested is 7 individuals per season. In our extended season from $s = 8/12, r = 12/12$, the yield harvested is again 7, and the maximum number of susceptible members is 12. So these two strategies are comparable in terms of meeting management targets. Figure 4.22 compares strategies $s = 8/12, r = 10/12$, $s = 10/12, r = 12/12$ and $s = 8/12, r = 12/12$, showing the differences in the maximum susceptible abundance, maximum infected proportion and harvest numbers for each harvest season with $h_0 = 2.5$. The longer harvest season is producing more yield. This is intuitive since it has more time to interact with the population to gain such yield. Despite the apparent benefits of this longer season, there may be difficulties in performing harvests over a longer period of time. Harvesting seasons of

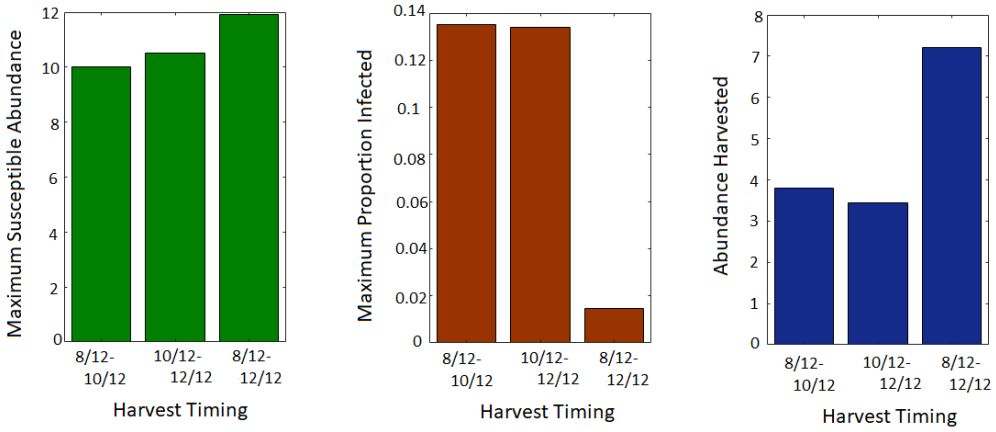

Figure 4.22: Comparing the maximum abundance of susceptible individuals, maximum infected proportion and numbers harvested during the season for the harvesting strategies $s = 8/12, r = 10/12$, $s = 10/12, r = 12/12$ and $s = 8/12, r = 12/12$, where $h_0 = 2.5$.

longer duration may not be possible for several reasons. For example the weather or climate may not be favourable for a long enough period, resources may be not available for an extended time, and a longer season requires a greater time-commitment from harvesting parties. Therefore, again we see that optimal strategies for different diseases and different systems would be dependent on other information, and not just on the results we produce from model simulations.

§ 4.5 Discussion

In this chapter we have shown that performing a seasonal harvest of a population who are subject to a fatal infectious disease, can help to increase susceptible population abundance whilst minimising infection and regulating the population cycle, when the population is subject to multiple periodic forcing in demographic rates. We implemented an SI model including seasonal variation in birth and transmission, and fixed the values of other parameters. An additional seasonal component representing a harvesting strategy, where strength, timing and duration could be altered, was included and we explored how different harvest tactics could impact population and disease dynamics. The success of the harvest strategy depended on its three elements: the strength of harvest, the time it was performed, and the length of the harvest season. Crucially, we found that the initial conditions and parameter values used for model simulation play an important role in determining the disease dynamics, and highlighted the bi-stability of the system from this. The bi-stable solutions can fundamentally change the behaviour of the host and disease

dynamics, so in managing a population, one must ensure the initial conditions are accurate. This is especially crucial for highly pathogenic and wide-spread diseases (Duke-Sylvester et al., 2011). As we seek to protect vulnerable wildlife populations, particularly due to our ever changing climate, predictive mathematical models are key for assessing the impact of management programmes and their effectiveness in maintaining wild populations (Gulland, 1995).

In many natural wildlife populations, groups aggregate at specific times in the year; for example whale sharks gather seasonally near Australian coastlines (Wilson et al., 2001). Such aggregation means that individuals are more densely populated, and hence in the presence of an infectious disease, direct host-host contacts will increase therefore raising transmission. Should such a disease require control, harvest/management strategies can be used. As well as minimising infection in a population, management strategies can be used for the benefit of the human population. For example, we may harvest a population for its meat, fur, or skin (Golden, 2011). As wildlife populations gather in larger groups, targetted harvests can be easier to manage since individuals live in closer quarters. Performing harvests at this time also coincides with the peak in possible disease transmission. We found that, for a harvest season coinciding with the increased transmission season, population and disease dynamics were dependent on the strength of harvest and the population abundances. Introduction of harvest settled the population and disease dynamics to more stable regimes, particularly as the harvest strength was increased. However, we highlighted the existence of bi-stability in the model, where differing population abundances could switch the dynamics between cycles of different lengths. This has been seen in other work, for example in Tang and Chen (2004). For smaller harvesting rates, dynamics were more likely to alter but as the baseline rate of harvest increased, dynamics became more stable. This was true up to a certain point, whereby beyond the harvest rate of $h_0 = 6$ in our original analysis of both models, the entire population was eradicated. Over-harvesting has occurred in the natural world, with one of the most prominent examples being the loss of whale species during the prolific whaling exploits in the 1800's (Pimm, 2020). For our chosen parameter values and initial conditions, we conclude that a harvest rate of $3 \leq h_0 \leq 5$ for the timing $10/12 - 12/12$ would be a good strategy. Such management is carried out at the most suitable time, and would avoid under or over harvesting. Of course, the parameter values used in our analysis are unlikely to be exactly as in the real world. However, the cases where we have highlighted the most stable dynamics in our analysis should be sufficient to cover any small errors or deviations in parameter values.

Although for practical reasons it may be easier to perform harvests at a time when populations are gathered together, other factors come into play. Managers would be required to think about factors such as costs, the availability of tools or resources, the weather and climate and perhaps even on any impact on tourism or the economy (Regehr et al., 2017; Gren et al., 2018). Therefore it is important

to determine how any targets of particular management can be achieved through harvesting at different times. If we want to maximise the harvest yield, whilst minimising infection within a population, we found that harvesting slightly before the peak in transmission improved results, though the difference between this and harvesting during maximum transmission were not substantial. This was for the specific set of initial conditions explored, where $S_0 + I_0 = 100$. Performing a population harvest at alternative times was unable to match the effectiveness of the two strategies where $s = 8/12, r = 10/12$ and $s = 10/12, r = 12/12$.

When considering population management, we often see short harvest seasons in order to maximise yield with minimum disruption to the population (Choisy and Rohani, 2006). In extending (doubling) the length of our season, we were able to reduce harvest rates by half to eradicate disease and maximise the abundance of susceptible population members. At the same harvest rates, the longer season increased population numbers and raised the harvested yield. At first sight it would therefore seem that a lengthened season is preferable, however we must consider other factors in this assumption. Performing harvest over a longer period of time could be more resource intensive, for example. In addition, it is likely that there would be a need for more time-commitment from hunters, therefore raising the cost of services (Diekert et al., 2016). These factors would need to be taken into consideration when designing an appropriate management strategy. Whether the benefits of a longer season (increased yield, etc.) outweigh the additional costs is important to discern.

As mentioned above, our analysis used specific parameter values and initial conditions which are not likely to be true to many real host-parasite systems, but our simulations are able to provide an insight into the possible patterns we may observe in population dynamics. In model simulations when making alterations to the harvest strength, timing and duration, bi-stable/multiple stable solutions were a common occurrence, meaning that it was possible for dynamics to change rapidly with a small change in conditions. Alongside the initial population conditions S_0, I_0, D_0, the rate of harvest h_0 played a large role in determining the specific disease dynamics we observed. In exploring different initial population conditions for varying harvest strengths, it was possible for population and disease dynamics to be highly unpredictable, causing a large degree of uncertainty in the model outcome. Through our analysis of both models, however, we found an abundance of stable solutions which would be robust to any small changes or alterations in parameter values. Higher rates of harvest (provided the rate was not too high so to cause extinction), gave the most stable solutions, where every set of initial conditions tested resulted in annual dynamics only. Such results are important for the potential design and implementation of management strategies that will be effective, and robust to small changes since it is important for strategies to be adaptable (Johnson et al., 1993; Morgan and Shepherd, 2006; Yletyinen et al., 2018).

Of course, we have made a number of assumptions in both the formulation

of the model, and in the analysis. As mentioned in chapters 2 and 3, there are numerous extensions that could be made to the models in order to suit other host-parasite systems. For example, we may need to add latency, vertical transmission or additional interacting populations. Also, we have fixed our seasonal components of breeding and aggregation. An extension of the models and analysis could consider different forms of the seasonality functions (see for example Hosseini et al. (2004)), or indeed could consider seasonality in other demographic processes, such as the death rate. On the whole, as in the previous chapters, the timing of seasonal processes is a key driver of population and disease dynamics. Any effective management strategies, therefore, need to consider how the timing of seasonality would impact results.

Seasonal fluctuations in the birth rates of wildlife, and in the transmission diseases, are common throughout the natural world. Many wildlife populations are harvested periodically for the benefit of humans; for meat, skin or fur, for example. Yet, theoretical studies of host-parasite relationships subject to multiple external periodic forcing have rarely considered how harvest can help to control, or even eradicate, disease. In this work I have shown that seasonal harvest can simultaneously maximise population abundance and maximise harvest yield, whilst minimising infection. This work shows, therefore, that both humans and the wildlife populations they manage, can benefit from a seasonal harvest in a fluctuating environment.

Chapter 5

Discussion

In this thesis I have explored mechanistic models of host-parasite relationships, where such hosts exhibit seasonal birth patterns and the transmission of disease is also modelled as a seasonal process. I have considered how recovery can influence the host-parasite dynamics, and how a seasonal harvest of the population can help to regulate disease cycles and maximise population abundance. I have specifically looked at how changing the timing of seasonal processes influences population and disease dynamics and have highlighted how very small changes can dramatically impact dynamics. This section brings together the work from each chapter, and highlights potential avenues for future work.

§ 5.1 Summary

Throughout this thesis, a key theme was the recurring importance of the timing of seasonal processes in determining the population and disease dynamics in our systems. Whether this was in the seasonal birth, transmission, or harvest, timing was crucial. Though previous studies have considered two seasonally varying rates in models of host parasite relationships (Swinton et al., 1998; Hosseini et al., 2004; Choisy and Rohani, 2006) for example, none have delved rigorously into the impact of the timing of seasons on the host and disease dynamics. The work contained in this thesis, therefore, brings new insight into how the dynamics of populations and the diseases they carry behave when affected by multiple seasonal components.

In chapters 2 and 3, where we explored SIR-style models with seasonal forcing in birth and transmission, we found that dynamics were most stable when births reached their peak shortly before the transmission rate. For the model in chapter 2, we explained this result in relation to the basic reproductive ratio (see section 2.3.2). When births peak, the pool of susceptible individuals is maximised as an influx of members enters the class. This raises the basic reproductive ratio R_0, allowing an epidemic to occur. The outbreak is accentuated by the rising transmission. With decreasing transmission and a dwindling susceptible pool, infections decrease, but

the susceptible population starts to build again as birth rates increase. This cycle allows a regular disease pattern to be observed. When the birth rate occurs at a different time in the annual calendar, the susceptible pool of members may not be high enough to cause a disease outbreak when transmission rises. This leads to a lag in the increase of disease, meaning an outbreak will occur in a following year after the sufficient recovery of the susceptible population. In chapter 3, we explained this pattern of behaviour in relation to the threshold for disease outbreak. This threshold was introduced in section 1.3 and defined in section 3.2. Similarly to above, the abundance of susceptible members determines the possibility of a rise in infection. When susceptible individuals reach and surpass the threshold level, infection will rise and lead to the cycle as explained above. With alternatively timed births, a wide array of dynamics are possible. Due to the abundance of observable dynamics from changes to the timing of seasonal forcing in both of the models, we conclude confidently that such timings are imperative. The determination of cycles is important in our study of host-parasite systems as it aids understanding of how the host and disease interact, and therefore how we might be able to mitigate negative impacts of infection in a population. With a more stable disease cycle, patterns are recognisable and consistent, hence helping in the process of managing populations.

For the harvest models presented in chapter 4, the seasonal forcing in birth and transmission were fixed with a five-month interval between their peaks. This allowed us to explore the impact of changing the timing of harvest with otherwise fixed seasonality. With harvest represented by a *constant effort* function and fixed to be performed for a two-month period, removing population members whilst transmission rates were rising/reaching their peak gave optimal management results in terms of maximising yield, minimising infection and maximising the susceptible population. When harvest was timed elsewhere within the annual population calendar, different and less optimal results were obtained through the strategy. Our analysis of this variation in seasonal timings showed again an array of possible dynamics, where in this case we required a management targeted during peak transmission times to achieve optimal results as described above. The application of harvest to both of the modelling frameworks used in chapters 2 and 3 was applied assuming fixed conditions in the original models. In this sense, we have explored a specific population system, varying only the harvest strategies. Therefore, it is important to note that the conclusion of harvest being optimal when timed to coincide with peak transmission may only be most suited to the host demographic situation explored in this chapter, where we assumed breeding and transmission peaks to be separated by a period of five months. Such pattern of breeding and transmission is commonly observed among wildlife, particularly in bird species where spring/summer breeding and autumn/winter migration (i.e. grouping leading to increased likelihood of direct transmission) is common (Rohwer et al., 2009; Curley et al., 2020).

In 2011, a study of the World's species estimated that there would be a total

of 8.7million (±1.3million) different lifeforms on Earth (Mora et al., 2011). Of this number, the estimated abundance of Animalia was 7.77million different species. Predictions for the current number of Animalia species that have been formally classified varies slightly between sources, though in Mora et al. (2011), the number was said to be around 1.2million. With such an abundance of unique species on Earth, social and breeding behaviours between types will be vastly different. In fact, even within species we can observe differences in behaviour. For example, a study on Acorn Woodpeckers showed that some formed cooperative groups on a year-round basis, whilst others chose to form temporary isolated pairs during the breeding season, but re-join the larger groups for migration (Stacey and Bock, 1978). In this system, we would expect an increased transmission rate during the migration season, as isolated pairs join with the larger group again. In addition, we could expect the seasonal fluctuation in such transmission rate to be of a small amplitude if the abundance of isolated pairs is far fewer than the year-round group. In contrast to this population behaviour, there are certain species who will gather to breed, and thus breeding and aggregation (transmission) would become part of the same biological process. For example, harbour seals congregate in certain months to find a partner and breed (Swinton et al., 1998), and this increase in population density would lead to an increasing transmission in directly transmitted diseases. Thus, in modelling specific populations, knowledge of the precise behaviours of hosts is required, since even within species, behaviour can vary.

The amplitude of our seasonally varying terms also determined the pattern of disease reoccurrence, though our two models from chapter 2 and chapter 3 showed different patterns of results. In the latter, where transmission of disease occurred through the environment as well as by direct contact, increasing seasonal amplitudes of birth and transmission led to the appearance of more complex dynamics. In contrast, when increasing amplitudes in our first model in chapter 2, dynamics moved through a period of complex behaviours, but settled to more stable cycles (biennial) with larger values. The fluctuation in seasonal rates, therefore, plays a role in determining disease cycles. We must note that the analysis was carried out for otherwise fixed parameter values and certain initial population conditions. In representing specific host-parasite systems therefore, detailed knowledge of appropriate parameter values would be vital for accurate disease modelling.

The initial population conditions used in model simulations were influential on the resulting population dynamics in all models explored in this thesis. The consequential existence of bi-stability and multiple-stable solutions had profound effects on our results. The presence of these types of solutions in our systems of differential equations is important due to their potential impact on population and disease dynamics. Bi-stability or multiple stable solutions occur when different attractors are simultaneously stable depending on the initial population conditions used for model simulation. Each stable solution has a specific *basin of attraction* (Keeling and Rohani, 2008), which contains all the initial conditions that will eventually settle

dynamics to the stable state observed. This means that, depending on how we compute our model simulations, we could see different results for the same parameter values (with different initial population conditions). This is an important property of seasonal models. Some basins of attraction may be extremely small, meaning certain dynamics could occur only for a very specific set of initial conditions. This means that we could omit acknowledging the presence of certain dynamics, because our simulations have not covered the initial conditions required to result in such behaviour.

In chapter 2 rapid switching between different dynamic attractors was observed, where small changes in population sizes could disrupt stable dynamics and alter the disease cycle. We saw several instances where dynamics switched between annual, biennial and higher-order cycles depending on population abundances. Such behaviour was found when altering the timing of seasons, when changing the amplitude of the seasonal components, and when investigating dynamics for highly virulent, transmissible diseases. Recovery, in general, stabilised the population dynamics. However, bi-stability was still evident in analysis where dynamics switched from annual to biennial cycles with different initial population conditions. The possibility of these rapid changes is important in the application of our models to existing natural populations. Recognising the potential for dynamic change to occur quickly under certain conditions means studies of populations and control of diseases can account for such behaviour.

With transmission possible through an environmental reservoir, as explored in chapter 3, bi-stability and multiple stable attractors were commonly observed. Depending on initial conditions and parameter values, we saw a multitude of dynamics and rapid switching between states, but the existence of biennial solutions was rare. For our chosen set of fixed parameter values we did not record any biennial dynamics. In exploring basins of attraction for the cycles discovered (annual, triennial and four-year cycles), we observed a clearly structured pattern in the basins (figure 3.10), where triennial dynamics were the most often occurring cycle. Fourier spectra confirmed this observation, in the dominance of the three-year signal, and the absence of biennial dynamics. We note here that, as explained above, basins of attraction for certain dynamic attractors can be very small. Therefore, it is possible that biennial dynamics occur more frequently, but we have not explored the initial conditions which lead to these cycles.

Seasonal removal of population members, both susceptible and infected, as explored in chapter 4 also gave rise to bi-stability. Whilst we observed changes in dynamics as a consequence of altering the timing and magnitude of harvest, changes in population abundance also had the potential to switch dynamics between different states. Similarly to chapter 3, biennial dynamics were rarely observed. However, in chapter 4, this absence was noticeable for both the basic SI model and the SID model. Again, we must highlight that our analysis used specific sets of parameter values, and additionally we predominantly varied initial conditions as integer val-

ues. Therefore, our analysis could be omitting the biennial dynamics due to the conditions in the basin of attraction not being explored.

The rapid switching of population dynamics we have observed in results from model simulations are reflective of situations that have been observed in real world populations. Anthropogenic changes present a huge challenge to wildlife, as populations must rapidly adapt to overcome alterations to their habitats and livelihoods. These human-mediated changes, be it in deforestation, construction, or excessive harvest, for example, often occur very quickly, meaning species must adapt quickly in order to survive (Wong and Candolin, 2015). Different studies have shown the behavioural changes adopted by certain wildlife species in response to anthropogenic change. For example, a study on the foraging behaviour of urban hedgehogs (Dowding et al., 2010) showed the species was more likely to forage later in the day to avoid human contact. The study showed differences in the responses of males and females, a result which could therefore have consequential impacts on breeding and hence population abundance. In their study, Legagneux and Ducatez (2013) demonstrated the ability of certain European bird species to alter their flight distances and speeds in response to new road developments. However, should a population be unable to respond quickly enough, newly built roads can be fatal for bird species. This could be due to the increased likelihood of collision with traffic, habitat loss or due to prey encountering predators more frequently. Immediate changes in the species environment can thus cause rapid population change, altering host abundance. Introduction of new species to existing habitats can be calamitous for native/existing species. Lehtonen et al. (2012) summarised the negative impact on a native fish species, the Arrow cichlid, when an invasive species, the bigmouth sleeper goby, was introduced to its habitat. The goby caused a decline in the success rate of breeding, leading to population reduction in the Arrow cichlid. In similar cases, where new species are introduced to existing ones, the inability of the existing species to respond could lead to catastrophic change in population abundance (Phillips and Suarez, 2012).

Additionally, anthropogenic changes can cause alterations in host-parasite relationships, and hence the dynamics of disease (Budria and Candolin, 2013). Desneux et al. (2007) highlighted how a particular parasitic wasp had a reduced ability to search for hosts due to the excessive use of pesticides in farming. Though this could benefit the host species, it could also lead to random change in host-parasite encounters, and hence disease dynamics. Certain species can regulate parasites through mutual grooming within the population (Okuno et al., 2012). This avoidance behaviour could be impacted by human-initiated rapid change, for example if habitats become fragmented or destroyed. Such activity may require populations to spend more time on foraging, and therefore time spent on grooming would reduce and lead to a sharp increase in parasitic success (Wong and Candolin, 2015). Therefore, these observed changes in species behaviour could lead to the altered population and disease patterns we discovered in the analysis of our models, lending our results

applicable to real-world situations.

The nature of transmission, as shown in chapters 2 and 3, has an impact on population and disease dynamics. We saw this through the consequential changes in dynamics when varying the parameters associated with the seasonal transmission, $\beta_0, \beta_1, \beta_2$. Since the seasonal transmission played a large role in determining the threshold for disease outbreak, we were able to attribute any changes to this threshold. There has been much debate on the most appropriate form of transmission to use in modelling disease (Mccallum et al., 2001; Begon et al., 2002), and perhaps one of the limitations to our definition of transmission is the assumption that contacts between population members are equally likely, regardless of their age, sex or hierarchy in the group. Despite this, SIR-style models, both with and without the presence of seasonally varying components, have been able to sufficiently model real-world host-parasite dynamics. For example, in the work of Anderson et al. (1981) rabies virus in European red foxes was explored, and the authors were able to provide models which matched empirical data, despite the limitations of their SEI model. Therefore, the mathematical modelling style we use can provide good approximations for population and disease dynamics, with transmission not necessarily needing to precisely match the exact real-world form to give suitable results. Of course, modelling techniques and model formulations can always be tweaked in some way, but we can be confident that our modelling framework can provide a solid guide in representing empirical observations.

In the 2018 review on infectious disease modelling of wildlife by Berg et al. (2018), the authors highlighted the need to explore how harvest strategies can impact disease spread, and how this modelling will be essential for informing managers in designing suitable practices. A compartmental modelling framework with inclusion of seasonality was suggested by the authors. In chapter 4, we have taken the first steps in exploring how different intensities of harvest can impact a host-parasite system, filling this knowledge gap as indicated by the Berg et al. (2018) review. We discussed that using our models and results in application to existing host-parasite systems requires some knowledge of both the host and disease behaviour, since reliable knowledge of the system helps to accurately parameterise the model, and thus gives us confidence in the simulation results. The data we deem necessary to obtain would be information on population size, lifespan of hosts, breeding and social habits and the virulence of the particular disease. With this information driving the parametrisation of models, our framework could be a useful tool for managing populations and disease.

§ 5.2 Future Work

In this thesis I have developed extensions to the classic SIR models originally formulated by Kermack and McKendrick (1927), by including two seasonally varying terms; one in host birth rate, and the other in transmission. Specifically, I have

explored the impact of changing the magnitude, amplitude and timing of such seasonal components on the population and disease dynamics, and have investigated the effects of changing initial conditions and other parameter values. The models consider density-dependence in the host death rate, and mostly assume that recovery is not possible. Additionally, I have considered how a seasonal harvest can influence population and disease dynamics. There are very few previous theoretical studies involving two seasonally varying terms in an SIR-type model for wildlife diseases, and only one known to us to also consider harvest. These studies take varying forms of seasonality, omit density-dependence in the death rate and consider that recovery is possible. Thus, this thesis contains unique work, giving scope for further developments to be made.

The first area we consider to be relevant for future work is consideration of alternative and/or additional transmission types, for example, vertical transmission. This type of transmission involves disease passing from mother to offspring, either during pregnancy or birth. To model this type of transmission, a fraction p of newborn individuals would go straight into the infection class I, giving the fraction $(1-p)$ of newborns to the susceptible class S. As we saw in chapter 3, the inclusion of an additional transmission pathway caused dynamics to alter. Thus for wildlife diseases where vertical transmission is possible, such as Bovine TB (Morris et al., 1994), Mycoplasma (Whithear et al., 1989) and Avian Encephalomyelitis (Calnek et al., 1960), where populations could also be influenced by seasonality in birth and transmission, our models would be more suitable for exploring the population and disease dynamics. We anticipate that the addition of vertical transmission into our model from chapter 2 would be likely to regulate dynamics to more stable cycles. This would be as a result of the addition of vertical transmission in the threshold for disease outbreak. Formulating a threshold whilst considering vertical transmission, we obtain a decreasing level as the fraction born infected, p, increases. Therefore, the susceptible population has a greater chance of surpassing the threshold to cause a rise in infection, leading to an increased chance of more stable dynamics. This is similarly the case should vertical transmission be incorporated into the environmental transmission model from chapter 3, due to the impact of the newborn infected fraction on the threshold for disease outbreak.

Numerous diseases have been observed to cause a so-called *latent* period of infection in their host, e.g. Avian Influenza (Hénaux et al., 2010), Phocine Distemper Virus (Duignan et al., 2014) and Ebola (Getz et al., 2019). This means that a susceptible host can contract disease, but remain unaffected for a period of time, before displaying symptoms/becoming infectious themselves. Models considering this delayed infection are known as $SEIR$ models (see section 1.4.3), and have been extensively studied in application to epidemiological systems. Studies using these models have considered externally forced systems (Aron and Schwartz, 1984; Grenfell et al., 1995; Earn et al., 2000; Bauch and Earn, 2003), but to the best of our knowledge have not taken account of both multiple external periodic forcing and

harvest. Therefore, the application of our models, adapted to include the possibility of latency, could be important in more accurately modelling several systems. In turn, the enhanced accuracy in modelling will assist in informing management strategies of populations and disease, helping to control outbreaks of infections.

Susceptibility to disease can be dependent on age. For example, naive members of a population, i.e. those that are very young, can experience an enhanced susceptibility to infectious agents due to their immaturity. We could also see the converse, where older generations become more susceptible to certain diseases as their age increases. Age-structured models have been used in abundance for human infectious diseases. Recently, age-structure has been used in work on coronaviruses (Colombo et al., 2020), and previously on diseases such as smallpox (Valle et al., 2013), measles and rubella (Anderson and May, 1983). Consideration of age-structure is also necessary for certain wildlife diseases, e.g. bovine spongiform encephalopathy, since susceptibility to disease decreases as age increases (Keeling and Rohani, 2008). If these populations and diseases occur in a seasonally varying environment, where births and disease transmission fluctuate, models should reflect this behaviour.

Recently we have seen increasing applications of spatially-structured models for representing disease transmission, for example during the COVID-19 pandemic (Colombo et al., 2020). In wildlife populations, for example, we have seen the need for space-structure in modelling the spread of rabies in the United States (Murray et al., 1986; Smith et al., 2002; Ruan, 2017). This spatial spread, teamed with the likelihood of seasonal breeding and social behaviour in populations, demands models including these when exploring infectious diseases. Spatial structure can be incorporated into models in different ways. Keeling and Rohani (2008) give a comprehensive review of different methods. One example is the concept of a metapopulation model which has been used previously in studies of infectious diseases in wildlife (White and Harris, 1995; Swinton et al., 1998; Smith et al., 2002). In these models, the population is sub-divided into different groups, where each has independent dynamics, but members can move between groups. For example, we could have two groups where dynamics are governed by differential equations $\frac{dS_A}{dt}$, $\frac{dI_A}{dt}$, $\frac{dS_B}{dt}$, $\frac{dI_B}{dt}$. Demographic rates (e.g. births, deaths) can be the same in each group, or different, and we could include a parameter to enable a group member from A to move into group B and vice versa if appropriate. Future models of wildlife disease and their control could consider space-structure in addition to seasonally varying components to more accurately represent certain systems (Cross et al., 2009; White et al., 2017). This will be particularly important in considering the impact of climate change and anthropogenic activities on wildlife populations (Rushing et al., 2019). With global warming, there is an increasing likelihood of disease spreading further. In Northern regions where climate change is being felt the most (IPCC Core Writing Team, 2014; Omazic et al., 2019), diseases are more likely to be spreading, particularly in the poleward direction. In fact, studies have shown that land-dwelling species are moving North with an average rate per decade of 17km (Chen et al.,

2011). This has profound impacts on host-parasite relationships. As highlighted by Hoberg and Brooks (2015), diseases that are sensitive to climate will have an opportunity to spread to new areas under the current impacts of global warming. This could also mean infection spreading to new species who have not previously been exposed to the travelling disease (Jones et al., 2008). Therefore, we can recognise the importance of spatial modelling in investigating host-parasite relationships, and how these may change through time.

In informing management strategies, results from data-driven models would be a more reliable source than our theoretical computations. For design of appropriate control strategies for specific diseases and populations, our models as described in chapter 4 could be quantified by host and infection data. Knowledge of population structure (contacts), abundance and breeding habits could provide appropriate parameter values for hosts, whilst historical data on the progression of infection numbers would help in estimating disease parameters. By quantifying a model in this way, disease dynamics can be more accurately studied, and therefore control strategies can be designed with greater accuracy (Pomeroy et al., 2017).

We recognise that we have only considered sinusoidal functions to represent our seasonally varying processes of birth and transmission in this thesis, and acknowledge that other functions could be more appropriate depending on the behaviour of the population being studied. In previous work we have seen seasonality represented by functions such as square-waves (Hosseini et al., 2004; Smith et al., 2008; Begon et al., 2009), or instantaneous pulses (Roberts and Kao, 1998; White et al., 1999). In some bat species for example (George et al., 2011), births occur in a very short time-frame (in this case, late June), at an annual interval. Therefore, an instantaneous pulse of birth would be more appropriate for a system like this. Other species exhibit longer breeding seasons, where outside of the season, births almost never occur. Birth seasons such as these have been observed in pandas (Owen et al., 2005), and so for populations such as these, a square function could more appropriately represent their seasonal birth. This reiterates our point that, should we wish to accurately model populations with the potential to manage infectious diseases, we must have a detailed understanding of the host demographics to obtain reliable modelling results. The number of possible forms that seasonality functions could take means that there are likely to be a variety of new results and dynamics observable in analysis of such systems. Review of different seasonality forms, when multiple seasonal processes act on a host-parasite system would be an interesting development to this thesis.

This thesis took a simulation based approach in analysing our mathematical models, using Matlab (*MATLAB version R2018a*), though we recognise that other methods are available and could be suitable. In extension to our work, we recognise that numerical continuation software such as MatCont (Dhooge et al., 2004) and AUTO (Doedel, 1981) could have complemented our results. The functionality of these software, in providing interactive analysis of dynamical systems and auto-

matic bifurcations, could have furthered our work by accompanying the simulations performed in Matlab. Alternative modelling approaches are available, including the use of stochastic simulation methods. For such models, a fixed set of parameter values and initial conditions will not necessarily lead to the same output, unlike in deterministic models (Allen, 2017). The use of stochastic methods in SIR models has been used widely, though they are less-common for non-domestic wildlife diseases since estimates for parameter values are not as easily obtainable or predictable for these populations (McCormack and Allen, 2007; Allen et al., 2011). Using stochastic models for the frameworks in this thesis could aid consideration of random movements (spatial structure) of individuals, and could help to explore the impact of random environmental effects. Asymptotic analysis is an alternative method of analysing an SIR model, with previous work having used this technique for both theoretical and empirical studies (Oli et al., 2006; Perasso and Razafison, 2014; Kröger and Schlickeiser, 2020). The method allows systematic analysis of approximate solutions, when exact solutions to systems of differential equations cannot be found (Murray, 1984; Howison, 2005). Due to the complexity of the models we proposed, numerical simulations provided us with the opportunity to explore multiple parameter combinations and initial conditions systematically and efficiently. This allows application of our models to a variety of host-parasite systems, with the possibility to explore the population and disease dynamics under different scenarios. Further extensions to our work could explore alternative analytical methods and modelling approaches.

With our ever-changing World, seasonal changes are becoming more prominent, affecting host-parasite systems globally. Increasing the accuracy of host-parasite models with control, for application to wildlife systems, is imperative if we wish to conserve species for generations to come.

References

Acevedo-Whitehouse, K. and A. L. J. Duffus
2009. Effects of environmental change on wildlife health. *Philosophical Transactions of the Royal Society*, 364:3429–3438.

Al-Shorbaji, F. N., R. E. Gozlan, B. Roche, J. Robert Britton, and D. Andreou
2015. The alternate role of direct and environmental transmission in fungal infectious disease in wildlife: Threats for biodiversity conservation. *Scientific Reports*, 5(April):1–9.

Albon, S. D., A. Stien, R. J. Irvine, R. Langvatn, E. Ropstad, and O. Halvorsen
2002. The role of parasites in the dynamics of a reindeer population. *Proceedings of the Royal Society B: Biological Sciences*, 269(1500):1625–1632.

Allen, L. J.
2017. A primer on stochastic epidemic models: Formulation, numerical simulation, and analysis. *Infectious Disease Modelling*, 2(2):128–142.

Allen, L. J. S., V. L. Brown, C. B. Jonsson, S. L. Klein, S. M. Laverty, K. Magwedere, J. C. Owen, and P. V. D. Driessche
2011. Mathematical Modeling of Viral Zoonoses in Wildlife. *Natural Resource Modeling*, (June):5–51.

Almberg, E. S., P. C. Cross, C. J. Johnson, D. M. Heisey, and B. J. Richards
2011. Modeling routes of chronic wasting disease transmission: Environmental prion persistence promotes deer population decline and extinction. *PLoS ONE*, 6(5).

Altizer, S., A. Dobson, P. Hosseini, P. Hudson, M. Pascual, and P. Rohani
2006. Seasonality and the dynamics of infectious diseases. *Ecology Letters*, 9(4):467–484.

Altizer, S., W. M. Hochachka, and A. A. Dhondt
2004. Seasonal dynamics of mycoplasmal conjunctivitis in eastern North American house finches. *Journal of Animal Ecology*, 73:309–322.

Altizer, S., R. S. Ostfeld, P. T. Johnson, S. Kutz, and C. D. Harvell
2013. Climate change and infectious diseases: From evidence to a predictive framework. *Science*, 341(6145):514–519.

Anderson, R. and R. May
1981. The Population Dynamics of Microparasites and Their Invertebrate Hosts. *Society*, 351(1278):605–654.

Anderson, R. and R. May
1991. *Infectious diseases of humans: dynamics and control*. Oxford University Press.

Anderson, R. M., C. A. Donnelly, N. M. Ferguson, M. E. Woolhouse, C. J. Watt, H. J. Udy, S. MaWhinney, S. P. Dunstan, T. R. Southwood, J. W. Wilesmith, J. B. Ryan, L. J. Hoinville, J. E. Hillerton, A. R. Austin, and G. A. Wells
1996. Transmission dynamics and epidemiology of BSE in British cattle. *Nature*, 382(6594):779–788.

Anderson, R. M., H. C. Jackson, R. M. May, and A. M. Smith
1981. Population dynamics of fox rabies in Europe. *Nature*, 289(5800):765–771.

Anderson, R. M. and R. M. May
1979. Population biology of infectious diseases: Part I. *Nature*, 280(5721):361–367.

Anderson, R. M. and R. M. May
1983. Vaccination against rubella and measles: Quantitative investigations of different policies. *Journal of Hygiene*, 90(2):259–325.

Aron, J. L. and I. B. Schwartz
1984. Seasonality and period-doubling bifurcations in an epidemic model. *Journal of Theoretical Biology*, 110(4):665–679.

Azar, C., J. Holmberg, and K. Lindgren
1994. Stability analysis of harvesting in a predator-prey model. *Journal of Theoretical Biology*, 174(1):13–19.

Azar, C., K. Lindgren, and J. Holmberg
1996. Constant quota versus constant effort harvesting. *Environmental and Resource Economics*, 7(2):193–196.

Bartmann, R., G. White, and L. Carpenter
1992. Compensatory Mortality in a Colorado Mule Deer Population. *Wildlife Monographs*, (121):3–39.

Bauch, C. and D. Earn
2003. Interepidemic intervals in forced and unforced SEIR models. *Dynamical Systems and Their Applications in Biology*, 36:33–44.

Begon, M., M. Bennett, R. G. Bowers, N. P. French, S. M. Hazel, and J. Turner
2002. A clarification of transmission terms in host-microparasite models: Numbers, densities and areas. *Epidemiology and Infection*, 129(1):147–153.

Begon, M., S. Telfer, M. J. Smith, S. Burthe, S. Paterson, and X. Lambin
2009. Seasonal host dynamics drive the timing of recurrent epidemics in a wildlife population. *Proceedings of the Royal Society B: Biological Sciences*, 276(1662):1603–1610.

Berg, S. S., J. D. Forester, and M. E. Craft
2018. Infectious Disease in Wild Animal Populations: Examining Transmission and Control with Mathematical Models. In *The Connections Between Ecology and Infectious Disease*, volume 5, chapter 7, Pp. 239–266.

Best, A.
2013. The Effects of Seasonal Forcing on Invertebrate-Disease Interactions with Immune Priming. *Bulletin of Mathematical Biology*, 75(11):2241–2256.

Blackburn, J. K., H. H. Ganz, J. M. Ponciano, W. C. Turner, S. J. Ryan, P. Kamath, C. Cizauskas, K. Kausrud, R. D. Holt, N. C. Stenseth, and W. M. Getz
2019. Modeling R0 for pathogens with environmental transmission: Animal movements, pathogen populations, and local infectious zones. *International Journal of Environmental Research and Public Health*, 16(6).

Boyce, M. S., K. Knopff, J. M. Northrup, J. A. Pitt, and L. S. Vors
2012. Harvest Models for Changing Environments. *Conserving Wildlife Populations in a Changing Climate*, (December):293–306.

Breban, R., J. M. Drake, D. E. Stallknecht, and P. Rohani
2009. The Role of Environmental Transmission in Recurrent Avian Influenza Epidemics. 5(4).

Budria, A. and U. Candolin
2013. How does human-induced environmental change influence host-parasite interactions? *Parasitology*, 141(4):462–474.

Cable, J., B. Boag, K. Murray, I. Barber, E. L. Pascoe, A. J. Wilson, A. R. Ellison, E. R. Morgan, S. M. Sait, and M. Booth
2017. Global change, parasite transmission and disease control: lessons from ecology. *Philosophical Transactions of the Royal Society B: Biological Sciences*, 372(1719):20160088.

Caley, P., G. Marion, and M. R. Hutchings
2009. Assessment of Transmission Rates and Routes, and the Implications for Management. In *Management of Disease in Wild Mammals*, R. J. Delahay, G. C. Smith, and M. R. Hutchings, eds., Pp. 31–51. Springer Japan.

Calnek, B. W., P. J. Taylor, and M. Sevoian
1960. Studies on Avian Encephalomyelitis. IV Epizootiology. *Avian Diseases*, 4(4):325.

Camacho, A., A. J. Kucharski, S. Funk, J. Breman, P. Piot, and W. J. Edmunds
2014. Potential for large outbreaks of Ebola virus disease. *Epidemics*, 9(2014):70–78.

Chen, I. C., J. K. Hill, R. Ohlemüller, D. B. Roy, and C. D. Thomas
2011. Rapid range shifts of species associated with high levels of climate warming. *Science*, 333(6045):1024–1026.

Choisy, M. and P. Rohani
2006. Harvesting can increase severity of wildlife disease epidemics. *Proceedings of the Royal Society B: Biological Sciences*, 273(1597):2025–2034.

Cid, B., F. M. Hilker, and E. Liz
2014. Harvest timing and its population dynamic consequences in a discrete single-species model. *Mathematical Biosciences*, 248(1):78–87.

Colombo, R. M., M. Garavello, F. Marcellini, and E. Rossi
2020. An age and space structured SIR model describing the Covid-19 pandemic. *Journal of Mathematics in Industry*, 10(1).

Cross, P. C., J. Drewe, V. Patrek, G. Pearce, M. D. Samuel, and R. J. Delahay
2009. Wildlife Population Structure and Parasite Transmission: Implications for Disease Management. In *Management of Disease in Wild Mammals*, R. J. Delahay, G. C. Smith, and M. R. Hutchings, eds., Pp. 9–29. Tokyo: Springer Japan.

Curley, S. R., L. L. Manne, and R. R. Veit
2020. Differential winter and breeding range shifts: Implications for avian migration distances. *Diversity and Distributions*, 26(4):415–425.

Deredec, A. and F. Courchamp
2003. Extinction thresholds in host-parasite dynamics. *Annales Zoologici Fennici*, 40(2):115–130.

Desneux, N., A. Decourtye, and J. M. Delpuech
2007. The sublethal effects of pesticides on beneficial arthropods. *Annual Review of Entomology*, 52:81–106.

Dhooge, A., W. Govaerts, and Y. A. Kuznetsov
2004. Matcont. *ACM SIGSAM Bulletin*, 38(1):21–22.

Diekert, F. K., A. Richter, I. M. Rivrud, A. Mysterud, and W. C. Clark
2016. How constraints affect the hunter's decision to shoot a deer. *Proceedings of the National Academy of Sciences of the United States of America*, 113(50):14450–14455.

Dietz, K.
1967. Epidemics and Rumours: A Survey. *Journal of the Royal Statistical Society.*, 130(4):505–528.

Dietz, K.
1976. The Incidence of Infectious Diseases under the Influence of Seasonal Fluctuations. In *Mathematical Models in Medicine*, J. Berger, W. J. Bühler, R. Repges, and P. Tautu, eds., Pp. 1–15, Berlin, Heidelberg. Springer Berlin Heidelberg.

Dobson, A. P. and P. J. Hudson
1992. Regulation and Stability of a Free-Living Host-Parasite System : Trichostrongylus tenuis in Red Grouse . *Journal of Animal Ecology*, 61(2):487–498.

Doedel, E. J.
1981. AUTO: A program for the automatic bifurcation and analysis of autonomous systems.

Donnelly, C. A., A. C. Ghani, G. M. Leung, A. J. Hedley, C. Fraser, S. Riley, L. J. Abu-Raddad, L. M. Ho, T. Q. Thach, P. Chau, K. P. Chan, T. H. Lam, L. Y. Tse, T. Tsang, S. H. Liu, J. H. Kong, E. M. Lau, N. M. Ferguson, and R. M. Anderson
2003a. Epidemiological determinants of spread of causal agent of severe acute respiratory syndrome in Hong Kong. *Lancet*, 361(9371):1761–1766.

Donnelly, C. A., R. Woodroffe, D. R. Cox, J. Bourne, G. Gettinby, A. M. Le Fevre, J. P. McInerney, and W. I. Morrison
2003b. Impact of localized badger culling on tuberculosis incidence in British cattle. *Nature*, 426(6968):834–837.

Dorélien, A. M., S. Ballesteros, and B. T. Grenfell
2013. Impact of Birth Seasonality on Dynamics of Acute Immunizing Infections in Sub-Saharan Africa. *PLoS ONE*, 8(10).

Dowding, C. V., S. Harris, S. Poulton, and P. J. Baker
2010. Nocturnal ranging behaviour of urban hedgehogs, Erinaceus europaeus, in relation to risk and reward. *Animal Behaviour*, 80(1):13–21.

Duarte, C. C.
1994. Renewable resource market obeying difference equations: Stable points, stable cycles, and Chaos. *Environmental & Resource Economics*, 4(4):353–381.

Duignan, P. J., M. F. Van Bressem, J. D. Baker, M. Barbieri, K. M. Colegrove, S. de Guise, R. L. de Swart, G. di Guardo, A. Dobson, W. P. Duprex, G. Early, D. Fauquier, T. Goldstein, S. J. Goodman, B. Grenfell, K. R. Groch, F. Gulland, A. Hall, B. A. Jensen, K. Lamy, K. Matassa, S. Mazzariol, S. E. Morris, O. Nielsen, D. Rotstein, T. K. Rowles, J. T. Saliki, U. Siebert, T. Waltzek, and J. F. Wellehan
2014. Phocine distemper Virus: Current knowledge and future directions. *Viruses*, 6(12):5093–5134.

Duke-Sylvester, S. M., L. Bolzoni, and L. A. Real
2011. Strong seasonality produces spatial asynchrony in the outbreak of infectious diseases. *Journal of the Royal Society Interface*, 8(59):817–825.

Eames, K. T. and M. J. Keeling
2003. Contact tracing and disease control. *Proceedings of the Royal Society B: Biological Sciences*, 270(1533):2565–2571.

Earn, D. J., P. Rohani, B. M. Bolker, and B. T. Grenfell
2000. A simple model for complex dynamical transitions in epidemics. *Science*, 287(5453):667–670.

Ferris, C. and A. Best
2018. The evolution of host defence to parasitism in fluctuating environments. *Journal of Theoretical Biology*, 440:58–65.

Fisman, D. N.
2007. Seasonality of Infectious Diseases. *Annual Review of Public Health*, 28(1):127–143.

Gallana, M., M.-P. Ryser-Degiorgis, T. Wahli, and H. Segner
2013. Climate change and infectious diseases of wildlife: Altered interactions between pathogens, vectors and hosts. *Current Zoology*, 59(3):427–437.

George, D. B., C. T. Webb, M. L. Farnsworth, T. J. O'Shea, R. A. Bowen, D. L. Smith, T. R. Stanley, L. E. Ellison, and C. E. Rupprecht
2011. Host and viral ecology determine bat rabies seasonality and maintenance. *Proceedings of the National Academy of Sciences of the United States of America*, 108(25):10208–10213.

Georgsson, G., S. Sigurdarson, and P. Brown
2006. Infectious agent of sheep scrapie may persist in the environment for at least 16 years. *Journal of General Virology*, 87(12):3737–3740.

Getz, W. M., R. Salter, and W. Mgbara
2019. Adequacy of SEIR models when epidemics have spatial structure: Ebola in Sierra Leone. *Philosophical Transactions of the Royal Society B: Biological Sciences*, 374(1775):1–7.

Gilg, O., K. M. Kovacs, J. Aars, J. Fort, G. Gauthier, D. Grémillet, R. A. Ims, H. Meltofte, J. Moreau, E. Post, N. M. Schmidt, G. Yannic, and L. Bollache
2012. Climate change and the ecology and evolution of Arctic vertebrates. *Annals of the New York Academy of Sciences*, 1249(1):166–190.

Gilman, S. E., M. C. Urban, J. Tewksbury, G. W. Gilchrist, and R. D. Holt
2010. A framework for community interactions under climate change. *Trends in Ecology and Evolution*, 25(6):325–331.

Golden, C. D.
2011. *The Importance of Wildlife Harvest to Human Health and Livelihoods in Northeastern Madagascar*. PhD thesis, University of California, Berkeley.

Greenhalgh, D.
1990. An epidemic model with a density-dependent death rate. *Mathematical Medicine and Biology*, 7(1):1–26.

Greenman, J. V. and R. A. Norman
2007. Environmental forcing, invasion and control of ecological and epidemiological systems. *Journal of Theoretical Biology*, 247(3):492–506.

Greenman, J. V. and V. B. Pasour
2011. Phase control of resonant systems: Interference, chaos and high periodicity. *Journal of Theoretical Biology*, 278(1):74–86.

Gren, I. M., T. Häggmark-Svensson, K. Elofsson, and M. Engelmann
2018. Economics of wildlife managementan overview. *European Journal of Wildlife Research*, 64(2).

Grenfell, B. T., B. M. Bolker, and A. Kleczkowski
1995. Seasonality and extinction in chaotic metapopulations. *Proceedings of the Royal Society B: Biological Sciences*, 259(1354):97–103.

Grimminck, K., L. Anne, M. Santegoets, F. C. Siemens, P. Leendert, A. Fraaij, I. Karl, M. Reiss, and S. Schoenmakers
2020. No evidence of vertical transmission of SARS- after induction of labour in an immune- suppressed SARS- CoV-2- positive patient. *BMJ*, Pp. 8–11.

Guerra, F. M., S. Bolotin, G. Lim, J. Heffernan, S. L. Deeks, Y. Li, and N. S. Crowcroft
2017. The basic reproduction number R(0) of measles: a systematic review. *The Lancet. Infectious diseases*, 17(12):e420–e428.

Gulland, F. M. D.
1995. Impact of infectious diseases on wild animal populations: A review. In *Ecology of Infectious Diseases in Natural Populations*, Pp. 20–51. Cambridge University Press, Cambridge.

He, D. and D. J. Earn
2007. Epidemiological effects of seasonal oscillations in birth rates. *Theoretical Population Biology*, 72(2):274–291.

Helm, B., T. Piersma, and H. van der Jeugd
2006. Sociable schedules: interplay between avian seasonal and social behaviour. *Animal Behaviour*, 72(2):245–262.

Hénaux, V., M. D. Samuel, and C. M. Bunck
2010. Model-based evaluation of highly and low pathogenic avian influenza dynamics in wild birds. *PLoS ONE*, 5(6):1–7.

Henning, J., J. Meers, P. R. Davies, and R. S. Morris
2005. Survival of rabbit haemorrhagic disease virus (RHDV) in the environment. *Epidemiology and Infection*, 133(4):719–730.

Hethcote, H. W.
1994. A Thousand and One Epidemic Models. In *Frontiers in Mathematical Biology*, S. A. Levin, ed., Pp. 504–515. Springer Berlin Heidelberg.

Hoberg, E. P. and D. R. Brooks
2015. Evolution in action: Climate change, biodiversity dynamics and emerging infectious disease. *Philosophical Transactions of the Royal Society B: Biological Sciences*, 370(1665):1–7.

Hosseini, P. R., A. A. Dhondt, and A. Dobson
2004. Seasonality and wildlife disease: how seasonal birth, aggregation and variation in immunity affect the dynamics of Mycoplasma gallisepticum in house finches. *Proceedings of the Royal Society B: Biological Sciences*, 271(1557):2569–2577.

Houghton, J., Y. Ding, D. Griggs, M. Noguer, P. van der Linden, X. Dai, K. Maskell, and C. Johnson
2001. *Climate Change 2001: The Scientific Basis. Contribution of Working Group I to the Third Assessment Report of the Intergovernmental Panel on Climate Change*. Cambridge Univ. Press.

Howison, S.
2005. *Practical applied mathematics: Modelling, analysis, approximation*. Cambridge Univ. Press.

Hudson, P. J., A. P. Dobson, and D. Newborn
1998. Prevention of population cycles by parasite removal. *Science*, 282(5397):2256–2258.

Imran, M. and S. Mahmood
2011. An overview of animal prion diseases. Pp. 1–8.

IPCC Core Writing Team
2014. Climate Change 2014: Synthesis Report. Contribution of Working Groups I, II and III to the Fifth Assessment Report of the Intergovernmental Panel on Climate Change. Technical report.

Ireland, J. M., B. D. Mestel, and R. A. Norman
2007. The effect of seasonal host birth rates on disease persistence. *Mathematical Biosciences*, 206(1):31–45.

Ireland, J. M., R. A. Norman, and J. V. Greenman
2004. The effect of seasonal host birth rates on population dynamics: The importance of resonance. *Journal of Theoretical Biology*, 231(2):229–238.

Johnson, F. A., B. K. Williams, J. D. Nichols, J. E. Hines, W. E. Kendall, G. W. Smith, and D. F. Caithamer
1993. Developing an adaptive management strategy for harvesting waterfowl in North America. *Transactions of the North American Wildlife and Natural Resources Conference*, 58(February 2016):565–583.

Johnston, K. M. and O. J. Schmitz
1997. Wildlife and climate change: Assessing the sensitivity of selected species to simulated doubling of atmospheric CO2. *Global Change Biology*, 3(6):531–544.

Jones, K. E., N. G. Patel, M. A. Levy, A. Storeygard, D. Balk, J. L. Gittleman, and P. Daszak
2008. Global trends in emerging infectious diseases. *Nature*, 451(7181):990–993.

Keeling, M. J. and P. Rohani
2008. *Modeling Infectious Diseases in Humans and Animals*. Princeton University Press.

Keeling, M. J., P. Rohani, and B. T. Grenfell
2001. Seasonally forced disease dynamics explored as switching between attractors. *Physica D: Nonlinear Phenomena*, 148(3-4):317–335.

Kermack, W. O. and A. G. McKendrick
1927. A Contribution to the Mathematical Theory of Epidemics. *Proceedings of the Royal Society A: Mathematical, Physical and Engineering Sciences*, 115(772):700–721.

Ketterson, E. D., A. M. Fudickar, J. W. Atwell, and T. J. Greives
2015. Seasonal timing and population divergence: When to breed, when to migrate. *Current Opinion in Behavioral Sciences*, 6:50–58.

Khan, A., M. Naveed, M. Dur-e Ahmad, and M. Imran
2015. Estimating the basic reproductive ratio for the Ebola outbreak in Liberia and Sierra Leone. *Infectious Diseases of Poverty*, 4(1):1–8.

Kokko, H. and J. Lindström
1998. Seasonal density dependence, timing of mortality, and sustainable harvesting. *Ecological Modelling*, 110(3):293–304.

Kröger, M. and R. Schlickeiser
2020. Analytical solution of the SIR-model for the temporal evolution of epidemics. Part A: time-independent reproduction factor. *Journal of Physics A: Mathematical and Theoretical*, 53(50).

Kucharski, A. J., P. Klepac, A. J. Conlan, S. M. Kissler, M. L. Tang, H. Fry, J. R. Gog, and W. J. Edmunds
2020. Effectiveness of isolation, testing, contact tracing, and physical distancing on reducing transmission of SARS-CoV-2 in different settings: a mathematical modelling study. *The Lancet. Infectious diseases*, 3099(20):1–10.

Kutz, S. J., E. P. Hoberg, L. Polley, and E. J. Jenkins
2005. Global warming is changing the dynamics of Arctic host-parasite systems. *Journal of Theoretical Biology*, 272:2571–2576.

Laakkonen, J., H. Henttonen, J. Niemimaa, and T. Soveri
1999. Seasonal dynamics of Pneumocystis carinii in the field vole, Microtus agrestis, and in the common shrew, Sorex araneus, in Finland. *Parasitology*, 118(1):1–5.

Lafferty, K.
2009. The ecology of climate change and infectious diseases. *Ecology*, 91(3):925–928.

Lange, M., S. Kramer-Schadt, and H. H. Thulke
2016. Relevance of indirect transmission for wildlife disease surveillance. *Frontiers in Veterinary Science*, 3(NOV):1–12.

Legagneux, P. and S. Ducatez
2013. European birds adjust their flight initiation distance to road speed limits. *Biology Letters*, 9(5).

Lehtonen, T. K., J. K. McCrary, and A. Meyer
2012. Introduced predator elicits deficient brood defence behaviour in a crater lake fish. *PLoS ONE*, 7(1).

Lincoln, G. A.
1992. Biology of Seasonal Breeding in Deer. In *The Biology of Deer*, R. D. Brown, ed., Pp. 565–574, New York, NY. Springer New York.

Lindgren, E., L. Talleklint, and T. Polfeldt
2000. Impact of climatic change on the northern latitude limit and population

density of the disease-transmitting European tick Ixodes ricinus. *Environmental Health Perspectives*, 108(2):119–123.

Lloyd-Smith, J. O., P. C. Cross, C. J. Briggs, M. Daugherty, W. M. Getz, J. Latto, M. S. Sanchez, A. B. Smith, and A. Swei
2005. Should we expect population thresholds for wildlife disease? *Trends in Ecology and Evolution*, 20(9):511–519.

Maji, C., D. Mukherjee, and D. Kesh
2018. Deterministic and stochastic analysis of an eco-epidemiological model. *Journal of Biological Physics*, 44(1):17–36.

Maunder, M. N.
2008. Maximum Sustainable Yield. Pp. 2292–2296. Oxford: Academic Press.

May, R.
1974. *Stability and Complexity in Model Ecosystems*, volume 1. Princeton University Press.

May, R. M.
1976. Simple mathematical models with very complicated dynamics. *Nature*, 261(5560):459–467.

May, R. M., J. R. Beddington, J. W. Horwood, and J. G. Shepherd
1978. Exploiting natural populations in an uncertain world. *Mathematical Biosciences*, 42(3-4):219–252.

Mccallum, H., N. Barlow, J. Hone, and H. Mccallum
2001. How should pathogen transmission be modelled? *Trends in Ecology & Evolution*, 16(6):295–300.

McCarthy, J. J., O. F. Canziani, N. A. Leary, D. J. Dokken, and K. S. White
2001. *Climate change 2001 : Impacts, Adaptation, and Vulnerability*. Cambridge Univ. Press.

McCormack, R. K. and L. J. Allen
2007. Multi-patch deterministic and stochastic models for wildlife diseases. *Journal of Biological Dynamics*, 1(1):63–85.

Millán, J., M. G. Candela, F. Palomares, M. J. Cubero, A. Rodríguez, M. Barral, J. de la Fuente, S. Almería, and L. León-Vizcaíno
2009. Disease threats to the endangered Iberian lynx (Lynx pardinus). *Veterinary Journal*, 182(1):114–124.

Miller, M. W. and M. M. Conner
2005. Epidemiology of Chronic Wasting Disease in Free-Ranging Mule Deer:

Spatial, Temporal, and Demographic Influences on Observed Prevalence Patterns. *Journal of Wildlife Diseases*, 41(2):275–290.

Miller, M. W., N. T. Hobbs, and S. J. Tavener
2006. Dynamics of prion disease transmission in mule deer. *Ecological Applications*, 16(6):2208–2214.

Miller, M. W., E. S. Williams, N. T. Hobbs, and L. L. Wolfe
2004. Environmental sources of prion transmission in mule deer. *Emerging Infectious Diseases*, 10(6):1003–1006.

Mora, C., D. P. Tittensor, S. Adl, A. G. Simpson, and B. Worm
2011. How many species are there on earth and in the ocean? *PLoS Biology*, 9(8):1–8.

Morgan, L. and S. Shepherd
2006. Population and Spatial Structure of Two Common Temperate Reef Herbivores: Abalone and Sea Urchins. Pp. 205–246. Burlington: Academic Press.

Morris, R. S., D. U. Pfeiffer, and R. Jackson
1994. The epidemiology of Mycobacterium bovis infections. *Veterinary Microbiology*, 40(1-2):153–177.

Murray, J., E. Stanley, and D. Brown
1986. On the Spatial Spread of Rabies among Foxes. *Proceedings of the Royal Society of London.*, 229(1255):111–150.

Murray, J. D.
1984. *Asymptotic Analysis*, Applied Mathematical Sciences. Springer-Verlag New York.

Okuno, M., K. Tsuji, H. Sato, and K. Fujisaki
2012. Plasticity of grooming behavior against entomopathogenic fungus Metarhizium anisopliae in the ant Lasius japonicus. *Journal of Ethology*, 30(1):23–27.

Oli, M. K., M. Venkataraman, P. A. Klein, L. D. Wendland, and M. B. Brown
2006. Population dynamics of infectious diseases: A discrete time model. *Ecological Modelling*, 198(1-2):183–194.

Omazic, A., H. Bylund, S. Boqvist, A. Högberg, C. Björkman, M. Tryland, B. Evengård, A. Koch, C. Berggren, A. Malogolovkin, D. Kolbasov, N. Pavelko, T. Thierfelder, and A. Albihn
2019. Identifying climate-sensitive infectious diseases in animals and humans in Northern regions. *Acta Veterinaria Scandinavica*, 61(1):1–12.

Owen, M., N. Czekala, R. Swaisgood, K. Steinman, and D. Lindburg
2005. Seasonal and diurnal dynamics of glucocorticoids and behavior in giant pandas. *Ursus*, 16(2):208–221.

Páez, D. J., O. Restif, P. Eby, and R. K. Plowright
2018. Optimal foraging in seasonal environments: Implications for residency of australian flying foxes in food-subsidized urban landscapes. *Philosophical Transactions of the Royal Society B: Biological Sciences*, 373(1745).

Parmesan, C.
2006. Ecological and Evolutionary Responses to Recent Climate Change. *Annual Review of Ecology, Evolution, and Systematics*, 37(1):637–669.

Parratt, S. R., E. Numminen, and A.-L. Laine
2016. Infectious Disease Dynamics in Heterogeneous Landscapes. *Annual Review of Ecology, Evolution, and Systematics*, 47(1):283–306.

Pascual, M. and A. Dobson
2005. Seasonal Patterns of Infectious Diseases. *PLoS Medicine*, 2(1):e5.

Paull, S. H. and P. T. Johnson
2011. High temperature enhances host pathology in a snail-trematode system: Possible consequences of climate change for the emergence of disease. *Freshwater Biology*, 56(4):767–778.

Peel, A. J., J. R. Pulliam, A. D. Luis, R. K. Plowright, T. J. O'Shea, D. T. Hayman, J. L. Wood, C. T. Webb, and O. Restif
2014. The effect of seasonal birth pulses on pathogen persistence in wild mammal populations. *Proceedings of the Royal Society B: Biological Sciences*, 281(1786).

Perasso, A. and U. Razafison
2014. Asymptotic behavior and numerical simulations for an infection load-structured epidemiological model: Application to the transmission of prion pathologies. *SIAM Journal on Applied Mathematics*, 74(5):1571–1597.

Phillips, B. L. and A. V. Suarez
2012. The role of behavioural variation in the invasion of new areas. In *Behavioural Responses to a Changing World*. Oxford: Oxford University Press.

Pimm, S. L.
2020. Overharvesting. *Encyclopædia Britannica, inc.*

Pomeroy, L. W., S. Bansal, M. Tildesley, K. I. M. Torres, N. Xiao, T. E. Capenter, and R. B. Garabed
2017. Data Driven Models of Foot and Mouth Disease Dynamics: A Review. *Transboundary and emerging diseases*, 64(3):716–728.

Porter, R., R. A. Norman, and L. Gilbert
2013. A model to test how ticks and louping ill virus can be controlled by treating red grouse with acaricide. *Medical and Veterinary Entomology*, 27(3):237–246.

Potapov, A., E. Merrill, and M. A. Lewis
2012. Wildlife disease elimination and density dependence. *Proceedings of the Royal Society B: Biological Sciences*, 279(1741):3139–3145.

Potapov, A., E. Merrill, M. Pybus, and M. A. Lewis
2016. Chronic wasting disease: Transmission mechanisms and the possibility of harvest management. *PLoS ONE*, 11(3):1–20.

Regehr, E. V., R. R. Wilson, K. D. Rode, M. C. Runge, and H. L. Stern
2017. Harvesting wildlife affected by climate change: a modelling and management approach for polar bears. *Journal of Applied Ecology*, 54(5):1534–1543.

Rinaldi, S. and S. Muratori
1993. Conditioned chaos in seasonally perturbed predator-prey models. *Ecological Modelling*, 69(1-2):79–97.

Roberts, M. G. and R. R. Kao
1998. The dynamics of an infectious disease in a population with birth pulses. *Mathematical Biosciences*, 149(1):23–36.

Rohani, P., R. Breban, D. E. Stallknecht, and J. M. Drake
2009. Environmental transmission of low pathogenicity avian influenza viruses and its implications for pathogen invasion. 106(25):10365–10369.

Rohwer, S., K. A. Hobson, and V. G. Rohwer
2009. Migratory double breeding in neotropical migrant birds. *Proceedings of the National Academy of Sciences of the United States of America*, 106(45):19050–19055.

Rowan, W.
1938. Light and Seasonal Reproduction in Animals. *Biological Reviews*, 13(4):374–401.

Ruan, S.
2017. Spatiotemporal epidemic models for rabies among animals. *Infectious Disease Modelling*, 2(3):277–287.

Rushing, C. S., J. A. Royle, D. J. Ziolkowski, and K. L. Pardieck
2019. Modeling spatially and temporally complex range dynamics when detection is imperfect. *Scientific Reports*, 9(1):1–9.

Sauvage, F., M. Langlais, N. G. Yoccoz, and D. Pontier
2003. Modelling hantavirus in fluctuating populations of bank voles: The role of indirect transmission on virus persistence. *Journal of Animal Ecology*, 72(1):1–13.

Schwartz, I. B.
1985. Multiple stable recurrent outbreaks and predictability in seasonally forced nonlinear epidemic models. *Journal of Mathematical Biology*, 21(3):347–361.

Shampine, L. and M. Reichelt
1997. Ode Matlab Solvers. *Journal of Scientific Computing*, 18:1–22.

Sharkey, K. J.
2008. Deterministic epidemiological models at the individual level. *Journal of Mathematical Biology*, 57(3):311–331.

Sharp, A. and J. Pastor
2011. Stable limit cycles and the paradox of enrichment in a model of chronic wasting disease. *Ecological Applications*, 21(4):1024–1030.

Silk, M. J., N. Weber, L. C. Steward, R. J. Delahay, D. P. Croft, D. J. Hodgson, M. Boots, and R. A. McDonald
2017. Seasonal variation in daily patterns of social contacts in the European badger meles meles. *Ecology and Evolution*, 7(21):9006–9015.

Smith, D. L., B. Lucey, L. A. Waller, J. E. Childs, and L. A. Real
2002. Predicting the spatial dynamics of rabies epidemics on heterogeneous landscapes. *PNAS*, 99(6):3668–3672.

Smith, H. L.
1983. Multiple stable subharmonics for a periodic epidemic model. *Journal of Mathematical Biology*, 17(2):179–190.

Smith, M. J., A. White, J. A. Sherratt, S. Telfer, M. Begon, and X. Lambin
2008. Disease effects on reproduction can cause population cycles in seasonal environments. *Journal of Animal Ecology 2008*, (77):378–389.

Soper, H.
1929. The Interpretation of Periodicity in Disease Prevalence. *Journal of the Royal Statistical Society.*, 92(1):34–73.

Stacey, P. and C. Bock
1978. Social Plasticity in the Acorn Woodpecker. *Science*, 202(4374):1298–1300.

Stirling, I., N. J. Lunn, and J. Iacozza
1999. Long-term trends in the population ecology of polar bears in western Hudson Bay in relation to climatic change. *Arctic*, 52(3):294–306.

Stokes, M.
2012. Population Ecology at Work: Managing Game Populations. *Nature Education Knowledge*, 3(10):5.

Stone, L., R. Olinky, and A. Huppert
2007. Seasonal dynamics of recurrent epidemics. *Nature*, 446(7135):533–536.

Sutherst, R. W.
2001. The vulnerability of animal and human health to parasites under global change. *International Journal for Parasitology*, 31(9):933–948.

Swinton, J., J. Harwood, B. T. Grenfell, and C. A. Gilligan
1998. Persistence thresholds for phocine distemper virus infection in harbour seal Phoca vitulina metapopulations. *Journal of Animal Ecology*, 67(1):54–68.

Tang, S. and L. Chen
2004. The effect of seasonal harvesting on stage-structured population models. *Journal of Mathematical Biology*, 48(4):357–374.

Taylor, R. A.
2014. *The Influence of Seasonal Forcing on the Population Dynamics of Ecological Systems*. PhD thesis.

Taylor, R. A., J. A. Sherratt, and A. White
2013. Seasonal forcing and multi-year cycles in interacting populations : lessons from a predator-prey model. *Journal of Mathematical Biology*, Pp. 1741–1764.

Taylor, R. A., A. White, and J. A. Sherratt
2015. Seasonal forcing in a host-macroparasite system. *Journal of Theoretical Biology*, 365:55–66.

Thomas, C. D., A. Cameron, R. E. Green, M. Bakkenes, L. J. Beaumont, Y. C. Collingham, B. F. N. Erasmus, M. F. de Siqueira, A. Grainger, L. Hannah, L. Hughes, B. Huntley, A. S. van Jaarsveld, G. F. Midgley, L. Miles, M. A. Ortega-Huerta, A. Townsend Peterson, O. L. Phillips, and S. E. Williams
2004. Extinction risk from climate change. *Nature*, 427(6970):145–148.

Tompkins, D., A. P. Dobson, and P. Arneberg
2001. Parasites and host population dynamics. *Trends in Ecology & Evolution*, 17(12):45–62.

Tompkins, D. M. and M. Begon
1999. Parasites can regulate wildlife populations. *Parasitology Today*, 15(8):311–313.

Tsikliras, A. C. and R. Froese
2019. Maximum Sustainable Yield. Pp. 108–115. Oxford: Elsevier.

Valle, S. Y., J. M. Hyman, and N. Chitnis
2013. Mathematical models of contact patterns between age groups for predicting the spread of infectious diseases. *Mathematical Biosciences and Engineering*, 10(5-6):1475–1497.

Van Den Driessche, P.
2017. Reproduction numbers of infectious disease models. *Infectious Disease Modelling*, 2(3):288–303.

Vasilyeva, O., T. Oraby, and F. Lutscher
2015. Aggregation and environmental transmission in Chronic Wasting Disease. *Mathematical Biosciences and Engineering*, 12(1):209–231.

Walther, G.-r., E. Post, P. Convey, A. Menzel, C. Parmesan, T. J. C. Beebee, J.-m. Fromentin, O. H.-g. I, and F. Bairlein
2002. Ecological Responses to Recent Climate Change. *Nature*, 416:389–395.

Wearing, H. J., P. Rohani, and M. J. Keeling
2005. Appropriate models for the management of infectious diseases. *PLoS Medicine*, 2(7):0621–0627.

White, A., R. G. Bowers, and M. Begon
1999. The Spread of Infection in Seasonal Insect-Pathogen Systems. *Oikos*, 85(3):487–498.

White, K. A., B. T. Grenfell, R. J. Hendry, O. Lejeune, and J. D. Murray
1996. Effect of seasonal host reproduction on host-macroparasite dynamics. *Mathematical Biosciences*, 137(2):79–99.

White, L. A., J. D. Forester, and M. E. Craft
2017. Dynamic, spatial models of parasite transmission in wildlife: Their structure, applications and remaining challenges. *Journal of Animal Ecology*, 87(3):559–580.

White, P. and S. Harris
1995. Bovine tuberculosis in badger (Meles meles) populations in southwest E ngland: the use of a spatial stochastic simulation model to understand the dynamics of the disease. *Philosophical Transactions of the Royal Society*, Pp. 391–413.

Whithear, K. G., G. S. Cottew, and K. E. Harrigan
1989. Virulence and transmissibility of Mycoplasma gallisepticum. *Australian Veterinary Journal*, 66(3):65–72.

Wiggins, R. C.
2009. Prion Stability and infectivity in the environment. *Neurochemical Research*, 34(1):158–168.

Williams, E. and M. Miller
2002. Chronic wasting disease in deer and elk in North America. *Revue Scientifique et Technique de l'OIE*, 21(2):305–316.

Williams, E., M. Miller, T. Kreeger, R. Kahn, and E. Thorne
2002. Chronic wasting disease of deer and elk: a review with recom- mendations for management. *The Journal of Wildlife Management*, 66(3):551–563.

Wilson, S. G., J. G. Taylor, and A. F. Pearce
2001. The seasonal aggregation of whale sharks at Ningaloo Reef, Western Australia: Currents, migrations and the El Niño/ Southern Oscillation. *Environmental Biology of Fishes*, 61(1):1–11.

Wobeser, G.
2002. Disease management strategies for wildlife. *OIE Revue Scientifique et Technique*, 21(1):159–178.

Wong, B. B. and U. Candolin
2015. Behavioral responses to changing environments. *Behavioral Ecology*, 26(3):665–673.

Woodroffe, R.
1999. Managing disease threats to wild mammals. *Animal Conservation*, 2(3):185–193.

Woodroffe, R., S. Cleaveland, O. Courtenay, M. K. Laurenson, and M. Artois
2004. Infectious disease: Infectious disease in the management and conservation of wild canids. In *The Biology and Conservation of Wild Canids*. Oxford: Oxford University Press.

Xu, C., M. S. Boyce, and D. J. Daley
2005. Harvesting in seasonal environments. *Journal of Mathematical Biology*, 50(6):663–682.

Yletyinen, J., J. Hentati-Sundberg, T. Blenckner, and Ö. Bodin
2018. Fishing strategy diversification and fishers' ecological dependency. *Ecology and Society*, 23(3).